ADVANCES IN GEOMATICS

Volume: 03 - Issue: 01 - October 2025 e-ISSN: 3023-4980

INTERNATIONAL REFEREED JOURNAL
PUBLISHED TWICE A YEAR
OPEN ACCESS

ADVANCES IN GEOMATICS

Volume: 03 - Issue: 01 - October 2025 e-ISSN: 3023-4980

INTERNATIONAL REFEREED JOURNAL
PUBLISHED TWICE A YEAR

OPEN ACCESS

Powered By
OJS
OPEN JOURNAL SYSTEMS

Special Thanks to
Assoc. Prof. Elvan ATAMTÜRK
for assuming the editorship of this issue and designing cover and interior pages...

October 30, 2025

Advances in Geomatics (AIG) is an international refereed journal which is published twice a year and it is open access. The responsibility related to the scope, content, and essence of the published papers in the journal adheres to the author(s). The papers published in the journal cannot be cited without showing reference.

ADVANCES
IN GEOMATICS
e-ISSN: 3023-4980

EDITOR

Erman ŞENTÜRK, Assoc. Prof. | Kocaeli University

MANAGING EDITOR

Elvan ATAMTÜRK, Assoc. Prof. | Kocaeli University

EDITORIAL BOARD

Aydın Üstün, Prof. | Kocaeli University

Yury Yasyukevich, Prof. | Russian Academy of Sciences

Ramazan Alpay Abbak, Prof. | Konya Technical University

Xiaodong Ren, Assoc. Prof. | Wuhan University

Erman Şentürk, Assoc. Prof. | Kocaeli University

Mohamed Freeshah, Asst. Prof. | Benha University

LANGUAGE EDITOR

Tuğba ATAMTÜRK

SECRETARY

Mohd Saqib, Ph.D. (C) | McGill University

CONTACTS

https://aigjournal.com advancesingeomatics@gmail.com

+90 262 303 32 46

ADVANCES IN GEOMATICS
e-ISSN: 3023-4980

INDEXES

ADVANCES
IN GEOMATICS
e-ISSN: 3023-4980

REVIEWERS OF THIS ISSUE

Gülcan Sarp, Prof.
Suleyman Demirel University - Turkey

Arzu Erener, Prof.
Kocaeli University - Turkey

Firdes Yenilmez, Assoc. Prof.
Akdeniz University - Turkey

Murat Selim Çepni, Assoc. Prof.
Kocaeli University - Turkey

Özer Akyürek, Assoc. Prof.
Kocaeli University - Turkey

Alev Mutlu, Assoc. Prof.
Kocaeli University - Turkey

Mohamed Freeshah, Asst. Prof.
Benha University - Egypt

Muhammad Arqim Adil, Ph.D.
Wroclaw University of Environmental and Life Sciences - Poland

Bissegue Jean Claude, Ph.D.
University of Ngaoundéré - Cameroon

Bishal Khatri, Ph.D.
Kathmandu University - Nepal

Hamdullah Livaoğlu, Ph.D.
Kocaeli University - Turkey

ADVANCES
IN GEOMATICS
e-ISSN: 3023-4980

ABOUT

Advances in Geomatics (AIG) is a peer-reviewed scientific journal dedicated to the dissemination of cutting-edge research in the field of geomatics. The Journal publishes English language original research articles, review papers, and technical notes in the multidisciplinary domain of geomatics.

AIM

Advances in Geomatics has started its publication life in 2023. This journal has embarked on the Open Access Policy with the idea that scientific information produced by academics, professionals, and others can be accessed by anyone, both locally and internationally, without any limitation. The journal aims to publish high-quality research articles, review papers, and technical notes that contribute to the understanding, development, and application of geomatics principles, technologies, and methodologies.

SCOPE

Advances in Geomatics welcomes contributions from researchers, academicians, professionals, and practitioners in the multidisciplinary domain of geomatics, including but not limited to the following areas: Geospatial data acquisition, geospatial data processing and analysis, geospatial data management, geospatial information systems, geospatial applications, geomatics for sustainable development, the journal encourages original research that pushes the boundaries of geomatics, promotes interdisciplinary collaborations, and addresses emerging challenges in the field.

PUBLICATION POLICIES

Advances in Geomatics is an international refereed journal that adopts double-blind peer-review process. Editorial board of our journal follows Editorial Policy of the Council of Scientific Committee.

PUBLICATION PERIOD

Advances in Geomatics is published twice a year in October and March. Publications are made from the following areas, which will contribute to the development of geomatics discipline and contribute to the literature: Other disciplines assessed in relation to geomatics, civil, geography, geophysics, geology, environmental and other engineering sciences, etc.

ADVANCES
IN GEOMATICS
e-ISSN: 3023-4980

FROM THE EDITOR

Dear academics, practitioners and our readers;

It is with great pleasure and enthusiasm that I welcome you to the inaugural issue of "Advances In Geomatics." As the Editor-in-Chief of this esteemed journal, I am honored to present a platform dedicated to the dissemination of cutting-edge research and innovation in the field of geomatics.

Geomatics, as a multidisciplinary science, plays a pivotal role in our understanding and management of the Earth's resources. The articles in this issue reflect the diverse range of topics within the geomatics domain, from geospatial technology and remote sensing to geographic information systems (GIS) and spatial analysis.

Our goal with "Advances In Geomatics" is to foster collaboration and exchange of knowledge among researchers, academics, and professionals in the geospatial community. The peer-reviewed articles featured in this issue represent the latest advancements and contribute to the ongoing discourse in geomatics.

I extend my gratitude to the authors for their valuable contributions and to the dedicated reviewers who have rigorously evaluated the manuscripts. Their commitment to maintaining the highest standards of scientific excellence is commendable.

As we embark on this scholarly journey together, I encourage readers to explore the diverse perspectives presented in this inaugural issue. "Advances In Geomatics" aims to be a catalyst for further advancements, discussions, and collaborations in the dynamic field of geomatics.

I look forward to your continued support and engagement with "Advances In Geomatics." May this journal serve as a source of inspiration and knowledge for all those passionate about advancing the frontiers of geomatics.

Sincerely,

Erman ŞENTÜRK, Assoc. Prof.
Editor

ADVANCES IN GEOMATICS

VOLUME 03 • ISSUE 01 • OCTOBER 2025
e-ISSN: 3023-4980

ORIGINAL ARTICLE

Submission: 30/03/2025
Accepted: 02/05/2025

REAL-TIME MONITORING OF ARTISANAL AND SMALL-SCALE GOLD MINING OPERATIONS USING ANDROID MOBILE GIS APPS AND GPS RECEIVER: FOCUS ON DEM, BOTE AND DIMAKO I MINING SITES (BATOURI GOLD DISTRICT, EASTERN CAMEROON)

Bissegue Jean CLAUDE[1,2,3]* Ravindra Nath TIWARI[2] Namit Kumar JHA[2] Mustapha ALAOUI[3] Tchameni RIGOBERT[1]

[1] Department of Earth Sciences, Faculty of Science, University of Ngaoundéré P.O. Box 454 Ngaoundéré, Cameroon.

[2] Geoinformatics Department, NETRA institute of Geoinformatics Management and Technologies Foundation, Dwarka Mor, New Delhi-110059, India.

[3] Centre des Compétences et Leadership (CCL), académie de formation professionnelle privée, Marrakech, Morocco.

* Corresponding Author: B. J. Claude, jeanclaudebissegue7@gmail.com 0009-0004-9821-744X

ABSTRACT

The concept of "sustainable mining" is also based on the requirement for rigorous monitoring of mining operations, in order to prevent abuses that can be exerted on the environment or the loss of income that can be recorded by the administrations of the countries owning the mines, either due to non-compliance by mining operators with the clauses of mining permits or because of the complacency of state agents in charge of mines. Android mobile GIS applications (AMGISA) with integrated GPS are a high-precision navigation, control, monitoring and terrestrial positioning system. This portable mapping and localized imaging system allows in real time addition of spatial information on the position of observation points, descriptions in the attribute table, collecting waypoints, tracks and taking geotagged photos, as well as capturing screenshots of said maps or images available on its interface. The interface is very dynamic, facilitating data collection via internet connection and their transfer to another workstation for offline processing version and submission of results to decision-makers. The automatic monitoring tests initiated with this technology in the Batouri gold district in the small mines of Dem, Bote and Dimako I have successfully enabled the control and monitoring of mining operations both in the exploration phase and in the exploitation phase. AMGISA and GPS thus constitute a viable alternative capable of being deployed in mining environments and meeting the requirements related to the control and monitoring of mining operations, especially in open-pit mines and particularly for countries located in forested or rugged or remote regions.

Keywords: Batouri, Artisanal and Small Scale Mining, Mobile GIS, GPS, Applied Geoinformatics.

Cited As: Claude, B. J., Tiwari, R. N., Jha, N. K., Alaoui, M. & Rigobert, T. (2025). Real-Time Monitoring of Artisanal and Small-Scale Gold Mining Operations Using Android Mobile GIS Apps and GPS Receiver: Focus on Dem, Bote and Dimako I Mining Sites (Batouri Gold District, Eastern Cameroon), Advances in Geomatics, 3(1), 1-19. https://doi.org/10.5281/zenodo.15596420

INTRODUCTION

In this modern era where the demand for rare and precious metals from the technological industry on which developed countries heavily depend is increasing day by day; in the so-called mining countries that supply these metals, on the other hand, there are scandals and crises linked to the mining sector. In most of these countries, particularly those located in forested or rugged or remote regions; the distance between the mining sites where the project manager operates and the capital where the project owner's institutions and services reside is often very great and difficult to access. On the field, there are often several problems related to the lack of control and rigorous monitoring of mining operations by the national administrative side. The most recurring problems are linked to: (1) anarchic exploitation due to non-compliance with the laws in force (environmental law, mining code) causing severe damage to the environment (soil pollution, water , air, visual pollution, destruction of ecosystems, etc.) and a significant shortfall in revenue for states; (2) non-compliance with the terms of mining titles (research permit, operating license) with the direct corollary of exaggerated extensions of the limits or perimeter of the mining title, authorized exploitation depths and often exploitation instead of research. In view of all these irregularities and their economic, environmental and social consequences; this article proposes an effective and adequate method for real-time monitoring and control of mining activities in the field. It presents the importance of integrating mobile GIS and the GPS receiver, which are two cutting-edge tools in the field of geoinformatics, in the mining sector. Furthermore, to date it is difficult to find works mentioning the role of mobile GIS and GPS in the monitoring of mining projects; however, several roles are assigned to GPS in the field of Geosciences such as environmental impacts and Water Resources (Castello et al., 2016; Schueler et al., 2011), and landslide hazard and risk (Roya Olyazadeh et al., 2017). The article is structured around three salient points: firstly the method of real-time data collection in the field (or station 1) with the android mobile GIS applications (AMGISA) and the GPS receiver (GPSr); secondly the transfer of data in real time to station 2 (offline/online); and finally thirdly the processing of the data at station 1(online/offline) or station 2 (offline/online) in order to submit them to decision-makers either in photographic or cartographic format, with the aim of making informed decisions and corrective measures if necessary.

1. LITERATURE REVIEW

1.1. Physiography of Study Area

The Batouri sector is located in the Adamaoua-Yade Domain (AYD) of the Pan African fold belt in Cameroon (Asaah et al., 2014) and is one of the areas affected by the Central Cameroonian Shear (Tchakounté et al., 2017). The sites of the small scale mining of Dem, Bote and Dimako I are located near the town of Batouri to the East and are aligned along the Mbil and Djengou rivers with a general NE-SW orientation constituting one of the subwatershed of the Kadey in the infrastructure of the

Kambele Shear. The study area stretches between latitudes 4° 20' N and 4° 28' N and longitudes 14° 22' E and 14° 27' E (Fig. 1). Access to mining sites is easily practicable due to a relatively dense road network made up of numerous rural roads opened and maintained, mostly by loggers and mining companies.

Batouri is under the influence of a hot and humid equatorial climate of the classic Guinean type with two rainy seasons, interspersed with two dry seasons (Tsaléfac, 2007). It extends to the forest-savannah boundary; the vegetation is very heterogeneous including a grassy savannah in the North and a lush forest in the South region (Bissegue, 2021). The geomorphological analysis based on the study of the SRTM DEM data with a spatial resolution of 30 m (Bissegue, 2021) showed that; the relief fluctuates between altitudes 600 and 900 m. Topographic variations show that the Batouri sector includes three geomorphological units: an upper surface (altitude > 680m), a lower surface (altitude < 600 m) and a transition zone (600 m < altitude < 680m).

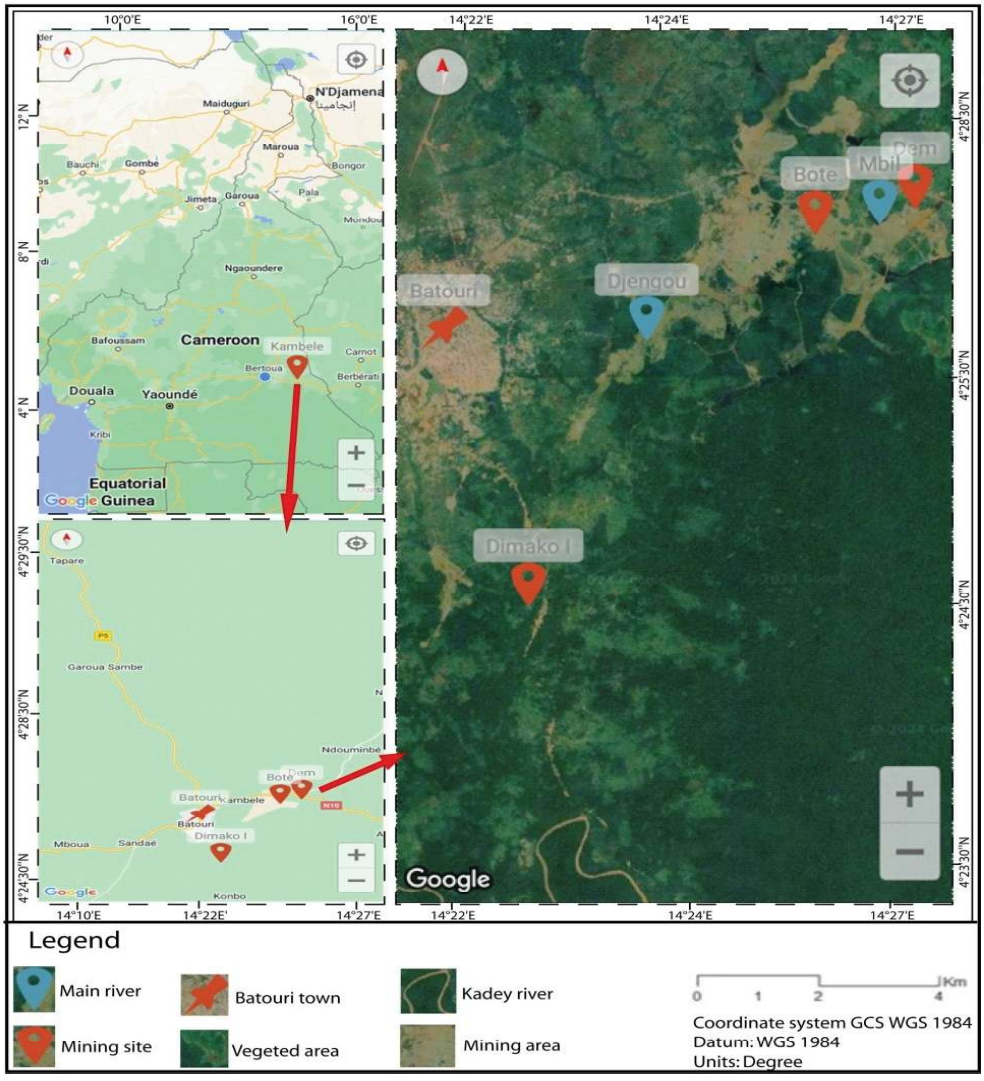

Figure 1. Location map of study area showing Dem, Bote and Dimako I mining sites.

1.2. Mining overview

Exploration by conventional methods and exploitation of Batouri gold remains an ancient activity. Numerous testimonies and stories from residents show that the gold ore deposits from Kambele and surrounding areas, located about 7 km to the East of the town of Batouri was discovered in March 1957 by MBANGO Collette in the Mboscoro stream by making a small well for water (Ntep Gweth, 2013). Several sites of mining activities with the exploitation of gold are located in the study area.

To date, the inventory of mining operations in the area allows, first of all, to identify the presence of several mining companies. Mining is preponderant in the Dem, Bote and Dimako I sites. This exploitation is mainly carried out in the beds, the banks of waterbodies and flats. In watercourses, it is done by dredging or suction and in banks and flats by digging using backhoes or excavators. The opening of mining sites has led to several considerable environmental problems in the operating areas such as water pollution, the destruction and diversions of waterways, deforestation and land degradation (Bissegue, 2021).

1.3. Background and key concepts

According to the functionalities and usages, Mobile Geographic Information Systems (Mobile GIS) extend traditional desktop GIS beyond the offices and allow individuals and organizations to localize, collect, store, visualize and even analyze geospatial data in both field and office environments. GIS have several extra functions in enhancing data performance. It can describe the spatial data on a map, such as the location and shape of geometric objects, and help analyze spatial relationships. It can also store attribute data of map features, and provide the capability to view the distribution network superimposed on different layers (Shin and Feuerborn, 2004). Lastly, GIS can support not only the analysis of features by using the graphical display, but also updating the data (Wei et al., 2010). For instance, about a good definition of Mobile GIS one can dive into more details through those references (Tomlinson 1987, 2007; Goodchild 1992, 2010; Mark, 2003; Egenhofer et al. 2016).

In this section, previous researches concerning field works using mobile GIS are reviewed to give an insight into the background of this study. Generally in geoinformatics, the different techniques for data collection are divided into (i) image interpretation; (ii) semi-automated classification; (iii) automated classification; and (iv) field navigation including total stations, GPS and recently mobile GIS. Data collection includes desk and field studies and involves different activities ranging from low cost to expensive (Soeters and van Westen, 1996). Geospatial information, spatial analysis, and spatial queries are no longer limited to a fixed environment but can be accessed at any place at any time (Shi et al. 2009). This is how many improvements in digital mapping and mobile GIS using geospatial technologies have been revealed in the field of data acquisition for landslide hazard and risk. Free and Open source Software for Geoinformatics has significantly improved the efficient mapping and management of post-disaster and impacted areas around the world (UNEP, 2014; Ushahidi, 2016;

GeoVille, 2016). A mobile GIS application for data collection of cadastral mapping using ESRI and Google Android Software has been developed (Bronder and Persson, 2013).

To end, in the domain of geographic information systems (GIS), advanced mobile information technologies have enabled a variety of novel applications which can help improve positioning and tracking accuracy, efficient field data collection, real-time mapping, ground truth validation, location intelligence and decision support, and so on (Lemmens, 2011; Abdalla, 2016).

2. RESEARCH DESIGN AND METHODOLOGY

2.1. Mobile database and online real-time field data collection

Sites monitoring across mining operations is central to many processes and has always been prevalent amongst exploration and mining operations over the entire course of the project lifecycle. This paper is aimed to provide an operational monitoring method as the project moves through its development phases. Our works focused on three sites whose national and international operators hold operating licenses granted by the State of Cameroon.

Mobile database maintains all the spatial and non-spatial data for mobile GIS applications. The geospatial data used here are essentially primary and come from direct field collection and analysis of cartographic databases available in the Mobile GIS software interface and GPS receiver (GPSr, Tab.1). These data are mainly composed of geotagged photographs, digital maps and Google Earth aerial images. The data thus collected is presented in four digital formats (JPG (.jpg) or PNG (.png) format and KMZ format (.kmz) for the AMGISA data source and GPX format for the GPS receiver). They contain significant information specifically linked to the extension of the perimeter or area of the operations site (size, shape), the precise position of the mining site, the layout and depth of the pits, the phases of mining operations (exploration, exploitation or ore processing) throughout the lifecycle of the mining project. GPS and Google Earth were used for collecting geographical location points of various utility features. The geographic coordinates in latitude and longitude determined by GPS in decimal degrees and surveyed in the global system WGS84/ ellipsoid IAG-GRS80 were arranged in an Excel database with a unique identifier (ID).

When doing field work with GIS technology, two aspects should be considered ; one is visualization (Pundt and Brinkkotter-Runde, 2000), and the other is data acquisition (Poorazizi et al., 2008). Field-based GIS has become the new solution for data visualization and acquisition. The control and monitoring of mining activities as proposed by this article consists of a full-time daily process of data collection, using mobile GIS by android applications (AMGISA) or other handheld GIS devices, GPS and internet connection, their preprocessing and/or their processing then sending in real time to decision-making services. For the convenience of this article, only the data collected during the period from August 29 to 30, 2024 are presented in order to support the approach. From the visualization

perspective, the actual mining sites are well displayed on a Mobile GIS-based map (AMGISA) ; this GIS technology is handling geographical and attribute data. With the visualization servers, user gets a better understanding of real world conditions, then views the attributes of area of interest on the digital graphical data displayed accordingly. For data acquisition during field surveys, different field processes have to be completed such as Geotagged photographs recording with both location and attribute and Screenshots of Collector (Fig.2).

Table 1. Database for real-time monitoring of artisanal and small-scale gold mining operations using Android Mobile GIS Apps and GPS receiver.

ID	Data inventory	Source/Description
1	Location	GPS Lat/Long coordinates
2	Date	GPS real-time
3	Type/Format	JPG/PNG/KMZ /GPX
4	Depth	GPS receiver
5	Volume	Measurement
5	Time	GPS real-time
7	Perimeter	GIS calculation
8	Path or track	GPS receiver
9	Polygon/area	GPS receiver
10	Geotagged photographs	Mobile GIS apps
11	Google maps	Mobile GIS-based map
12	Google satellite images	Mobile GIS-based map
13	Google Earth aerial photos	Google Earth pro
14	Photographs	Digital camera

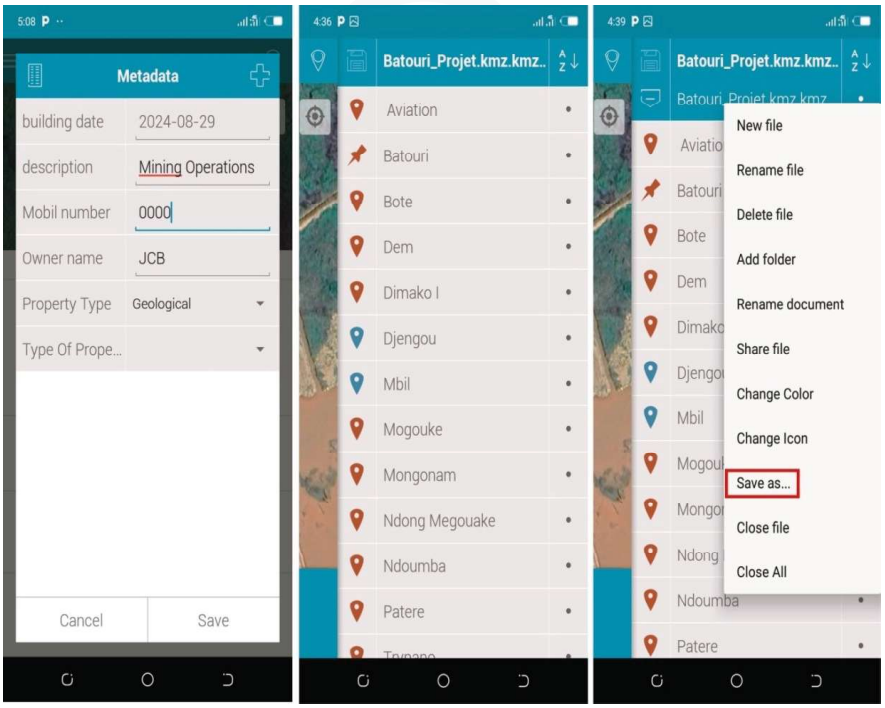

Figure 2. Attribute table editing and field data recording with AMGISA.

2.2. Online real time data pre-processing and transmission

Preprocessing consisted of correcting the position of observation points collected by the AMGISA, deleting unnecessary data and transferring data from mobile device and GPSr to in-office computer effortlessly. The process of correcting the position of a point after data collection is done in three steps: (1) Simple navigation through the application to the location of the point considered, then placement of a new waypoint which modifies the incorrect coordinates and automatically gives the real coordinates of the location, (2) noting the coordinates then deleting the waypoint with false co-ordinates and, (3) editing the location to be corrected. The corrected points were recorded in Table 2. The method of deletion, verification of the accuracy of the data and recovery of GPS data and their export to the computer is classic. Using a cable, the GPS is connected to the computer ; then using specialized software, the data in GPX format including positions of observation points, lines or tracks (in lines or polygons) of spaces mining operations were converted and saved in shapefile and KML formats.

Online data access for field work needs handheld devices such as laptops, smartphones and tablets. Smartphone was adopted for this work in the field because of its own graphical user interface, touch keyboard, wireless communication capabilities and the ease of having the Android mobile GIS application (AMGISA) online through the Playstore platform with Android as Operating Systems (OS). For data gathering, updating via mobile GIS and transferring to another users (Fig.3), the availability of wireless communication is important. Typical technologies used here it's cellular networks well supported by Android devices and available in the field. 4G is the most commonly cellular network used in Cameroon facilitating online mobile GIS functionalities and making the communication fast and stable. Communication among different devices (e.g. station 1 in the field and station 2 in the office) and data transfer is therefore established by mobile network connection. Online mobile GIS (AMGISA) also enables a real-time data updates and exchanges between centralized map servers and distributed mobile.

Table 2. Correction of observation point coordinates using the GIS Mobile apps (AMGISA).

		Incorrect coordinates		Real coordinates	
ID	Placemark	X(DMS)	Y(DMS)	X(DMS)	Y(DMS)
1	**Dem**	360.000 0.000 0.000	360.000 0.000 0.000	14.000 26.000 30.103E	4.000 27.000 42.738N
2	**Djengou**	360.000 0.000 0.000	360.000 0.000 0.000	14.000 23.000 54.596E	4.000 26.000 14.841N
3	**Dimako I**	360.000 0.000 0.000	360.000 0.000 0.000	14.000 22.000 42.510E	4.000 23.000 22.586N
4	**Mongonam**	360.000 0.000 0.000	360.000 0.000 0.000	14.000 22.000 06.728E	4.000 24.000 52.339N
5	**Pater**	360.000 0.000 0.000	360.000 0.000 0.000	14.000 23.000 14.133E	4.000 25.000 20.370N

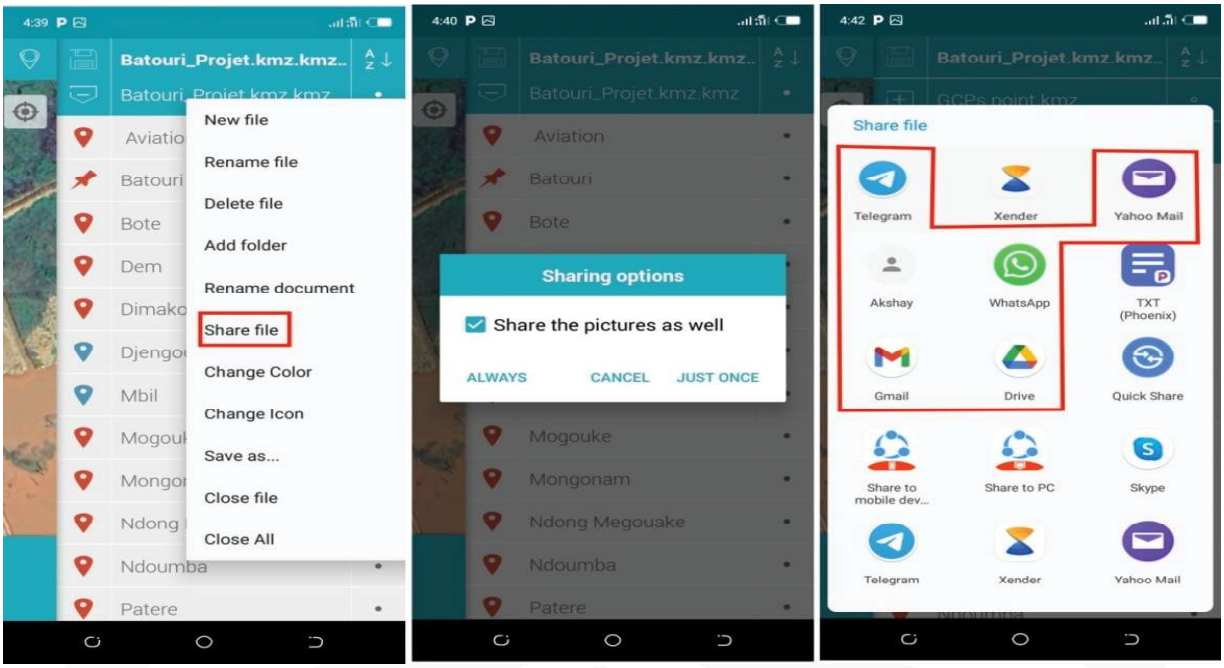

Figure 3. Data transfer process from mobile device to in-office computer effortlessly based on the use of internet and common web apps from the field.

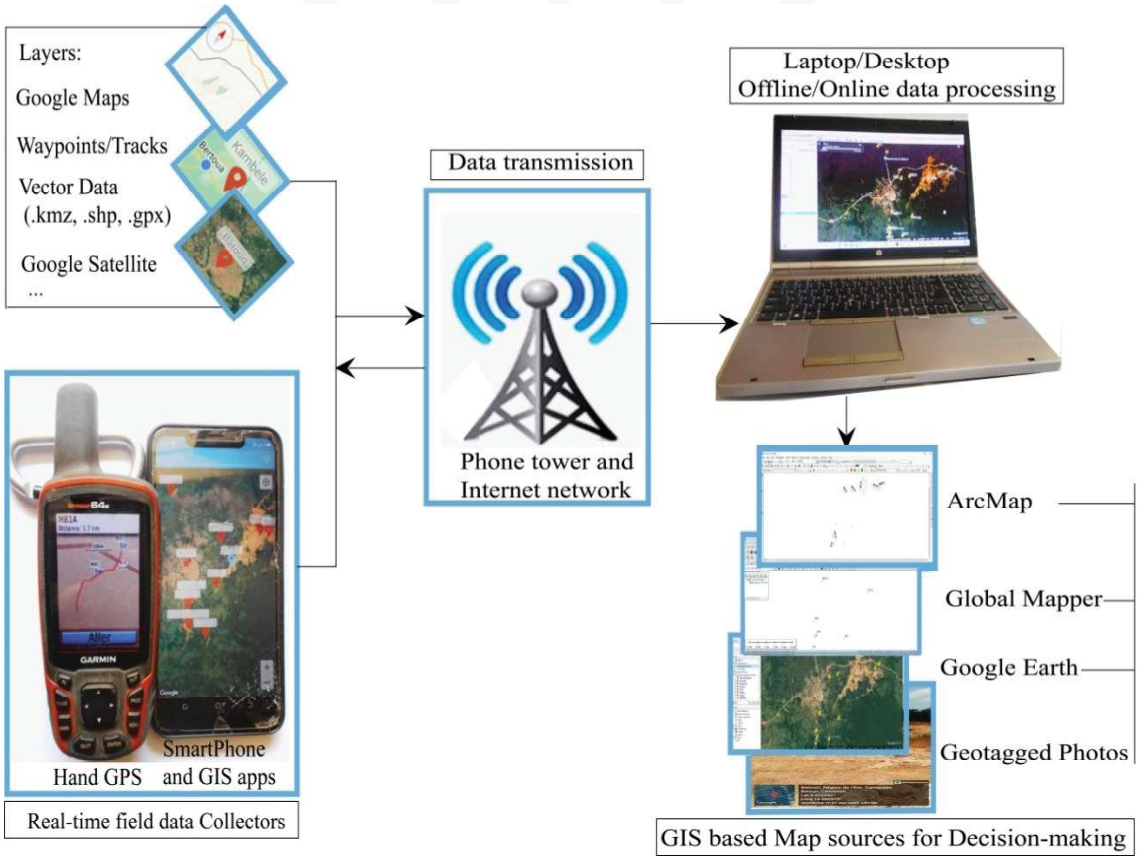

Figure 4. Conceptual workflow of real-Time GPS handed and Mobile GIS Data Acquisition System for gold mining operations monitoring.

2.3. Offline data processing and post-processing

Real-Time Data Collection enables immediate data upload and synchronization with cloud-based GIS systems or data transfer to another users (workstation). Once the fieldwork has been completed for the day, the mobile GIS apps (AMGISA, as indicated in section above) allow to gather field data including GPS coordinates, geotagged photos, basemap and feature attribute information. Then, daily data can be downloaded quickly and effortlessly. Offline mode data processing consists of the data visualization and analysis; this stage (station 2) permits to utilize GIS softwares (such as ArcGIS, Google Earth, Global Mapper, …) to analyze the collected data and create maps, reports, and visualizations to aid decision making. Thereafter, post-processing enables the analysis and interpretation of the collected field data using desktop GIS softwares, creation of informative maps ; helps to perform spatial analysis, and generate reports. The conceptual workflow is briefly described as seen in Figure 4.

3. RESULTS

3.1. Monitoring of Dem Mining open pit

Early mobile GIS and GPS monitoring was conducted in Dem, Bote and Dimako I in order to define the different mining operations carried out in these mining sites and consequently collect accurate data and transfer them in real time for decision-making. Firstly, GPS data is basically point oriented ; whereas GIS data is more complex comprising points (GPS coordinates), lines (tracks) and polygons (areas) and images and Relational Databases. However, the only prerequisite for collecting data is to actually be on the ground; no image data can be collected outside the field. The location of mining sites on the basemap served by the mobile GIS app (AMGISA) interface also allows for taking pictures of the observed points, which generates two types of data, namely maps of mining sites and geotagged photos. Thus, accurate and up-to-date data for the entire mining site can be viewed in the field via the basemaps available on the mobile GIS application interface.

The centered map (Fig.5) presents the mining site of the small Dem mine, this map shows the extent of the activities and allows spatially to appreciate the scale of the exploitation whose observation elements are the perimeter, the position, the type of activity, the equipment used and even the evolution over time. The geotagged images around centered map provide details and precision on the type of activity and its degree. These activities include the stage of the mine opening, stripping of waste rock, transport of mining waste, backfilling and ore deposition among others. The most important thing here is the geographical position of the mine site, its size, nature, extension and depth in accordance with the provisions of the research title.

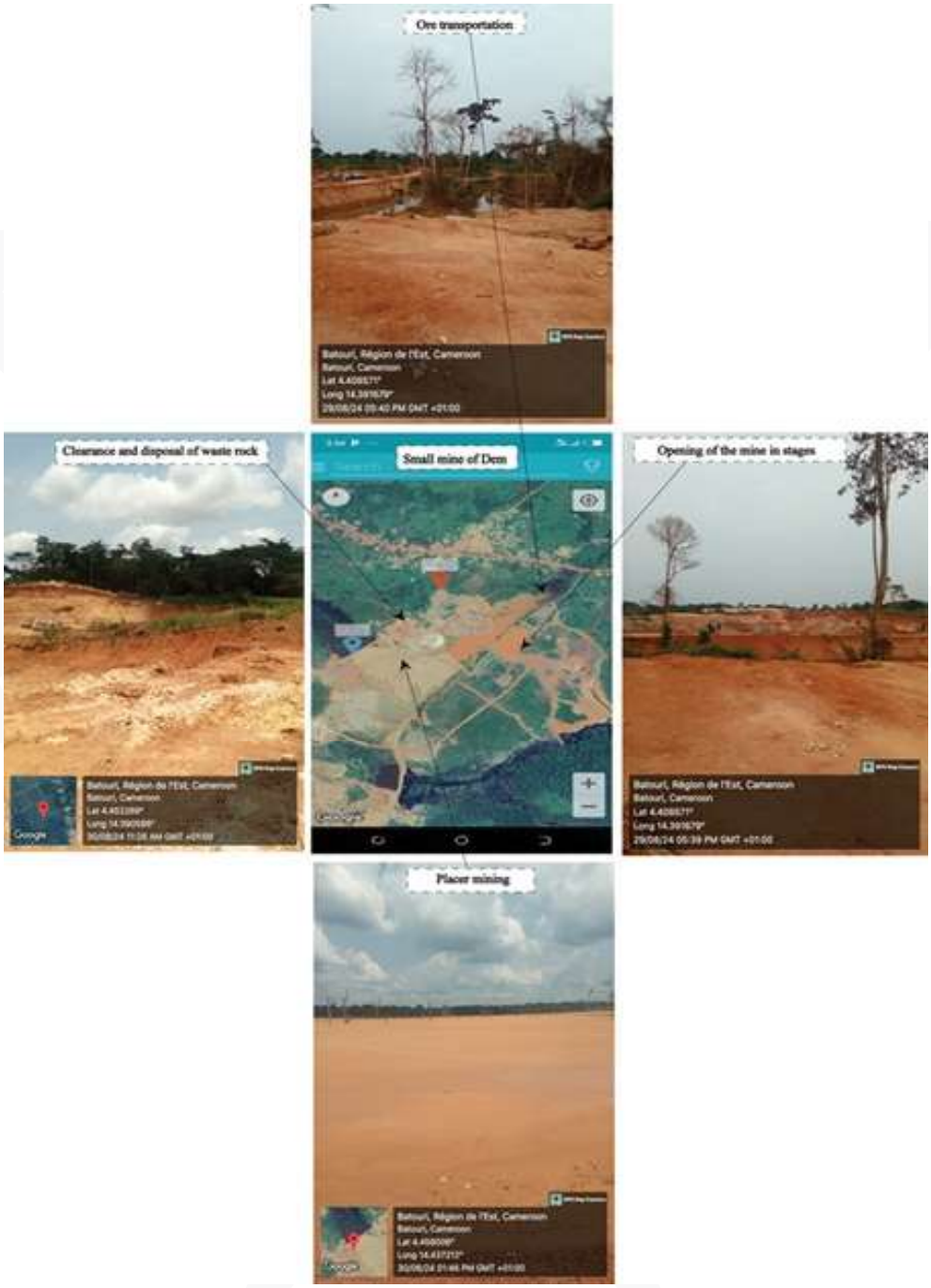

Figure 5. Screenshot of centered Google satellite image of Dem's small open pit mine and geo-tagged photos of operations.

3.2. Monitoring of Bote Mining open pit

An important application of Mobile GIS apps (AMGISA) alone or in combination with GPS is the monitoring of mining and geological operations related to all phases of a mining project such as prospecting, exploration, mine development and exploitation. Data collection tests by mobile GIS applications downloaded from playstore conducted in Dem, Bote and Dimako I demonstrated their

interest in being associated with GPS in order to improve the availability of coordinates and, consequently, the accuracy of the data. Comparison with 2D coordinates obtained from an geotagged image at station 1(in field) confirmed a repeatability of less than 0.01 degree, as well as an accuracy of less than 0.01 degree (assuming no movement of the device) with the 3D coordinates taken by the GPS receiver (GPSr). Figure 6 presents the monitoring images of the mining operations at the small Bote mine, carried out using AMGISA and GPSr. Bote is the largest mining site in the study area. The mine consists of several pits, each approximately 1.5 km length and 750 m width, reaching depths of almost 50 m in places. The data collected, mainly consisting of geotagged photos, tracks, and GPS coordinates indicate that the site is located between 14° longitude and 4° latitude. The mining phase is very advanced in terms of the extension of the mine perimeter and the depth that almost reaches the granite bedrock. Activities also include, among others, mine opening, stripping of waste rock, transport of mine waste, backfilling, ore deposition, as well as ore processing and enrichment. Irregular or illegal activities can now be detected through rigorous real-time monitoring using mobile GIS and an internet connection. Appropriate measures can be taken in real time by decision-makers to ensure strict implementation of the clauses of the various contracts or the provisions of the various mining titles awarded to mining companies.

3.3. Monitoring of Dimako I Mining open pit

Android mobile GIS is a portable mapping and imaging system, operating simultaneously in harsh urban and rural environments, and often used for mining in environments where good sky visibility is not guaranteed. It is a positioning/orientation device imposing strict requirements in this regard; the solution to the positioning/orientation problem increasingly relies on the integration of several technologies. Therefore, in this paper as a reminder, a hybrid system based on Android mobile GIS applications (AMGISA) and GPS receiver (GPSr) is used.

The small Dimako mine is in the data collection phase of its opening. The Dimako locality is located in the middle of a dense forest; the installation of a mine in this site is the cause of the loss of a strong forest cover. The GPSr made it possible to collect the coordinates and tracks of the extension of the exploitation perimeter. The mobile GIS interface permitted to access the maps and take precise geotagged photos of the observation points. Mining operations at this stage include the opening of the mine, stripping of waste rock, excavation and transport of mining waste. The image data presented in Figure 7 are thus integrated in offline mode into desktop GIS tools for visualization, analysis, interpretation and creation of maps useful for decision-making.

Figure 6. Screenshot of centered Google satellite image of Bote's small open pit mine and geotagged photos of operations.

Figure 7. Screenshot of centered Google satellite image of Dimako I's small open pit mine and geo-tagged photos of operations.

4. DISCUSSION OF FINDINGS

4.1. Mapping and data assessment for decision-making

Several cartographic and image editing platforms available, such as GIS, make it possible to produce maps and carry out data evaluations, necessary to support the taking of appropriate measures by decision-makers in accordance with the mining and environmental law in force in the host country. Figure 8 presents the field data projected on the Google Earth image basemap, the rapid visualization and evaluation of which allow the extent of activities on the ground to be assessed. The superposition of spatial terrain information on aerial imagery therefore makes it possible to faithfully visualize the reality as it is on the ground and to induce informed decision-making. Thus presented, the online mobile GIS and offline office work aim to reduce the costs and time required for data collection/modification/loading, increase data accuracy, make data for the entire study area visible and complete the mapping of the study area within the time limit for informed daily decision-making.

Researchers in the environmental field are increasingly interested in the use of geolocation and mobile mapping devices such as GPS devices (Zheng et al. 2008, Yue et al. 2014) and mobile phones (Kang et al. 2010, Gao 2015, Xu et al. 2016, Zhao et al. 2016). Thus, the popularization of mining operations monitoring technology and the processing approaches of data collected online or offline by mobile GIS via smartphones will therefore advance informed decision-making and geospatial intelligence based on them.

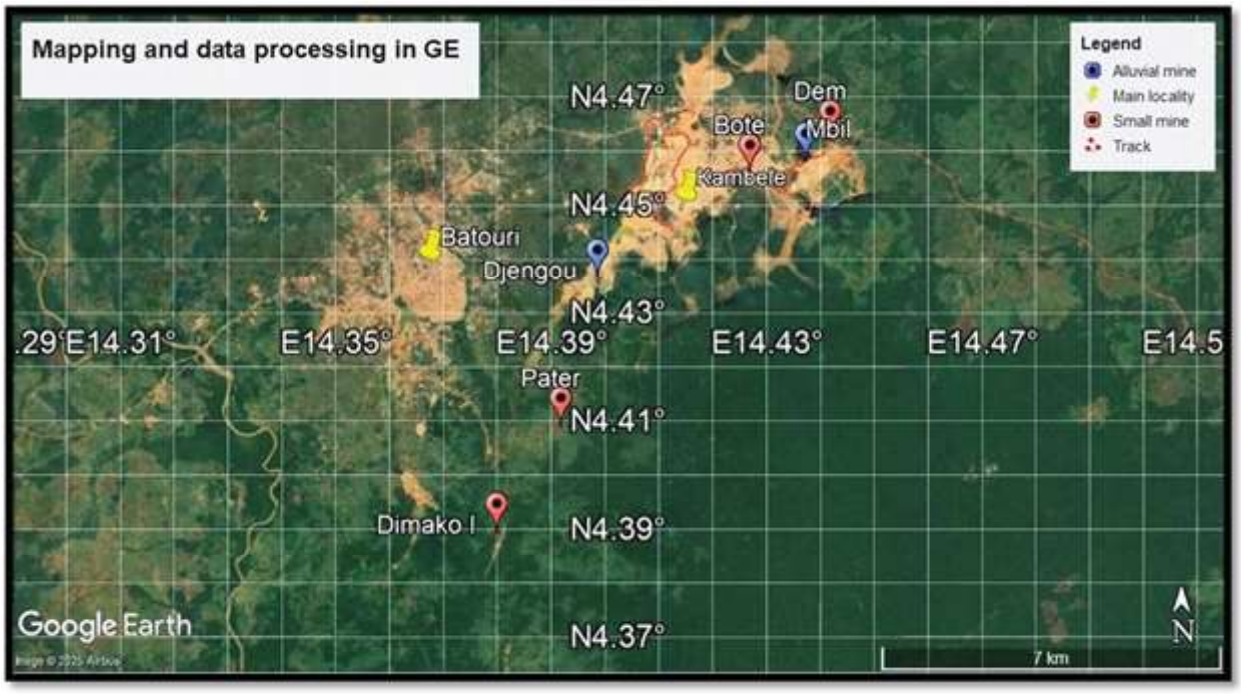

Figure 8. Display and visualization on Google Earth of data including observation points and routes of mining site extensions.

4.2. Map publishing

To publish a map to support informed decision-making, it was first necessary to create a map project in a desktop GIS in offline mode and connect all the data layers. The test map template produced in this example therefore contains several feature layers. The built-up, land-use, waterbody, and road network layers were chosen as background layers. All these layers were used as operational layers for visualization, queries, querying, and editing to better assess the location of the various mining sites and the nature of their operations. Figure 9 presents an overview of the test map, it is important to mention that this map comes from the data collected during the monitoring test using AMGISA in the test area of the Dem, Bote and Dimako I mining sites. Users (mining operators and decision-makers) can identify the symbols of the mining sites, their geographical position, the paths of their extension and their relationship with the environment, as well as several other characteristics can be evaluated. These geospatial data layers on the mining sites thus represented are essentially the reflection of the work carried out by the field agents responsible for monitoring mining activities. The choice of symbology and colors make each element of the map easily readable and identifiable.

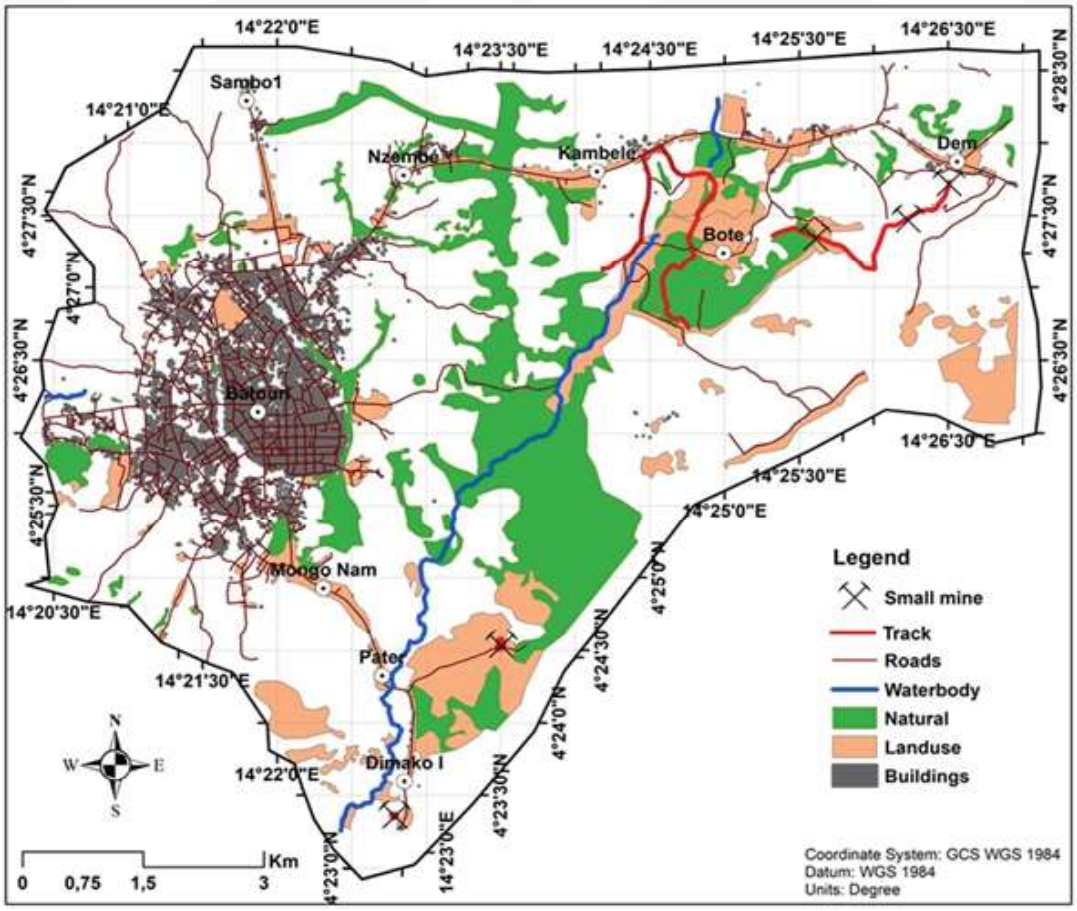

Figure 9. Informed decision support map edited in an offline GIS mode using field data collected by the mobile GIS apps and GPS receiver then plotted on land use-land cover basemap of the study area.

The results of this research have shown how mobile GIS via smartphones have facilitated the tasks of monitoring mining operations and collecting field data. In terms of data access, collecting, querying, and modifying or correcting data on a mobile device and transferring it to another workstation for offline processing and mapping have become possible. From a visualization perspective, they help mining stakeholders visualize the spatial distribution information of mining sites on digital maps. However, this research also has some limitations. To this end, the development of a mobile GIS application for use in the environmental field must address certain challenges, including: i) the limitation of system resources, such as processor speed, memory size, and battery power; ii) the limitation of network connection during field survey; and iii) the size of the screen and keyboard, as well as the interface as indicated by Fu and Sun (2011). As additional practical solutions, it is suggested here to use optimized mobile GIS applications and other alternative devices such as power banks, solar charging systems, internet modems and tablets. Fu and Sun (2010) also pointed out that it is essential to choose a widely used system and mobile device to maximize the acceptance of this application by different target groups (such as mining authorities). Therefore, Android mobile GIS has proven valuable as the main platform in this study, thanks to its free resources, accessible online to all on playstore. From this point of view, Android also helps reduce the costs of controlling and monitoring mining works because it makes it possible to edit data in real time through its graphical interface, as mentioned by Wei et al. (2010).

CONCLUSION

Android mobile GIS applications (AMGISA) are a new type of portable mapping and localized imaging system, capable of providing high-precision positioning coverage when accompanied by the GPS receiver (GPSr). It is therefore a navigation system allowing to locate oneself on the map and to mark the precise position of the observation point and take geotagged photos. This article presents some technical aspects of this technology, summarizes the strengths and describes the various applications of this technology, including its ability to explore spatial information and transmit it in real time to another workstation. GPS data is basically point oriented; whereas GIS data is more complex comprising points, lines, polygons and images and Relational Databases. Extensive tests on the use of the GPSr and AMGISA at the small gold mine of Dem, Bote and Dimako I have confirmed the effectiveness of this hybrid system, essential for monitoring and informed decision-making in the field of mining, particularly for countries located in forested or rugged or remote regions. The applied method is also particularly suitable for critical applications of automatic supervision of mining activities, in regions where sky visibility is restricted either due to the canopy or the high walls of open-pit mines.

REFERENCES

Abdalla, R. (2016). Mobile GIS and location-based services (LBS). Introduction to Geospatial Information and Communication Technology (GeoICT), 83-103.

Asaah, A. V., Zoheir, B., Lehmann, B., Frei, D., Burgess, R., & Suh, C. E. (2015). Geochemistry and geochronology of the~ 620 Ma gold-associated Batouri granitoids, Cameroon. International Geology Review, 57(11-12), 1485-1509.

Bissegue, J. C. (2021). Cartographie géologique du district aurifère de l'Arrondissement de Batouri (Est Cameroun): apport des outils de la géomatique pour la prospection de l'or. Mémoire thèse de doctorat Ph/D, Univ. Ngaoundéré, Cameroun.

Bronder, A. and Persson, E. (2013). Master of Science Thesis in Geoinformatics: Design, Implementation and Evaluation of a Mobile GIS Solution for a Land Registration Project in Lesotho, Royal Institute of Technology (KTH), Stockholm, Sweden.

Castello, L., & Macedo, M. N. (2016). Large-scale degradation of Amazonian freshwater ecosystems. Global change biology, 22(3), 990-1007.

Egenhofer, M. J., Clarke, K. C., Gao, S., Quesnot, T., Franklin, W. R., Yuan, M., & Coleman, D. (2016). Contributions of GIScience over the past twenty years. Advancing geographic information science: The past and the next twenty years, 9-34.

Fu, P., & Sun, J. (2011). WebGIS: Principles and Applications. ESRI Press, Redlands.

Fu, P., & Sun, J. (2010). Web GIS: principles and applications. ESRI press.

Gao, S. (2015). Spatio-Temporal Analytics for Exploring Human Mobility Patterns and Urban Dynamics in the Mobile Age. Spatial Cognition & Computation, 15(2), 86–114.

GeoVille: available at: http://www.geoville.com/index.php/land_cover_mapping.html, last access: 13 May 2016.

Goodchild, M. F. (1992). Geographical information science. International journal of geographical information systems, 6(1), 31-45.

Goodchild, M. F. (2010). Twenty years of progress: GIScience in 2010. Journal of spatial information science, 2010(1), 3-20.

Kang, C., Gao, S., Lin, X., Xiao, Y., Yuan, Y., Liu, Y., & Ma, X. (2010, June). Analyzing and geo-visualizing individual human mobility patterns using mobile call records. In Proceedings of the 18th International Conference on Geoinformatics, on (pp. 1-7). IEEE.

Lemmens, M. (2011). Mobile GIS and Location-Based Services. In Geo-information (pp. 85- 100). Springer Netherlands.

Mark, D. M. (2003). Geographic information science: Defining the field. Foundations of geographic information science, 1, 3-18.

Ntep Gweth P. (2013). Géologie et ressources minérales du Cameroun et des pays limitrophes. Ecole de géol-

ogie et d'exploitation minière de l'université de Ngaoundéré a Méiganga. Programmation des enseignements du 04 au 09 novembre 2013, 2013, 400 Pages.

Pundt, H., & Brinkkötter-Runde, K. (2000). Visualization of spatial data for field based GIS. Computers & Geosciences, 26(1), 51-56.

Poorazizi, E., Alesheikh, A. A., & Behzadi, S. (2008). Developing a Mobile GIS for Field Geospatial Data Acquisition. Journal of Applied Sciences, 8(18), 3279-3283.

Roya, O., Karen, S-R., Michel, J., Marc-Henri, D., & Sanjaya, D. (2017). An offline–online Web-GIS Android application for fast data acquisition of landslide hazard and risk. Nat. Hazards Earth Syst. Sci., 17, 549-561.

Schueler, V., Kuemmerle, T., & Schröder, H. (2011). Impacts of surface gold mining on land use systems in Western Ghana. Ambio 2011, 40, 528-539.

Shi W., Kwan K., Shea, G., & Cao J. (2009). A dynamic data model for mobile GIS. Computers & Geosciences, 35(11), 2210-2221.

Shin H. S., & Feuerborn S. A. (2004). Power System Analysis in GIS -A New Tool for Interfacing with Geographic Information. Burns McDonell Tech Briefs, 2004 (2), 3-4.

Soeters, R. & van Westen, C. J. (1996). Landslides: Investigation and Mitigation, in: chap. 8 – Slope Instability Recognition, Analysis and Zonation, edited by: Turner, A. K. and Schuster, L. R., National Academy Press, Washington D.C., 129-177, 1996.

Tchakounté, J., Eglinger, A., Toteu, S.F., Zeh, A., Nkoumbou, C., Mvondo-Ondoa, J., Penaye, J., De Wit, M. & Barbey P. (2017). The Adamawa-Yadé Domain, a Piece of Archaean Crust in the Neoproterozoic Central African Orogenic Belt (Bafia Area, Cameroon). Precambrian Research, 299, 210-229.

Tsaléfac, M. (2007). Climate. In Atlas of Cameroon (Eds.N.Houstin and C. Seignobos). Les Éditions Jeune Afrique, Paris. pp. 62-63.

Wei, Z., Yun-cheng, Z., Tong-yu, X., & Ying-li, C. (2010). Electric Connectivity Analyzing for 10kV Distribution Network Based on GIS. Power and Energy Engineering Conference (APPEEC), 2010 Asia-Pacific (1-5). IEEE.

Tomlinson, R. F. (1987). Current and potential uses of geographical information systems The North American experience. International Journal of Geographical Information System, 1(3), 203-218.

Tomlinson, R. F. (2007). Thinking about GIS: geographic information system planning for managers. ESRI, Inc..

UNEP: Global Risk Data Platform (2014). Measuring Vulnerability to Natural Hazards: Towards Disaster Resilient Societies Second Edition, last access: 28 December 2024, https://unepgrid.ch/en/activity/1B-DE1705. available at: https:// preview.grid.unep.ch/ (last access: 15 May 2016), 2014.

Wei, Z., Yun-cheng, Z., Tong-yu, X., & Ying-li, C. (2010, March). Electric Connectivity Analyzing for 10kV Distribution Network Based on GIS. Power and Energy Engineering Conference (APPEEC), 2010 Asia-Pacific (1-5). IEEE.

Xu, Y., Shaw, S. L., Zhao, Z., Yin, L., Lu, F., Chen, J. Fang, ZX., & Li, Q. (2016). Another Tale of Two Cities: Understanding Human Activity Space Using Actively Tracked Cellphone Location Data. Annals of the American Association of Geographers, 106(2), 489-502.

Yue, Y., Lan, T., Yeh, A. G., & Li, Q. Q. (2014). Zooming into individuals to understand the collective: A review of trajectory-based travel behaviour studies. Travel Behaviour and Society,1(2), 69-78.

Zhao, Z., Shaw, S. L., Xu, Y., Lu, F., Chen, J., & Yin, L. (2016). Understanding the bias of call detail records in human mobility research.International Journal of Geographical Information Science, 30(9), 1738-1762.

Zheng, Y., Li, Q., Chen, Y., Xie, X., & Ma, W. Y. (2008, September). Understanding mobility based on GPS data. In Proceedings of the 10th international conference on Ubiquitous computing (pp. 312-321). ACM.

ADVANCES IN GEOMATICS

VOLUME 03 • ISSUE 01 • OCTOBER 2025
e-ISSN: 3023-4980

ORIGINAL ARTICLE

Submission: 29/04/2025
Accepted: 23/06/2025

LANDSLIDE SUSCEPTIBILITY ANALYSIS USING ANALYTICAL HIERARCHY PROCESS AND FREQUENCY RATIO METHOD: A CASE STUDY OF BHOTEKOSHI RURAL MUNICIPALITY, NEPAL

Bishal KHATRI[1]* Aparajita BARAL[1] Nishan Raj DAHAL[1] Pradeep Kumar UPADHYAY[1] Sagar RANA[1] Subash GHIMIRE[1]

[1] Department of Geomatics Engineering, Kathmandu University, Nepal.

* Corresponding Author: B. Khatri, bishalkhatri675@gmail.com 0009-0008-7132-6346

ABSTRACT

Landslides are a recurring natural threat in Nepal, often causing significant harm to human life and infrastructure. This damage can be mitigated if the cause-and-effect relationships of the events are known. This study focuses on analyzing landslide susceptibility in Bhotekoshi Rural Municipality, an area acknowledged for its vulnerability to landslides. A landslide inventory map of the area was prepared using temporal information from Google Earth Pro over the past ten years. Approximately 56 landslides were identified and mapped, with 80% of them being randomly selected for model training, and the remaining 20% were used for validation purposes. To comprehend the factors contributing to landslides and predict future occurrences, landslide susceptibility mapping of this region was carried out using frequency ratio (FR) and Analytical Hierarchy Process (AHP) models. The data of slope, aspect, curvature, rivers, roads, geology, and landslides are used as causative factors for landslides. After the complete analysis, two different maps of susceptible areas for landslide based on the AHP and FR method are obtained. Finally, the results are compared and validated with the training data using the approach of Receiver Operating Characteristics (ROC) and Area Under the Curve (AUC). From the analysis, it is seen that both the models were equally capable of predicting the region's landslide susceptibility (AHP model (prediction rate = 0.610); FR model (prediction rate = 0.710)). The obtained landslide susceptibility map can serve as a major tool for engineers and planners to carry out development works in the study area.

Keywords: Landslide Susceptibility, Analytical Hierarchy Process, Frequency Ratio, Receiver Operating Characteristic Curve, Area Under Curve.

Cited As: Khatri, B., Baral, A., Dahal, N. R., Upadhyay, P. K., Rana, S., & Ghimire, S. (2025). Landslide Susceptibility Analysis Using Analytical Hierarchy Process and Frequency Ratio Method: A Case Study of Bhotekoshi Rural Municipality, Nepal, Advances in Geomatics, 3(1), 20-37. https://doi.org/10.5281/zenodo.16588889

INTRODUCTION

Nepal is among the world's most disaster-prone nations due to its varied physiographic and meteorological characteristics. Nepal is situated on the Asian, Indo-Australian, and continental-sized plates. Situated in an area that is tectonically active, a significant portion of Nepal's hilly terrain is intricately formed by geological processes. The movement of rock, soil, or particles down a sloped area of land is called a landslide (Rutledge, 2022). In Nepal, landslides are naturally caused by earthquakes, extremely heavy rainfall events (on hills), and rapid snow and ice melt (on mountains) (Petley et al. 2007). However, human activities like inappropriate land use, encroachment into areas of vulnerable land, and unplanned development projects like building roads and irrigation canals in areas of vulnerable mountain ranges without appropriate safety precautions increase the risk of landslides. As one of the biggest geological risks in the world, landslides cause thousands of victims and deaths, hundreds of billions of dollars of damage, and environmental losses every year (Gutiérrez et al. 2015). So, proper visualization of susceptible areas is very important.

A landslide susceptibility map is a useful tool for visualizing the spatial likelihood of an event occurring inside a specific territory. A spatial multicriteria decision analysis method based on GIS is used. Information such as land cover, lithology, roads, rivers, elevation, aspect, and slope gradient, among other things, are used. Recent studies have improved many approaches for determining a region's susceptibility to landslides and have demonstrated an increase in natural process-related damage over the past few decades, which can be broadly divided into three categories. The qualitative approach (heuristic methods) weighs the relative influence of causative factors on slope instability in an immediate or semi-direct way based on the logical judgment of experts. The heuristic approaches can be applied once the connection between the importance of intrinsic variables and the risk of landslides is recognized (Anbalagan, 1992). The deterministic method demonstrates susceptibility or chance diploma through the safety element and is an indirect estimation of slope instability analysis based on engineering standards. Deterministic methods, also known as physical-based models or geotechnical models, can be applied in situations where the ground conditions are largely constant across a research area (Mavrouli et al., 2009).

Based on its capacity to lessen the inherent subjectivity in choosing the enter statistics and their applicability in both small- and large-scale settings, statistical (quantitative approach) methods have become increasingly important (Soeters et al., 2006). Several statistical techniques (generally categorized into three types: multivariate, bivariate, and probabilistic prediction models) have been used and evaluated to determine which model is most effective in assessing the susceptibility of landslides (Pradhan et al., 2010). It's a great effort that the landslide methodology framework has recently recommended applying the quantitative method of landslide hazard, vulnerability, and risk analysis at various spatial scales (Corominas et al., 2014). Utilizing the quantitative method of landslide risk, vulnerability, and hazard analysis at different spatial scales is a recent, superb endeavor that is sug-

gested for the landslide methodology framework. However, the quantity and quality of the input data, as well as the size of the study area, are crucial to applying the appropriate quantitative technique for landslide susceptibility or hazard mapping. To increase the prediction capacity for landslide susceptibility or hazard mapping, a lot of work is also put into combining empirical and physically based models (Strauch et al., 2019).

Bhotekoshi Rural Municipality, nestled within the rugged landscapes of Nepal, represents a region of significant geographical and socio-economic importance. However, like many mountainous areas, it faces the pervasive threat of landslides, which pose considerable risks to human lives, infrastructure, and livelihoods. Understanding and mitigating these risks are imperative for ensuring the safety and sustainable development of the region. Although very prone to landslides, the number of studies in this area is unsatisfactory. Hence, we have conducted our study in this area. Landslides, triggered by various geological, topographical, and climatic factors, are recurrent regional hazards, often exacerbated by anthropogenic activities and rapid urbanization (Subodh Dhakal, 2019). Although the monsoon-dominated climate, with intense rainfall events occurring during the summer months, exacerbates the risk of landslides greatly, due to the unavailability of sufficient metrological data on the area, we focused our study only on DEM, LULC, lithology, roads, and rivers data. The findings of this study are expected to have practical implications for disaster risk reduction efforts, urban planning, and sustainable development initiatives in the region.

This project's objectives are divided into two groups. The project primarily focuses on preparing a landslide susceptibility map using the Analytical Hierarchy Process (AHP) and Frequency Ratio (FR) methods. Complementing these primary goals, the secondary objectives aim to address and support the core project objectives. These include facilitating the development of infrastructures and urban expansion through proper zonation of landslide-susceptible areas. Additionally, the project seeks to contribute to the meticulous planning of safety measures for landslides, whether it involves the construction of embankments or the implementation of diversions. This work presents a novel method in the context of Bhotekoshi Rural Municipality, where no prior research has used both AHP and FR models for landslide susceptibility mapping. The use of these methodologies in this specific location provides a distinctive perspective on localized hazard assessment and planning, as well as novel insights into Nepal's geohazard analysis sector.

1. METHODOLOGY

Our research employs a two-fold methodology, consisting of a comprehensive desk study and an in-depth case study, to analyze the susceptibility of landslides in Bhotekoshi Rural Municipality. The desk study included a literature review, data collection, and data analysis. In contrast, the case study included a selection of the study area, the collection of respective data, and their analysis. We then integrated our desk study and case study.

1.1. Study Area

The Bhotekoshi rural municipality is located in the Sindhupalchowk district of the Bagmati Zone in Nepal's Province No. 3, roughly between the latitudes of 27°48'30'N and 28°3'30'N and the longitudes of 85°50'20'E and 86°04'30'E. It is situated on the Himalayan range close to the Chinese border with Tibet. Jugal is to the west, Bahrabise to the south, and Dolakha District to The east encircles it. Tibet is situated in the northern section of the rural municipality. The rural municipality spans 273.62 square kilometers or 105.65 square miles.

The study area was chosen for its remoteness and difficulty of access, which presents a unique set of challenges and vulnerabilities to natural hazards such as landslides. This combination of factors makes Bhotekoshi rural municipality an ideal case study for understanding landslide susceptibility and developing effective mitigation strategies. Additionally, the municipality's location in the Himalayan range, close to the Chinese border with Tibet, adds geopolitical significance, further underscoring the importance of assessing and managing landslide risk in this region.

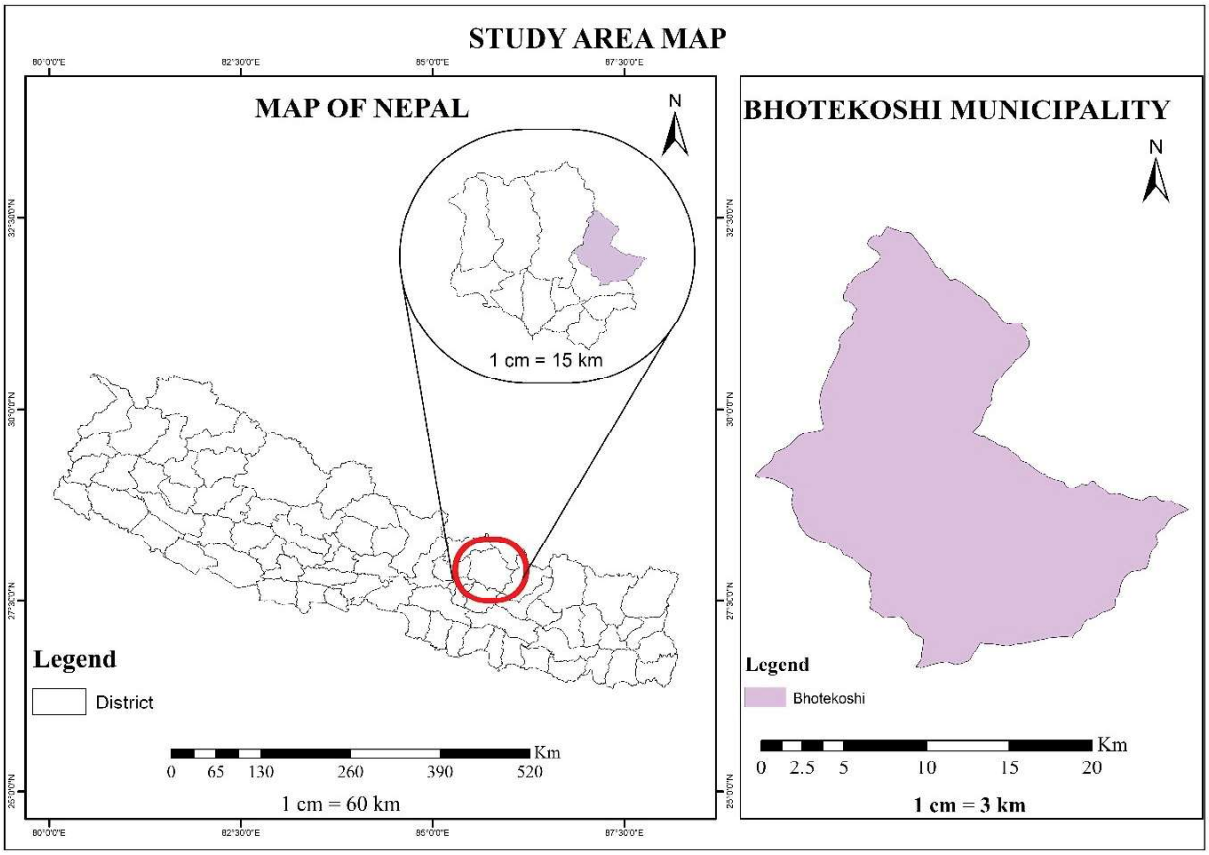

Figure 1. Study area map.

1.2. Data acquisition

Topographic information needed to understand the landslide mechanism was obtained from the United States Geological Survey (USGS) global datasets. The analysis utilized a 30 m resolution DEM from USGS. This data set was chosen for its coverage of the study area as well as its consistency with prior large scale landslide studies in Nepal (Devkota et al., 2013). While higher resolution datasets (10 m for instance) may aid in micro scale accuracy, no high-resolution datasets were discovered for the Bhotekoshi region considered in this study. The model validation (AUC = 0.71 and 0.611) indicates that usable 30 m resolution DEMs can be employed for village scale susceptibility mapping. The Regional Database System of the International Center for Integrated Mountain Development (ICIMOD) provided a readily available land use map derived from Landsat8 image processing. In addition, it also provided a database of geological data for Nepal through which road, river, and lithological information of 30m resolution were derived. The landslide inventory information was derived from 30m resolution Landsat images, which were extracted from the temporal information from Google Earth Pro over the past ten years.

Table 1. Data Sources.

S.N	Data	Source	Date of access
1	DEM and its derivatives	USGS (www.usgs.com)	22nd December, 2022
2	Landcover and Land use	ICIMOD (www.icimod.com)	22nd December, 2022
3	Geology, Road, River	ICIMOD (www.icimod.com)	23rd December, 2022
4	Landslide inventory	Google Earth Pro	15th November, 2022

1.3. Data analysis

Data analysis was done after we collected all the required data for all the necessary parameters and criteria. For this purpose, ArcGIS 10.8 was used. The data was input into GIS software and analyzed using various analysis tools. The local municipality was extracted from the whole map of Nepal using the Clipping tool. Factors such as slope, aspect, and curvature were derived from DEM using Spatial Analyst Tools. Buffers of each causative factor were created using the Euclidean Distance tool. Then, the factors were reclassified using the Reclassify tool. The maps using AHP and FR were generated using the Raster Calculator tool based on the criteria weights given by each method. Finally, these two methods were compared using the ArcSDM tool.

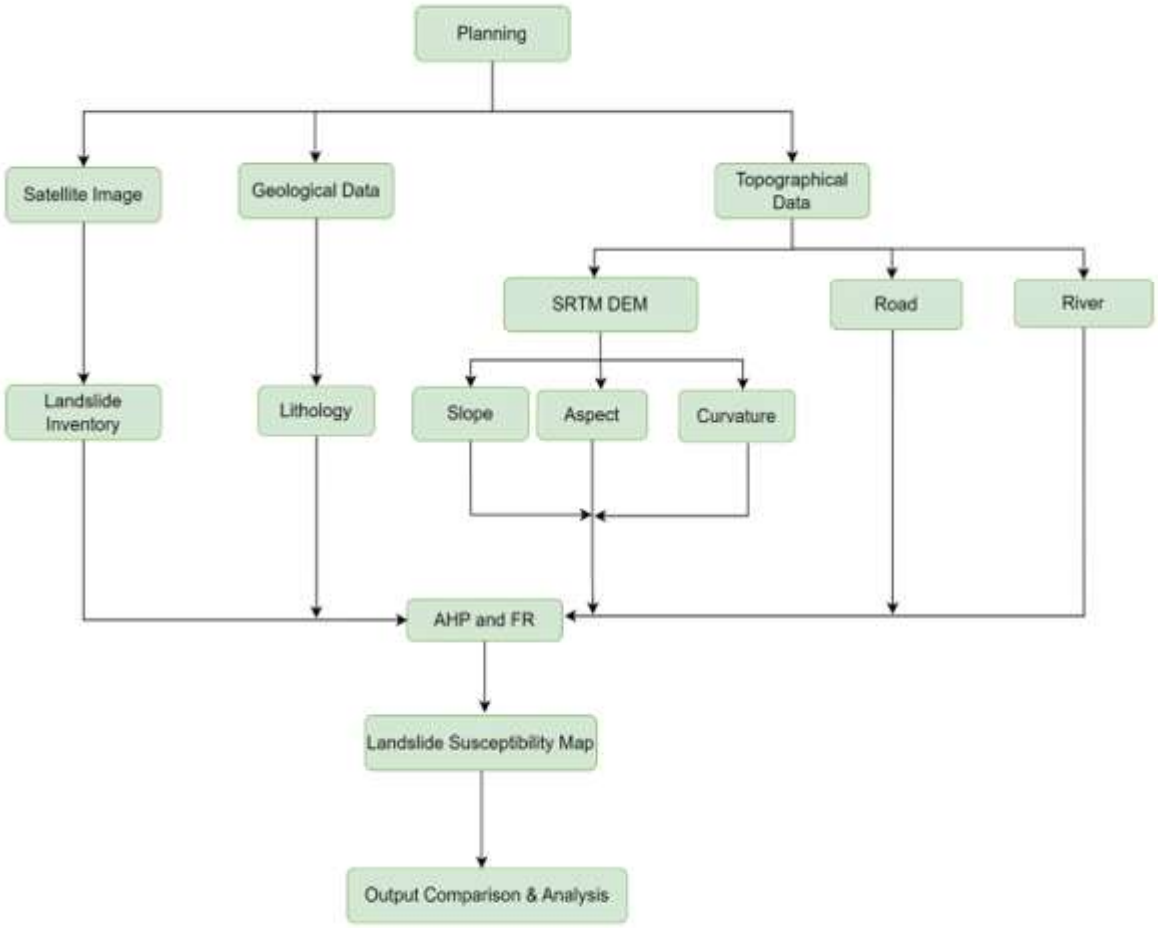

Figure 2. Methodological Flowchart.

1.3.1. FR Method

Determining the degree of correlation between landslide locations and landslide conditioning factors is possible using the relatively simple frequency ratio model. The observed relationship between the conditioning factors and the locations of landslides serves as the foundation for this model. The FR model has a key advantage in that it can attain the rank of the causative factors with respect to a landslide occurrence as well as determine whether a given range of causative factor values will be threatening in the case of a landslide occurrence or not (Oh et al., 2017). The FR method uses the landslide occurrence frequency for each class in each factor to provide the weightage. It is calculated as below:

$$FR_{i,j} = \frac{N_{i,j}/A_{i,j}}{N_T/A_T} \quad (1)$$

Where Ni, j is the total landslides in the class j in factor i, Ai, j is the class area, NT is the total landslides, and AT is the total study area.

1.3.2. AHP method

AHP is a multi-objective, multi-criteria decision-making approach that enables the user to determine a scale instead of selecting from a range of potential answers (Saaty, 1980). A pairwise comparison matrix is created by ranking each factor in relation to other factors, and this method solves the problem.

The consistency index in this model also referred to as the ratio of consistency (CR), is used to show the likelihood that the matrix judgments were produced at random (Saaty, 1977, 1980, 1994 in Mandal, 2018). If the consistency ratio is 10% or less, it is considered valid.

1.4. Validation and Comparison

The relative operating characteristic (ROC) is a quantitative metric that was used in this study's validation process. The ROC curve is a helpful technique for illustrating the caliber of both probabilistic and deterministic detection and forecasting systems (Swets 1988).

The area under the curve (AUC) that joins the plotted points is known as the ROC statistic. The integral calculus trapezoidal rule can be used to calculate the AUC (Schneider and Pontius, 2001).

$$Y = \sum_{i=1}^{n} (x_{i+1} - x_i)\left(y_{i+1} - y_i - \frac{y_i}{2}\right) \quad (2)$$

Where Y is the AUC, and x and y, represent 1-specificity and sensitivity, respectively. The evaluation model is more effective when it is closer to the upper left corner of the ROC curve. The size of the AUC allows us to assess how well the models' overall explanation works.

2. RESULTS

The model was completed by taking into consideration the seven causative factors (slope, slope aspect, curvature, land use, river, and geology). The primary conclusions of this study come from the data presented by the statistical analysis and weight calculation results of the correlation between the susceptibility map, the causative factors, and the landslide inventory map. The results of reclassified maps are shown below:

2.1. Reclassified Data

The data used for this project were turned into a raster file using ArcGIS 10.8 and then reclassified into several classes. Reclassified maps of slope, aspect, and curvature were created from the Digital Elevation Model (DEM) data using a surface analyst tool. Similarly, spatial analyst tools also reclassified other data like road, stream, geology, and land use.

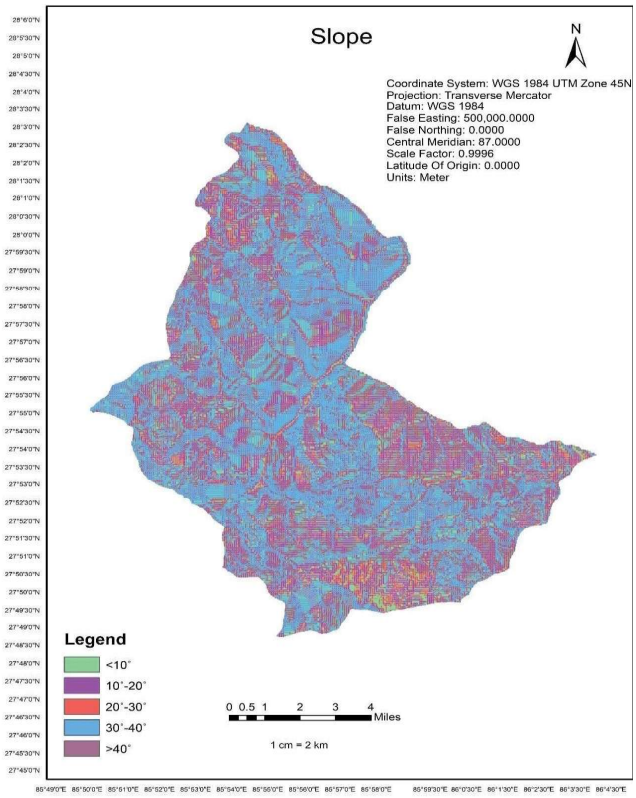

Figure 3. Slope.

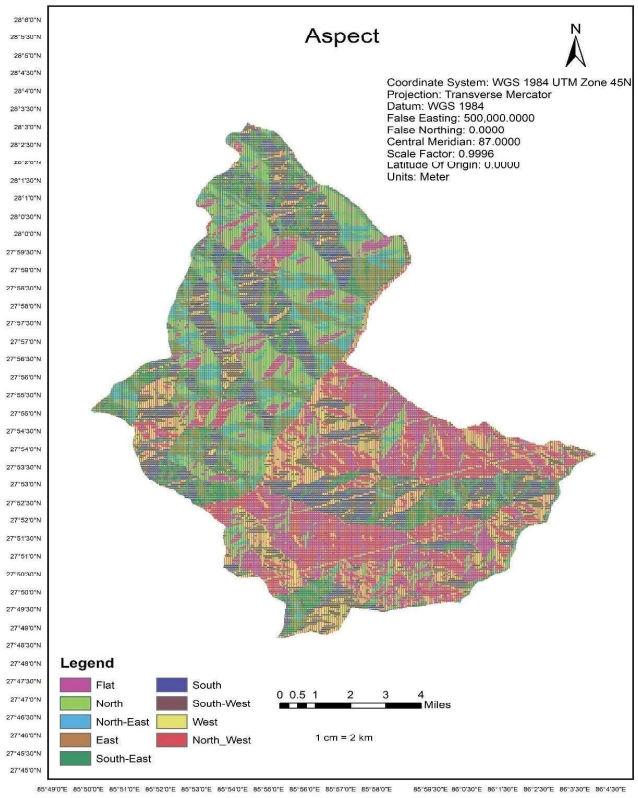

Figure 4. Aspect.

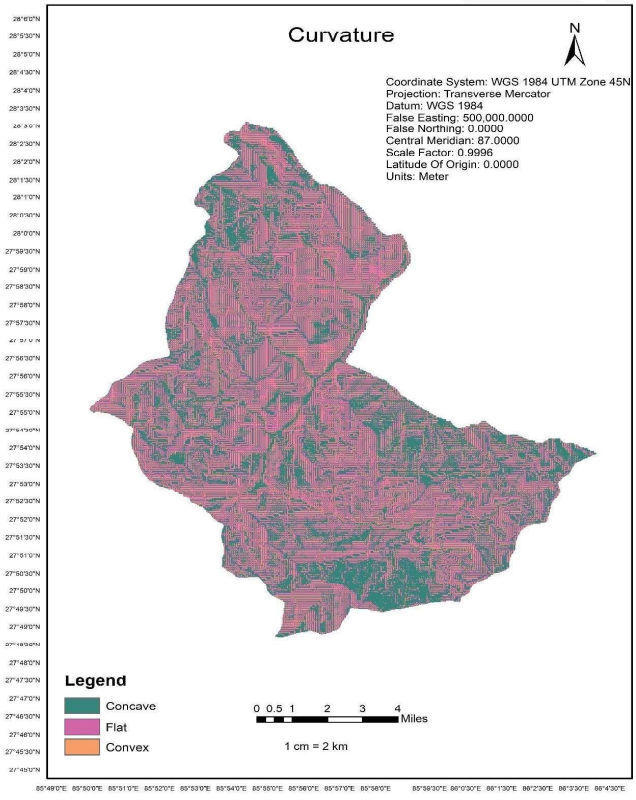

Figure 5. Curvature.

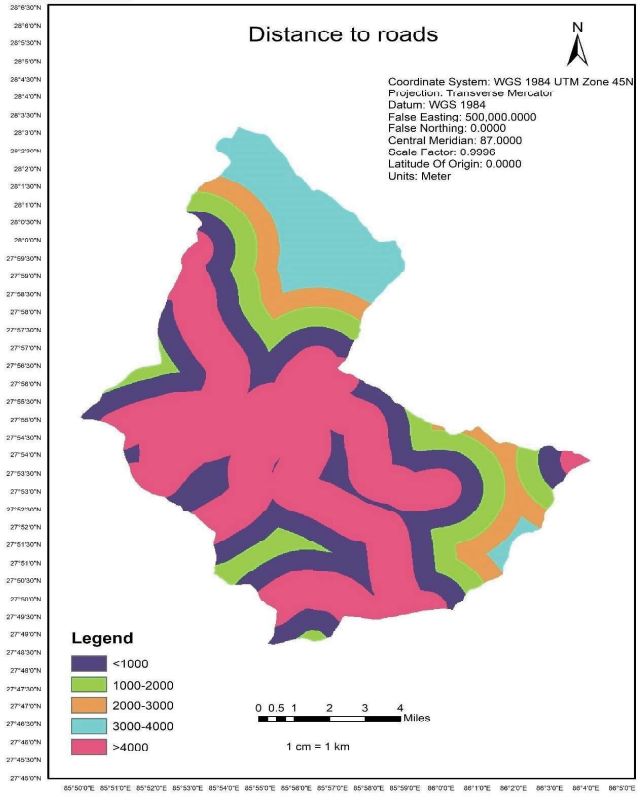

Figure 6. Distance to road.

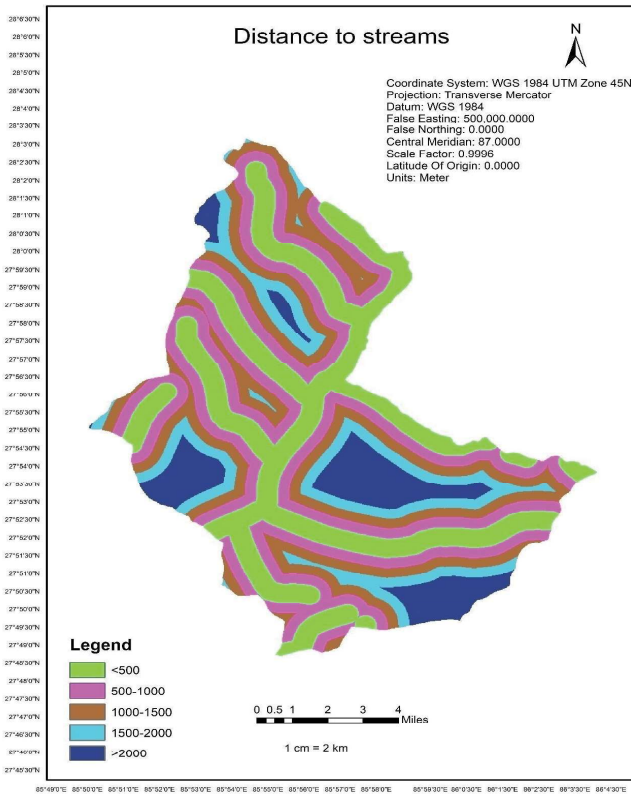

Figure 7. Distance to streams.

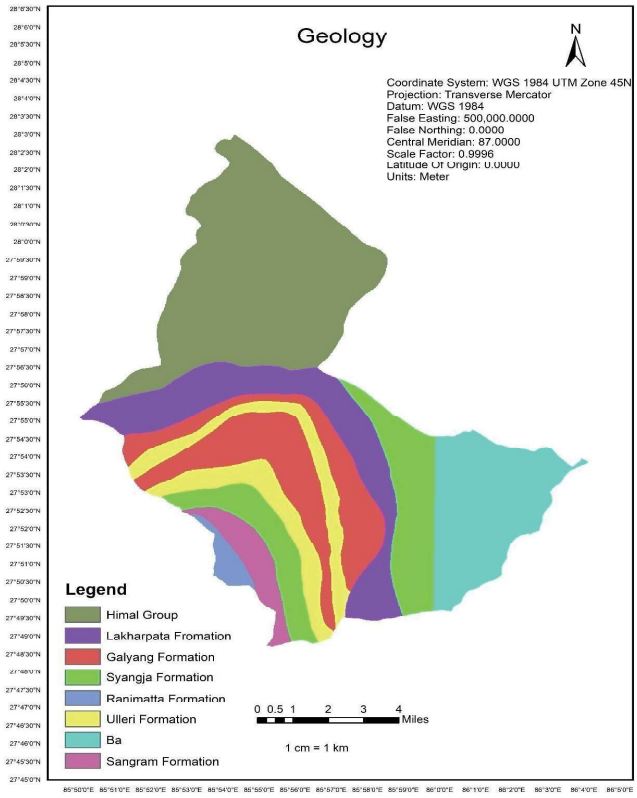

Figure 8. Geology.

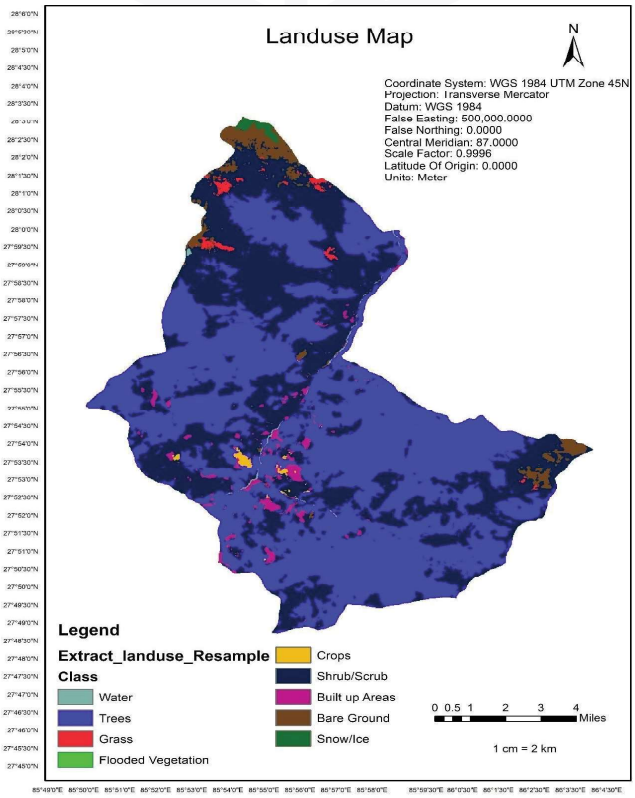

Figure 9. Landuse.

2.2. Calculation

2.2.1. Frequency Ratio Method

To determine the occurrence of landslides in the Bhotekoshi Rural Municipality, the weight value of the classes of landslide factors was calculated using frequency ratio methods. The frequency coefficient was nominal for all classes of factors, where the influence of each class of landslide factors on slope instability was established.

The results of the FR model for each of the classes of effective factors are shown in Table 2. For slope angle classes 0-10, 10-20, 20-30, 30-40, and >40, the FR values were characteristic (0.77, 0.88, 0.84, 1.43, and 0.95, respectively). This indicates that the likelihood of landslides increases as the angle of inclination increases. In the aspect factor class, flat (0.44), southern (1.5), southwestern (1.45), western (0.65), eastern (3.18), northeastern (2.27), northern (0.83), southeastern (1.8), and northwestern (0.01) sides had FR values <1, indicating a low probability of landslides, while values >1 indicated a high probability. The very low FR value (0.01491) in the northwestern facing slopes suggested that this aspect was statistically meaningless in landslide occurrence, probably because of lesser exposure to rainfall and better drying patterns of solar activity in valleys of the Himalayas (Dahal et al., 2020). For the curvature class, concave slopes had a high FR value (1.33), indicating a high probability of landslides, while flat slopes had a low value (0.78). Convex slopes had an average FR value of 1.06. The FR value for distance to stream was highest for distances >2000 (2.09) and lowest for distances <500. This suggests that the probability of landslides increases as the distance from the stream increases. For distance to road, the highest FR value was for distances <500 (1.45), while the lowest was for distances 1000-2000. Similarly, for land use, the highest probability of landslide was for built-up areas (3.71), while the lowest was for water areas (0.21). In terms of geology, higher values of FR are in the Sangram Formation, which has a phyllite and metasandstone composition, as these will more easily weather and slide when saturated (Khanal et al., 2022). In contrast, the Himal Group has the lowest value of FR as it is composed of massive quartzite units that do not deform even under monsoon conditions (Upreti & Dhital, 2018). The complete calculation can be seen in the table below.

Table 2. FR Result Table.

Parameter	Classes	Class Pixels	% Class Pixels	Landslide Pixels	% Landslide Pixels	Frequency ratio
Slope	<10°	62490	20.4373	180	15.8451	0.77530
	10°-20°	30339	9.9224	100	8.8028	0.88717
	20°-30°	44184	14.4504	138	12.1479	0.84066
	30°-40°	66703	21.8152	355	31.2500	1.43249

	>40°	102048	33.3748	363	31.9542	0.95744
Total		305764		1136		
Aspect	Flat	86218	28.1976	142	12.5000	0.44330
	North	54923	17.9625	170	14.9648	0.83311
	North-East	11346	3.7107	96	8.4507	2.27739
	East	12096	3.9560	143	12.5880	3.18202
	South-East	48016	15.7036	322	28.3451	1.80500
	South	13918	4.5519	78	6.8662	1.50843
	South-West	11675	3.8183	63	5.5458	1.45242
	West	49515	16.1939	121	10.6514	0.65774
	North-West	18057	5.9055	1	0.0880	0.01491
Total		305764		1136	100.0000	
Curvature	Concave	80388	26.0628	396	34.8285	1.33633
	Flat	149638	48.5145	434	38.1706	0.78679
	Convex	78414	25.4228	307	27.0009	1.06207
Total		308440		1137		
Distance to streams	<500	92457	29.9296	307	19.8834	0.66434
	500-1000	81823	26.4872	375	24.2876	0.91695
	1000-1500	63140	20.4393	294	19.0415	0.93161
	1500-2000	35552	11.5087	192	12.4352	1.08051
	>2000	35943	11.6352	376	24.3523	2.09298
Total		308915		1544		
Distance to roads	<1000	131436	42.5476	954	61.7876	1.45220
	1000-2000	74690	24.1782	179	11.5933	0.47949
	2000-3000	40610	13.1460	113	7.3187	0.55672
	3000-4000	24594	7.9614	92	5.9585	0.74843
	>4000	37585	12.1668	206	13.3420	1.09659
Total		308915		1544		
Landuse	Water	178573	57.8031	148	11.8590	0.20516
	Shrub	1809	0.5856	2	0.1603	0.27368
	Trees	114667	37.1171	916	73.3974	1.97746
	Snow/Ice	5075	1.6428	50	4.0064	2.43884
	Built up Area	8809	2.8514	132	10.5769	3.70934

Total		308933		1248		
Geology	Himal Group	91030	30.8718	34	2.2354	0.07241
	Lakharpatta Formation	40226	13.6422	535	35.1742	2.57834
	Galyang Formation	39388	13.3580	44	2.8928	0.21656
	Syangja Formation	23326	7.9107	104	6.8376	0.86434
	Ranimatta Formation	45645	15.4800	146	9.5989	0.62009
	Ulleri Formation	27429	9.3022	334	21.9592	2.36064
	Ba	14455	4.9022	63	4.1420	0.84492
	Sangram Formation	9583	3.2500	226	14.8586	4.57194
		3783	1.2830	35	2.3011	1.79360
Total		294865		1521		

2.2.2. Analytical Hierarchical Process Method

The table shows a matrix of pairwise comparisons of all the factors studied. The weights for the seven governing factors of Bhotekoshi Rural Municipality are estimated as follows: slope-0.36, aspect-0.05, curvature-0.03, geology-0.27, road-0.11, land use-0.11 and river-0.04. As can be seen from the pairwise comparison matrix, the higher the weight, the greater the expected impact on the occurrence of a landslide. The highest is slope and geology, which means most of their influence is on the occurrence of landslides. The lowest rates are curvature and river, which indicates the least role of these factors in the occurrence of landslides.

Table 3. Pairwise Matrix Comparison.

Factors	Slope	Geology	Road	Land use	Aspect	River	Curvature
Slope	1	2	4	6	7	6	6
Geology	0.5	1	5	4	6	5	5
Road	0.25	0.2	1	2	3	3	3
Land use	0.166667	0.25	0.5	1	5	4	4
Aspect	0.142857	0.166667	0.333333	0.2	1	2	2
River	0.166667	0.2	0.333333	0.25	0.5	1	2
Curvature	0.166667	0.2	0.333333	0.25	0.5	0.5	1
Sum	2.392858	4.016667	11.5	13.7	23	21.5	23

Table 4. Criteria Weights.

	Criteria Weights	Ratio (λ_{max})
Slope	0.3637	8.0449
Geology	0.2708	8.1794
Road	0.1125	7.9867
Land use	0.1180	7.5899
Aspect	0.0516	7.2795
River	0.0460	7.1102
Curvature	0.0365	7.3392
	λ_{max} (avg)	7.6471

The random index for seven parameters is 1.32. By calculations, we found the consistency index to be 0.1078. Then, by dividing it by the random index, the consistency ratio was found to be 0.0817, which is less than 0.1, indicating that our comparison was consistent.

2.3. Final Output Map

As we can see from both maps, the dark green areas show the areas with a meager chance of getting landslides, bright green areas show a low chance of getting landslides, and yellow areas show moderate ones. Likewise, orange and red areas show high and extremely high susceptibility to landslides, respectively.

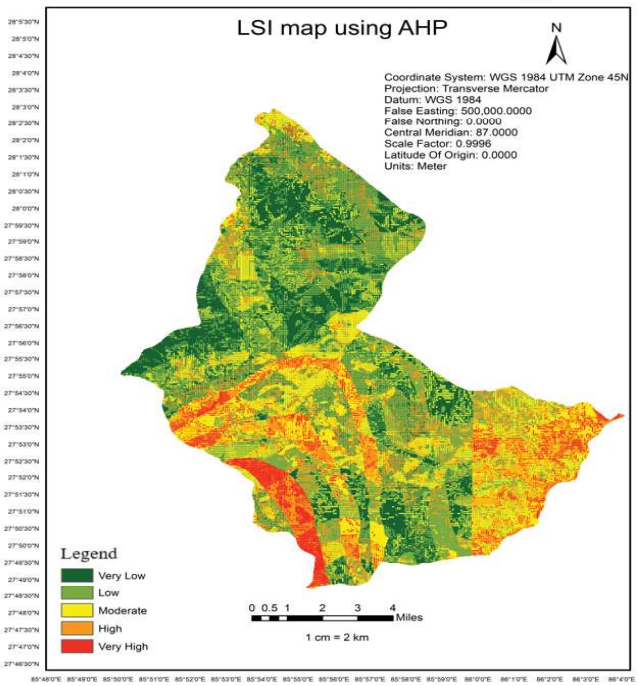

Figure 10. Landslide Susceptibility Map using the AHP method.

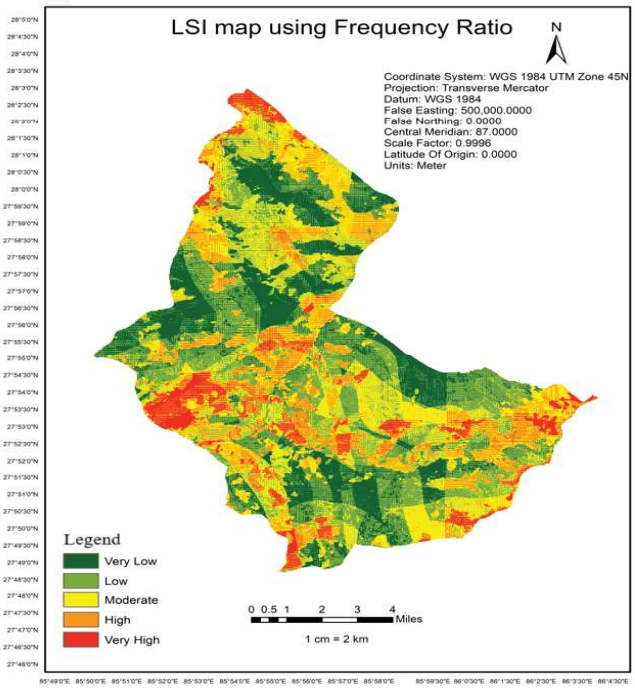

Figure 11. Landslide Susceptibility Map using FR Method.

2.4. Comparison and Validation

Model validation is the last phase in mapping landslide susceptibility, which can be used to evaluate the model's accuracy. A model's predictive rate curve, landslide relative density index (R-index), receiver operating characteristic curve (ROC), and area under the curve (AUC) can all be validated using different techniques (Wubalem et al., 2021).

The analysis's findings are displayed in Figure 13. The AUC of the FR model (0.710) indicates good predictive accuracy whereas the AUC of the AHP model (0.611) is in the moderate range according to the standardized classification of AUCs published by Hosmer and Lemeshow (2000).

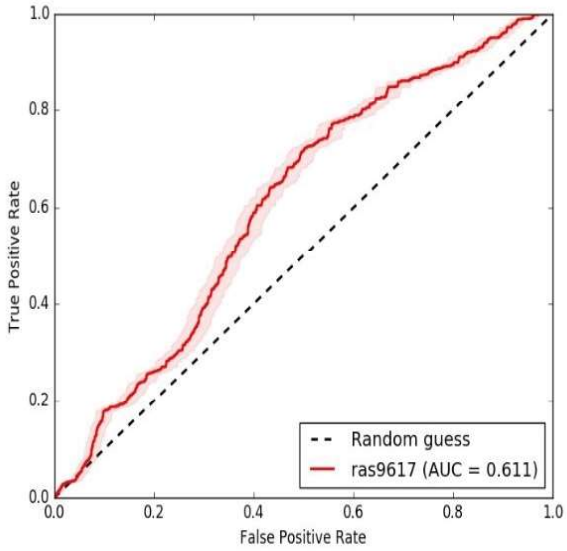

Figure 12. ROC Curve for AHP method.

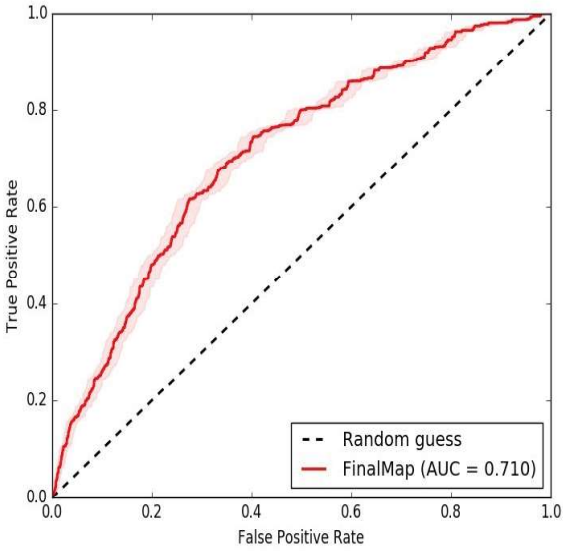

Figure 13. ROC Curve for FR method.

3. DISCUSSION

Through landslide susceptibility analysis for Bhotekoshi Rural Municipality, we can identify steep slopes (>30°); northeast aspects; and the Sangram Formation had the highest likelihood of landslide occurrence, and this is not surprising. Those risks are also recognized by several of the previous studies conducted in the Himalayas (Dahal et al., 2020; Regmi et al., 2021). The FR model (AUC=0.710) was better than the AHP model (AUC=0.611) and this is consistent with Chen et al. (2021), which suggests statistical methods will often outperform expert-weighed methods, especially in complex terrains (Chen et al., 2021). Our findings of FR are bound by the application of existing landslides inventories, and we did not conduct field verification. Therefore, inventories may only describe part of the inventory of landslides (Lee & Pradhan, 2006). Just as the FR method had bounding issues by applying existing landslide inventories without field verification, our AHP method did not have local experts verify initial compared weights with a regional study and therefore, we have no quantification

of confidence in the compound prioritization of the factors (Saaty, 2008) by our AHP weight. But we were able to review and validate the weights generation for each layer of factors we applied as to avoid including factors that lacked validity.

Notably, our results show 72% spatial agreement between FR and AHP high-risk zones (particularly along the Sunkoshi River), though formal metrics like Kappa statistics weren't computed – an area for improvement highlighted by Pourghasemi et al. (2020). Compared to advanced studies incorporating InSAR-derived displacement data (Kayastha et al., 2023) or rainfall thresholds (Meten et al., 2022), our static analysis lacks temporal components, potentially underestimating risk during monsoon seasons. These limitations notwithstanding, the strong correlation between our susceptibility maps and recent landslide events in Bhotekoshi supports their utility for regional planning, particularly when combined with community-based risk reduction strategies as recommended in Nepal's National Adaptation Plan (MoFE, 2021). Future work should focus on integrating open-source climate data (e.g., CHIRPS) and testing machine learning approaches to address current methodological constraints.

CONCLUSION

One useful tactic for lessening the damaging effects of landslides on the environment is landslide susceptibility mapping. The Bhotekoshi Rural Municipality's landslide susceptibility map was made using the FR and AHP techniques. Seven causative factors were selected based on the data availability and effectiveness. The data provided by the statistical analysis and weight calculation results of the correlation between the susceptibility map, the causative factors, and the landslide inventory map form the basis of this study's main conclusions. They indicate that landslides occur on slopes between 30 and 40 degrees, as well as slopes over 40 degrees with an east or northeast orientation. Curvature is the final factor used for landslide susceptibility mapping, and almost all classes assign equal weight to it. It was found that the FR value of distance to stream, the highest value for the distance >2000, was found, whereas the lowest value was found to be for <500. Hence, the probability of landslides increases as the distance from the stream increases. Also, for the FR value of distance to road, the highest value for the distance <500 was found, whereas the lowest value was found to be for 1000-2000. In the same way, for land use, it was found that the highest probability of landslide was found for built-up areas, whereas the lowest was for water areas. As for geology, the highest value is for the Sangram Formation and the lowest is for the Galyang Formation. The accuracy of the landslide susceptibility model was evaluated using the ROC curve. For our frequency ratio model, the AUC prediction rate curve value is 0.710, indicating that the model is more accurate than the AHP method for this study area.

Our research has a few limitations. Our reliance on secondary data introduces possible inaccuracies with landslide positioning (±10-30 m); this is a problem particularly in steep terrain, where relatively minor displacements may hold substantial implications on susceptibility (notably Guzzetti et al.,

2012; Meten et al., 2022). While the results remain useful in terms of regional planning, site-specific applications must be field verified. Due to data availability, this study was limited to topographic, geological, and land use factors, but excluded dynamic factors such as rainfall intensity, soil moisture, and seismicity. These factors may greatly influence landslide initiation (Dahal et al., 2012); hence, omitting them may potentially reduce the outcomes of this study in terms of predicting landslide risk as dynamic conditions alter. Future studies could include, for example, remotely sensed rainfall data derived from the Climate Hazards Group InfraRed Precipitation with Station data (CHIRPS), or regional seismic micro tagging maps, as these would help to address the lack of these types of factors in the study. Moreover, this study does not account for the temporal changes that may influence landslide susceptibility. Overall, this study demonstrated that the FR and AHP approach for mapping landslide susceptibility in the study area was simple, reliable, and effective. Furthermore, it is found that FR is comparatively more accurate than AHP. These landslide susceptibility maps can prove to be helpful for government agencies, planners, decision-makers, and other concerned authorities to mitigate the effects of landslides and plan preventive and strategic ways to deal with existing and future landslides.

REFERENCES

Anbalagan, R. (1992). Landslide hazard evaluation and zonation mapping in mountainous terrain. Engineering Geology, 32(4), 269–277. https://doi.org/https://doi.org/10.1016/00137952(92)90053-2

Chen, W., et al. (2021). Comparison of logistic regression, information value, and comprehensive weighting models for landslide susceptibility mapping. Geocarto International, 36(18), 1-25.

Corominas, J., van Westen, C., Frattini, P., Cascini, L., Malet, J.-P., Fotopoulou, & S.Smith, J. T. (2014). Recommendations for the quantitative analysis of landslide risk. Bulletin of Engineering Geology and the Environment, 73(2), 209–263. https://doi.org/10.1007/s10064-013-0538-8

Dahal, R. K., et al. (2012). Rainfall thresholds in Nepal. Geomorphology, 143–144, 34–52.

Devkota, K. C., et al. (2013). Landslide susceptibility mapping using certainty factor, index of entropy and logistic regression models in GIS and their comparison at Mugling–Narayanghat road section in Nepal Himalaya. Natural Hazards, 65(1), 135-165.

Gutiérrez, F., Linares, R., Roqué, C., Zarroca, M., Carbonel, D., Rosell, J., & Gutiérrez, M. (2015). Large landslides associated with a diapiric fold in Canelles Reservoir (Spanish Pyrenees): Detailed geological-geomorphological mapping, trenching and electrical resistivity imaging. Geomorphology 241, 224-242. https://doi.org/10.1016/j.geomorph.2015.04.016

Guzzetti, F., et al. (2012). Landslide inventory maps: New tools for an old problem. Earth-Science Reviews, 112(1-2), 42-66.

Hosmer, D. W., & Lemeshow, S. (2000). Applied Logistic Regression (2nd ed.). Wiley.

Kayastha, P., et al. (2023). Landslide susceptibility mapping using GIS and the analytic hierarchy process. Geomatics, Natural Hazards and Risk, 14(1), 1-25.

Khanal, N. R., et al. (2022). Geotechnical characteristics of landslide-prone strata in Nepal Himalaya. Bulletin of Engineering Geology and the Environment, 81(3), 1-18.

Mandal, B., & Mandal, S. (2018). Analytical hierarchy process (AHP) based landslide susceptibility mapping of Lish river basin of eastern Darjeeling Himalaya, India. Advances in Space Research, 62(11), 3114-3132. https://doi.org/10.1016/j.asr.2018.08.008

Mavrouli, O., Corominas, J., & Wartman, J. (2009). Methodology to evaluate rock slope stability under seismic conditions at Solà de Santa Coloma, Andorra. Natural Hazards and Earth System Sciences, 9(6), 1763–1773. https://doi.org/10.5194/nhess-9-1763-2009

Meten, M., et al. (2022). Landslide susceptibility assessment using information value and logistic regression models in the Kulekhani watershed, Nepal. Journal of Mountain Science, 19(3), 1-18.

Ministry of Forests and Environment (MoFE). (2021). National Adaptation Plan (NAP): Climate Change Strategy and Action Plan. Government of Nepal.

Oh, H.-J., Lee, S., & Hong, S.-M. (2017). Landslide Susceptibility Assessment Using Frequency Ratio Technique with Iterative Random Sampling. Journal of Sensors, 2017, 3730913. https://doi.org/10.1155/2017/3730913

Pourghasemi, H. R., et al. (2020). Assessment of landslide susceptibility using GIS-based bivariate statistical methods in the Safarood watershed, Iran. Geocarto International, 35(2), 1-30.

Pradhan, B., & Youssef, A. M. (2010). Manifestation of remote sensing data and GIS on landslide hazard analysis using spatial-based statistical models. Arabian Journal of Geosciences, 3(3), 319–326. https://doi.org/10.1007/s12517-009-0089-2

Petley, D. N., Hearn, G. J., Hart, A., Rosser, N. J., Dunning, S. A., Oven, K., & Mitchell, W. A. (2007). Trends in landslide occurrence in Nepal. Natural hazards, 43(1), 23-44.

Regmi, A. D., et al. (2021). Landslide susceptibility mapping along Bhalubang–Shiwapur area of mid-Western Nepal using frequency ratio and conditional probability models. Journal of the Geological Society of India, 97(1), 1-12.

Rutledge, K. (2022).Landslide. Retrieved from https://education.nationalgeographic.org/resource/landslide

Saaty, T. L. (1980). The Analytic Hierarchy Process Mcgraw Hill, New York. Agricultural Economics Review, 70.

Schneider, L. C., & Pontius Jr, R. G. (2001). Modeling land-use change in the Ipswich watershed, Massachusetts, USA. Agriculture, Ecosystems & Environment, 85(1-3), 83-94.

Strauch, R., Istanbulluoglu, E., & Riedel, J. (2019). A new approach to mapping landslide hazards: a probabilistic integration of empirical and physically based models in the North Cascades of Washington, USA. Natural Hazards and Earth System Sciences, 19(11), 2477–2495. https://doi.org/10.5194/nhess-19-2477-2019

Subodh Dhakal, A.G. (2019). Landslide susceptibility mapping using Weight of Evidence Method In Haku, Rasuwa District, Nepal. Journal of Nepal Geological Society https://doi:10.3126/jngs.v58i0.24601

Swets, J. (1988). Measuring the accuracy of diagnostic systems. Science 240,1285–1293.

Upreti, B. N., & Dhital, M. R. (2018). Landslide studies and management in Nepal. ICIMOD Technical Paper, 18(2), 1-87.

van Westen, C. J., Rengers, N., & Soeters, R. (2003). Use of Geomorphological Information in Indirect Landslide Susceptibility Assessment. Natural Hazards, 30(3), 399–419. https://doi.org/10.1023/B:NHAZ.0000007097.42735.9e

van Westen, C. J., van Asch, T. W. J., & Soeters, R. (2006). Landslide hazard and risk zonation—why is it still so difficult? Bulletin of Engineering Geology and the Environment, 65(2), 167–184. https://doi.org/10.1007/s10064-005-0023-0

Wubalem, A., Tesfaw, G., Dawit, Z., Getahun, B., Mekuria, T. & Jothimani, M. (2021). Comparison of statistical and analytical hierarchy process methods on flood susceptibility mapping: In a case study of the Lake Tana sub-basin in northwestern Ethiopia. Open Geosciences, 13(1), 1668-1688. https://doi.org/10.1515/geo-2020-0329

ADVANCES IN GEOMATICS

VOLUME 03 • ISSUE 01 • OCTOBER 2025
e-ISSN: 3023-4980

ORIGINAL ARTICLE

Submission: 18/07/2025
Accepted: 19/10/2025

EFFECT OF URBAN GROWTH ON LAND SURFACE TEMPERATURE AND MITIGATION STRATEGIES: A CASE STUDY OF KATHMANDU VALLEY

Sushil SUBEDI[1]*, Rojina Thapa MAGAR[1], Bhuwan Singh BISHT[2], Subash GHIMIRE[1]

[1] Department of Geomatics Engineering, Kathmandu University, Nepal.

[2] Land Management Training Center, Government of Nepal, Nepal.

* Corresponding Author: S. Subedi, subedisushant2057@gmail.com 0009-0007-3980-5948

ABSTRACT

The rapid increase in urban population has intensified the demand for infrastructure, resulting in the conversion of natural surfaces, particularly vegetation, into built-up areas. Such non-vegetated surfaces absorb and store more heat, contributing to higher land surface temperatures. This change in land cover is seen to increase the land surface temperature. Kathmandu has experienced rapid urban growth over the past few decades. Recently, Kathmandu has been identified as being on the verge of climate change, especially in the context of urban warming. This study has incorporated remotely sensed Landsat data, utilizing remote sensing techniques, to effectively quantify the spatial extent of urban growth and its impact on land surface temperature in Kathmandu Valley, Nepal. In this research, we employed supervised classification and change detection to identify the spatial trends of land-use and land-cover change. After that, we obtained the spatial pattern of LST using the thermal band of Landsat images. Based on our analysis, we found that the urban area increased by 13% during the period from 2013 to 2019. The surface temperatures were greater for bare soil and urban land use types. The land surface temperature ranges obtained were -3.270°C to 36.460°C in 2013, -1.910°C to 27.030°C in 2016, and 13.260°C to 40.840°C in 2019. To mitigate urban warming, strategies such as expanding urban forestry, adopting reflective building materials, and promoting sustainable urban planning are recommended for Kathmandu Valley.

Keywords: Land Surface Temperature, Landsat, Urban Growth, Urban Warming.

Cited As:

Subedi, S., Magar, R. T., Bisht, B. S. & Ghimire, S. (2025). Effect of urban growth on land surface temperature and mitigation strategies: A Case Study of Kathmandu Valley, Advances in Geomatics, 3(1), 38-54. https://doi.org/10.5281/zenodo.18087219

INTRODUCTION

Urban population growth increases the need for infrastructure, resulting in the loss of vegetation and its replacement with heat-absorbing built surfaces. This change in land cover results in an increase in land surface temperature. Nepal is one of the ten least urbanized countries in the world (Joshi, 2023). However, it is also one of the top ten fastest urbanizing countries. In 2014, the level of urbanization was 18.2%, with an urban population of 5,130,000, and a rate of urbanization of 3% (Timsina et al., 2020). Between 1978 and 2000 A.D., studies in the Kathmandu Valley found a growth rate of approximately 450% in urban areas. Additionally, the temperature in the Kathmandu Valley has been recorded as 30 °C in 2005, 31 °C in 2012, and 35 °C in 2015 (Ishtiaque et al., 2017).

Land surface temperature means the skin temperature of the surface. It depends on isolation and the nature of the surface or object material. Generally, water bodies, vegetative areas, and wet soil are cooler than bare soil, sand, metal, and built-up areas. Therefore, a positive relationship exists between LST and urbanisation (K.C. & Shepherd, 2015). Satellite-based LST can be determined from thermal emission at wavelengths in either infrared or microwave, which are "atmospheric windows". However, many uncertainties are involved in retrieving LST from radiance, which is directly measured by sensors onboard. Thermal infrared (TIR)-based LST retrievals are less uncertain than microwave-based ones because of the smaller range of variation of surface emissivity in the TIR domain and the stronger dependence of the radiance on temperature (Hulley et al., 2019).

Thus, urban growth has been identified as a critical process in the valley. It has led to population influx, environmental deterioration, urban fragmentation, haphazard landscape development, stress on ecosystem structure, and alteration of land use patterns (Akher & Chattopadhyay, 2017). According to UN-HABITAT (2015), Kathmandu is vulnerable to the impact of climate change. Therefore, this research claims to investigate the effect of urban growth on land surface temperature in the valley, since LST is an essential factor controlling urban climate (Kathmandu Valley, Nepal: Climate Change Vulnerability Assessment (Inu Pradhan Salike, 2015)

The main objective of this study is to quantify the spatial extent of urban growth, assess its influence on land surface temperature patterns, and examine temporal changes in thermal behaviour across the Kathmandu Valley. Additionally, the study aims to provide evidence-based insights to support sustainable urban planning and climate-responsive strategies.

1. MATERIALS AND METHODS

1.1 Study Area

The study area is Kathmandu Valley of Nepal, which is in the Latitude range of 27°34'33"N to 27°49'4" N and the Longitude range of 85° 11' 19" E to 85° 34' 57" E as shown in Figure 1. The Kathmandu

Valley comprises the districts of Kathmandu, Lalitpur, and Bhaktapur. The average elevation is 1300 meters above mean sea level (Thapa & Murayama, 2012). It is surrounded by four high hills: Shivpuri in the northwest, Chandragiri in the southwest, Nagarjun in the northeast, and Phulchoki in the southeast. Their altitude ranges from 1500 m. to 2800 m (Bhattarai et al., 2017).

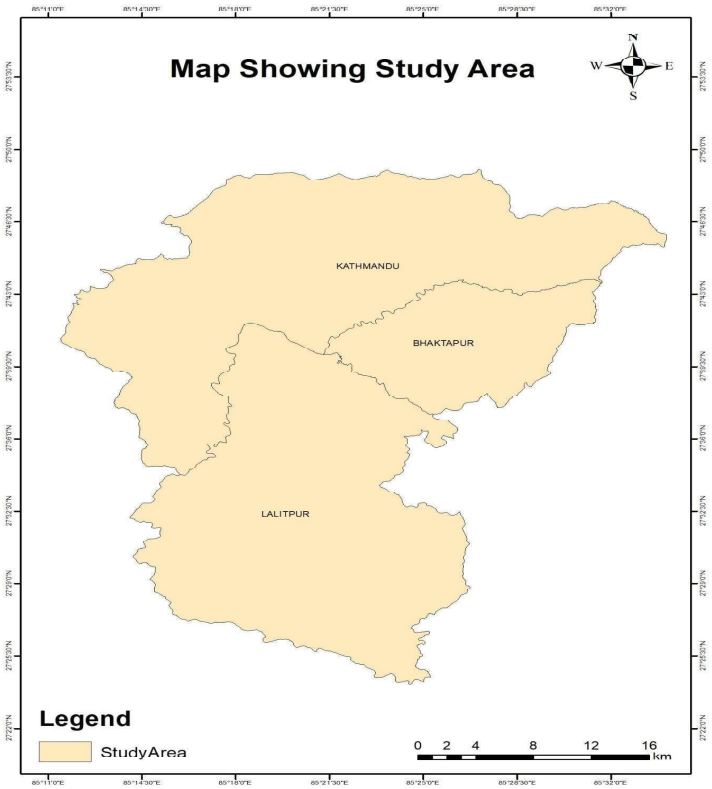

Figure 1. Study Area.

This valley was selected for this research due to its status as a rapidly urbanizing region experiencing significant landscape transformation, which provides a critical context for analyzing urban thermal impacts (Rimal et al., 2018).

1.2 Workflow

The overall workflow adopted for analyzing land surface temperature (LST) and urban growth in Kathmandu Valley is shown in Figure 2. The process begins with the acquisition of Landsat images for the years 2013, 2016, and 2019, followed by preprocessing steps including radiometric correction, atmospheric correction, and subsetting (clipping) to focus on the study area. LST is then derived from the thermal bands, and image classification is performed to identify different land cover types. Subsequently, LST classification and urban area analysis are carried out, followed by change detection to examine spatial and temporal trends. The final step involves analysis and verification to ensure the accuracy and reliability of the results.

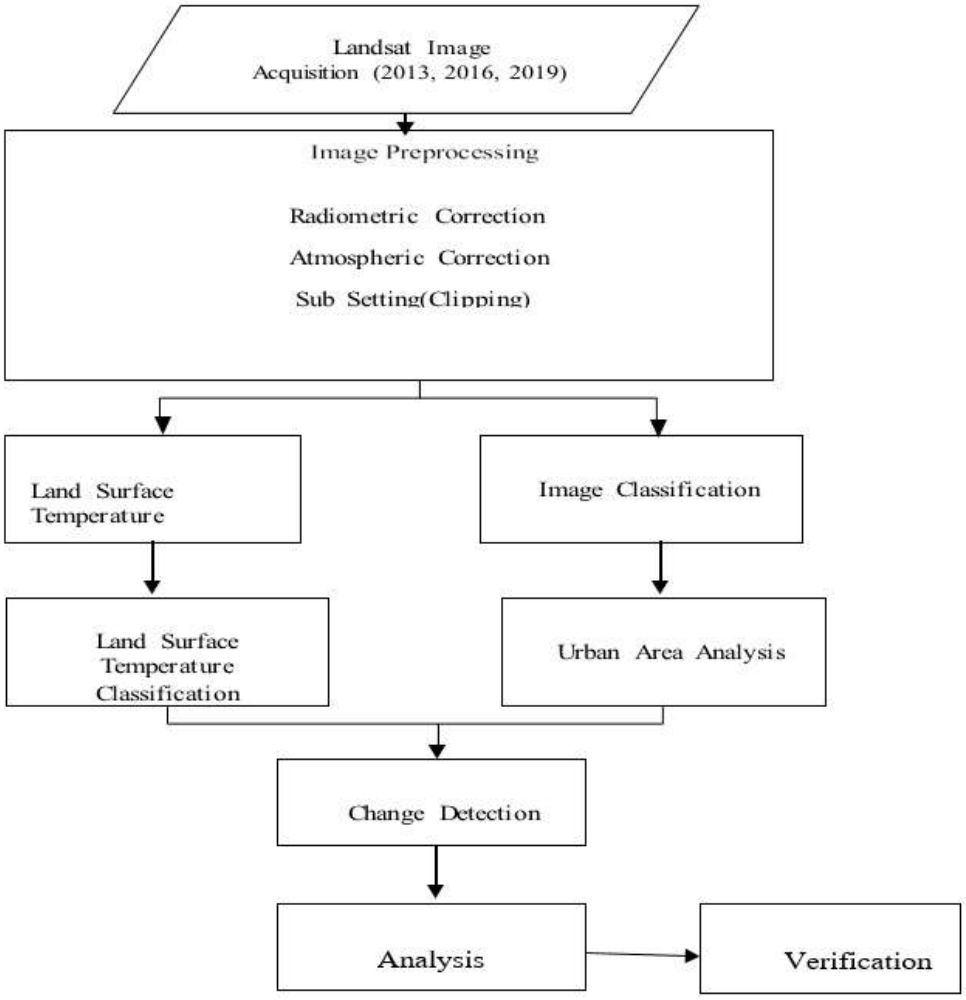

Figure 2. Workflow.

1.3 Data Source

The primary dataset for this research consists of Landsat 8 imagery from the Operational Land Imager (OLI) and Thermal Infrared Sensor (TIRS), Collection 1 Level-1 products, acquired on March 26, 2013; March 15, 2016; and January 3, 2019. Although more recent Landsat images (e.g., 2022, 2025) could provide updated information on land surface changes, this study focuses on the period 2013–2019 due to data availability and to maintain temporal consistency for trend analysis. Future research could incorporate more recent imagery to examine ongoing urban growth and LST dynamics.. These Landsat data can be freely accessed from the USGS portal and are processed by NASA to generate radiometric calibration and atmospheric correction algorithms for the Level-1 products. Landsat images are among the widely used satellite remote sensing data. Their spatial, spectral, and temporal resolution made them useful for mapping and planning projects (Wulder et al., 2019).

1.4 Radiometric Correction

Radiometric correction was applied to minimize errors in the satellite image's digital numbers (DN). This process enhances the quality and comparability of remotely sensed data, especially across multiple time periods (Chander et al., 2009). We used the empirical formula method for radiometric calibration. DN values were converted to Top-of-Atmosphere (TOA) reflectance using band-specific gain and bias values from the metadata:

$$TOA\ Reflectance = Gain * DN + Offset \quad (1)$$

After conversion, TOA reflectance was adjusted for solar elevation using band math with the following expression:

$$Corrected\ Reflectance = TOA\ Reflectance / \sin(44.34755968°) \quad (2)$$

1.5 Atmospheric Correction

Atmospheric correction removes the effects of the atmosphere to derive surface reflectance, improving image interpretability (Rumora et al., 2020). Accurate correction requires parameters like water vapor and aerosol distribution. Without such data, we used the Dark Object Subtraction (DOS) method, which assumes some pixels are in complete shadow and their radiance is due to atmospheric scattering. This path radiance is subtracted from all pixels. While less accurate, DOS is helpful when atmospheric data is unavailable.

1.6 Land Surface Temperature

Land surface temperature was retrieved from the thermal infrared band of Landsat images (band 10 of Landsat 8). The basic steps for the retrieval of LST are given below:

Conversion of pixel values to radiance:

The pixel values from digital number units were converted into radiance using the header file's parameters of Landsat images as follows:

$$L_\lambda = ML * QCAL + AL \quad (3)$$

This converts raw digital numbers (DN) from the satellite sensor into spectral radiance values, where ML represents the multiplicative rescaling factor, QCAL is the quantized calibrated pixel value, and AL is the additive rescaling factor, both obtained from the Landsat metadata file.

Atmospheric correction:

Removal of atmospheric effects from the thermal bands is essential to convert radiance to reflectance measures. Therefore, atmospheric correction uses the Dark Object Subtraction (DOS) Method.

Conversion of spectral radiance to at-sensor brightness temperature (BT):

Radiance values were then converted to at-sensor brightness temperature (in Celsius).

$$BT = \frac{K_2}{\ln\left(\frac{K_1}{L_\lambda} + 1\right)} - 273.15 \quad (4)$$

Here, – 273.15 is the Kelvin temperature constant.

Determination of Land Surface Emissivity (LSE):

Emissivity was estimated based on land cover type. The Portion of Vegetation (PV) is calculated as given in equation (5).

$$PV = \left(\frac{NDVI - NDVI_{\min}}{NDVI_{\max} - NDVI_{\min}}\right)^2 \quad (5)$$

$$LSE = 0.004 * PV + 0.986 \quad (6)$$

Land surface emissivity is calculated using the vegetation proportion, where the coefficients 0.004 and 0.986 are empirically derived constants that account for the emissivity characteristics of vegetated and non-vegetated surfaces.

Land Surface Temperature retrieval:

LST was calculated using the corrected brightness temperature and emissivity, applying the following formula:

$$LST = \frac{BT}{1 + \left(\lambda * \frac{BT}{C_2}\right) * \ln(LSE)} \quad (7)$$

Where, λ is the central band wavelength of emitted radiance (11.45 μm)

$$C_2 = \left(\frac{h * c}{\sigma}\right) = (1.438 * 10^{-2} mK) \quad (8)$$

with h is Planck's constant ($6.62*10^{-34}$ Js), c is the velocity of light ($2.998*10^8$ m/s) and σ is the Boltzmann constant ($1.38*10^{-23}$ J/K).

1.7 Image Classification

In image classification, we prefer supervised classification, which is a pixel-based approach. Since supervised classification has generally been recommended for evaluating segmentation results, and because classification accuracy is also believed to be highly dependent on the quality of segmentation (Liu & Xia, 2010). Hence, supervised classification was thought to lead to a more accurate classification of our project work (Maxwell et al., 2018). Similarly, this method uses the spectral signature defined in the satellite image (Talukdar et al., 2020).

1.8 Change Detection

The change detection approach is based on subtracting images acquired twice. This is performed on a pixel-by-pixel level to create the difference image. In the process, the pixel value is deducted from the initial and final images. Image differencing was used to detect urban changes in the images acquired in 2013, 2016, and 2019, specifically comparing the 2013 image.

2. RESULTS

2.1 Land Use Land Cover Change

Supervised maximum likelihood classification was applied to Landsat imagery to generate Land Use Land Cover (LULC) maps for 2013, 2016, and 2019 (Figures 3-5). The classification identified three primary land cover categories: urban areas, forest cover, and cultivated land. This categorization enabled systematic analysis of spatial and temporal changes associated with rapid urbanization in Kathmandu Valley.

The classified maps reveal distinct spatial patterns of land cover transformation. Urban areas are predominantly concentrated in the central valley floor, while forest cover remains largely distributed along the peripheral hills. Cultivated land occupies the intermediate zones between urban centers and forested hillsides. Over the six-year study period, a clear trend of urban expansion emerged, characterized by the conversion of both agricultural and forest lands into built-up areas.

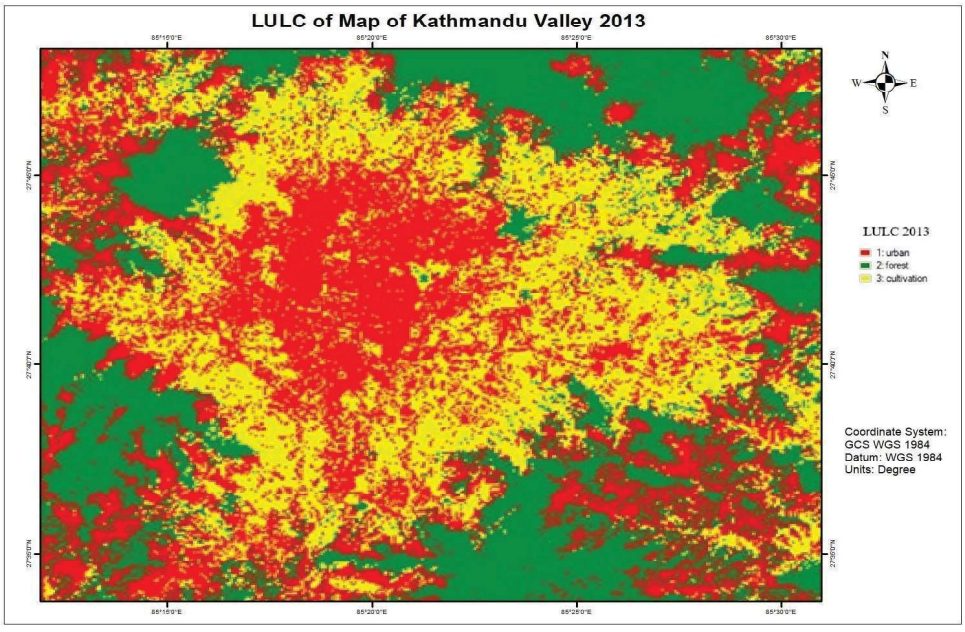

Figure 3. Supervised the Classification of Land Cover for analyzing the urban growth in 2013

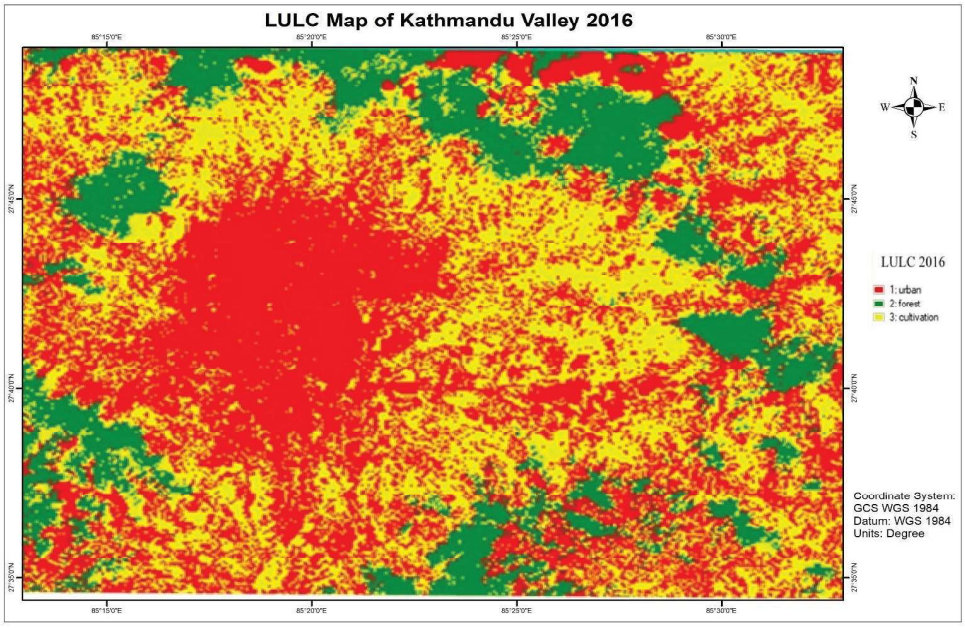

Figure 4. Supervised the Classification of Land Cover for analyzing the urban growth in 2016.

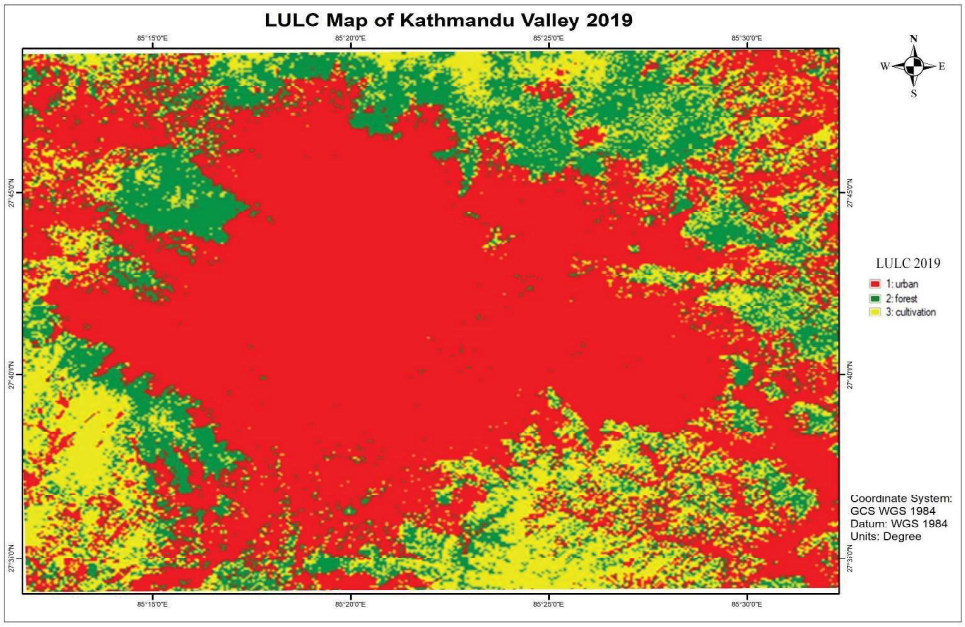

Figure 5. Supervised the Classification of Land Cover for analyzing the urban growth in 2019.

Table 1 presents the pixel count for each land cover class across the three time periods. The urban class showed a substantial increase from 681,405 pixels in 2013 to 1,026,126 pixels in 2019, representing approximately 50% growth. Conversely, forest cover declined dramatically from 650,982 pixels in 2013 to 339,749 pixels in 2016, though it showed partial recovery to 438,169 pixels by 2019. Cultivated land exhibited fluctuating trends, increasing from 572,177 pixels in 2013 to 745,718 pixels in 2016, before declining to 640,269 pixels in 2019.

Table 1. Total Pixels of Every Land Cover Class.

	2013	2016	2019
Urban	681405	819097	1026126
Forest	650982	339749	438169
Cultivation	572177	745718	640269

Table 2 translates these pixel counts into actual area coverage (in square meters), providing a more tangible understanding of landscape transformation. Urban areas expanded from 613.26 million m^2 in 2013 to 923.51 million m^2 in 2019, reflecting an increase of over 310 million m^2. Forest cover decreased from 585.88 million m^2 to 394.35 million m^2, representing a loss of approximately 191.53 million m^2 over the study period. Cultivated land increased initially to 671.15 million m^2 in 2016 but subsequently declined to 576.24 million m^2 by 2019.

Table 2. Total Area coverage of every land cover class.

	2013	2016	2019
Urban	613264500	737187300	923513400
Forest	585883800	305774100	394352100
Cultivation	514959300	671146200	576242100
Total	1714107600	1714107600	189410760

The percentage distribution of land cover classes (Table 3) provides critical insights into the proportional changes across the landscape. Urban areas increased from 35.78% of the total study area in 2013 to 48.76% in 2019, marking an increase of nearly 13 percentage points. This substantial growth came primarily at the expense of forest cover, which declined from 34.18% to 20.82%. Cultivated land maintained relatively stable coverage, varying between 30.04% and 30.42% across the study period, though it experienced intermediate fluctuations.

Table 3. Total percentage coverage of every land cover class.

	2013	2016	2019
Urban	35.7774798	43.0070609	48.75717726
Forest	34.1801063	17.8386759	20.8199418
Cultivation	30.0424139	39.1542631	30.42288094

2.2 Temporal Change Detection Statistics of Urban Growth

Change detection analysis was performed to quantify land cover transitions between the study periods. Tables 4 and 5 present the change statistics between 2013 and 2016, while Tables 6 and 7 show the changes between 2016 and 2019.

Table 4 presents the percentage change matrix for the 2013–2016 period. The matrix shows that 76.66% of urban areas remained stable, while 17.42% of new urban area came from forest conversion and 32.04% from cultivated land. Forest areas experienced significant transformation, with only 50.11% remaining as forest, and 49.90% undergoing class changes. Cultivated land showed 67.12% stability, with losses primarily to urban expansion. The image difference row indicates urban areas increased by 20.21%, forest decreased by 47.81%, and cultivated land increased by 30.33%.

Table 4. Percentage Change Statistics Table between years 2013-2016.

Percentage	Urban	Forest	Cultivation	Row Total	Class Total
Urban	76.661	17.418	32.042	100	100
Forest	1.291	50.105	0.834	100	100
Cultivation	22.048	32.477	67.123	100	100
Class Total	100	100	100	0	0
Class Changes	23.339	49.895	32.877	0	0
Image Difference	20.207	-47.81	30.33	0	0

Table 5 translates these percentages into actual area changes (in square meters) for 2013–2016. Urban areas expanded by 123.93 million m², growing from 613.26 million m² to 737.19 million m². This expansion occurred through the conversion of 102.05 million m² of forest and 165.00 million m² of cultivated land. Forest cover declined dramatically by 280.11 million m², decreasing from 585.88 million m² to 305.77 million m². Cultivated land showed a net increase of 156.19 million m², rising from 514.96 million m² to 671.15 million m².

Table 5. Area Change Statistics between years 2013-2016.

Area (sq. m)	Urban	Forest	Cultivation	Row Total	Class Total
Urban	470135700	102047400	165004200	737187300	737187300
Forest	7919100	293558400	4296600	305774100	305774100
Cultivation	135209700	190278000	345658500	671146200	671146200
Class Total	613264500	585883800	514959300	0	0
Class Changes	143128800	292325400	169300800	0	0
Image Difference	123922800	-280109700	156186900	0	0

Table 6 presents the percentage change matrix for the period 2016–2019. Urban areas maintained 64.04% stability, with 40.30% of new urban areas derived from cultivated land and a minimal contribution (0.31%) from forest. Forest areas exhibited only 35.58% stability, with 64.42% of the land undergoing class changes, while cultivated land had the lowest stability at 28.00%, with 72.00% of the land transitioning. The image difference indicates urban areas increased by 0.86%, forests increased by 28.97%, and cultivated land decreased by 14.14%.

Table 6. Percentage Change Statistics Table between years 2016-2019.

	Urban	Forest	Cultivation	Row Total	Class Total
Urban	64.039	0.31	40.301	100	100
Forest	9.88	35.58	31.695	100	100
Cultivation	26.081	64.111	28.003	100	100
Class Total	100	100	100	0	0
Class Changes	35.961	64.42	71.997	0	0
Image Difference	0.858	28.968	-14.141	0	0

Table 7 presents the area-based change statistics for 2016–2019. Urban areas expanded by 186.32 million m², increasing from 737.19 million m² to 923.51 million m². This growth primarily came from cultivated land conversion (270.48 million m²). Forest cover increased by 88.58 million m², rising from 305.77 million m² to 394.35 million m², largely through conversion from cultivated areas (196.03 million m²). Cultivated land declined by 94.90 million m², decreasing from 671.15 million m² to 576.24 million m².

Table 7. Area Change Statistics between years 2016-2019.

Area (sq. m)	Urban	Forest	Cultivation	Row Total	Class Total
Urban	472086000	946800	270480600	743513400	743513400
Forest	72837000	108792900	212722200	394352100	394352100
Cultivation	192264300	196034400	187943400	576242100	576242100
Class Total	737187300	305774100	671146200	0	0
Class Changes	265101300	196981200	483202800	0	0
Image difference	6326100	88578000	-94904100	0	0

Overall, the change detection analysis reveals that urban areas expanded by approximately 310.25 million m² between 2013 and 2019, with cultivated land serving as the primary source of urban expansion throughout the study period. Forest cover showed a net decline of 191.53 million m² despite the partial recovery in the later period.

The urban growth graph for the study area's time periods is illustrated in Figure 6. The graph shows us that the urban growth is gradually increasing. The temporal LULC trend, illustrated in Figure 6, demonstrates a consistent upward trajectory of urban growth over the six-year study period. The data clearly reveal that urbanization has been the dominant driver of land transformation, often occurring at the expense of forest and agricultural lands. This pattern suggests unplanned urban sprawl and underscores the urgent need for effective land-use management strategies to ensure sustainable urban development.

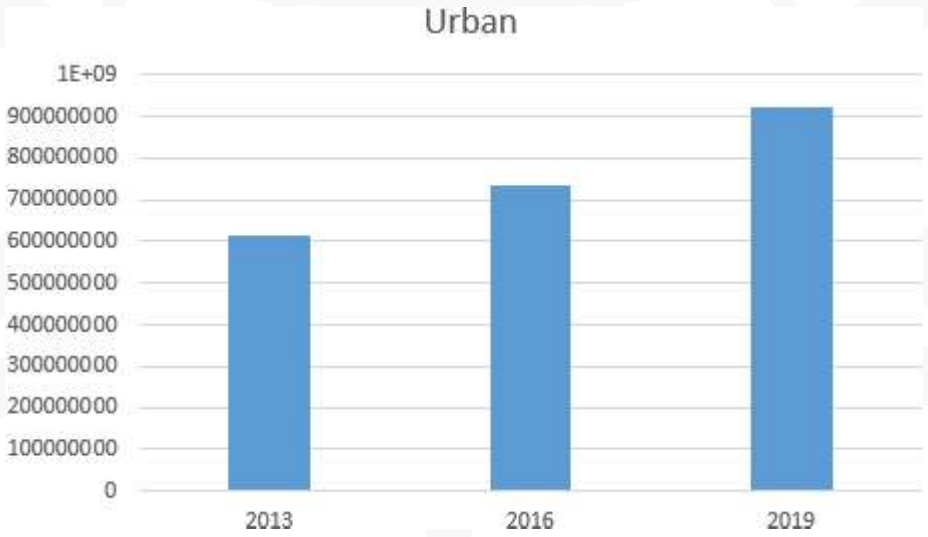

Figure 6. Chart of total area coverage by urban growth.

3. MITIGATION STRATEGIES

To mitigate the impacts of rapid urban growth and rising land surface temperatures in Kathmandu Valley, targeted actions are needed. Expanding green spaces through tree planting along the Ring Road, major city areas, and dense neighborhoods, as well as promoting green roofs can reduce heat buildup. Cool roofs in industrial zones, light pavements in public spaces, and reflective facades in new residential areas should be encouraged. Integrating climate-responsive architecture that blends traditional Nepali design with modern passive cooling can further reduce heat stress. Strengthened public awareness, community involvement, and strict enforcement of planning and building codes are also vital for effective heat mitigation in the Valley.

The implementation of these mitigation strategies requires coordinated efforts from government agencies, municipal authorities, private developers, and citizens. While individual measures provide benefits, the synergistic effect of combined strategies would be most effective in addressing the urban warming challenge. Given the rapid pace of urbanization documented in this study, immediate action is imperative to ensure a sustainable and livable future for Kathmandu Valley.

4. DISCUSSION

4.1 Land Surface Temperature

The LST maps of the study area in 2013, 2016, and 2019 are shown below. LST ranged from -3.270°C to 36.460°C in 2013, -1.91°C to 27.030°C in 2016, and 13.260°C to 40.840°C in 2019. The maximum temperature declined sharply in the year 2016 by around 90°C. However, the minimum temperature has been increasing in subsequent years. There is a sudden decline in the maximum temperature from 2013 to 2016, as some days of the year in the past could have been hotter, despite the influence of the urban warming phenomenon caused by urban growth over time. LST pattern analysis indicates a low temperature, represented by a blue tone, at the edges of all maps, which corresponds to the forest area. The yellow patch in the middle represents the urban settlements, and the red patches at the edges represent bare soil and even rocks in the high cliffs. A similar trend was observed in studies conducted by Tran et al. (2017)

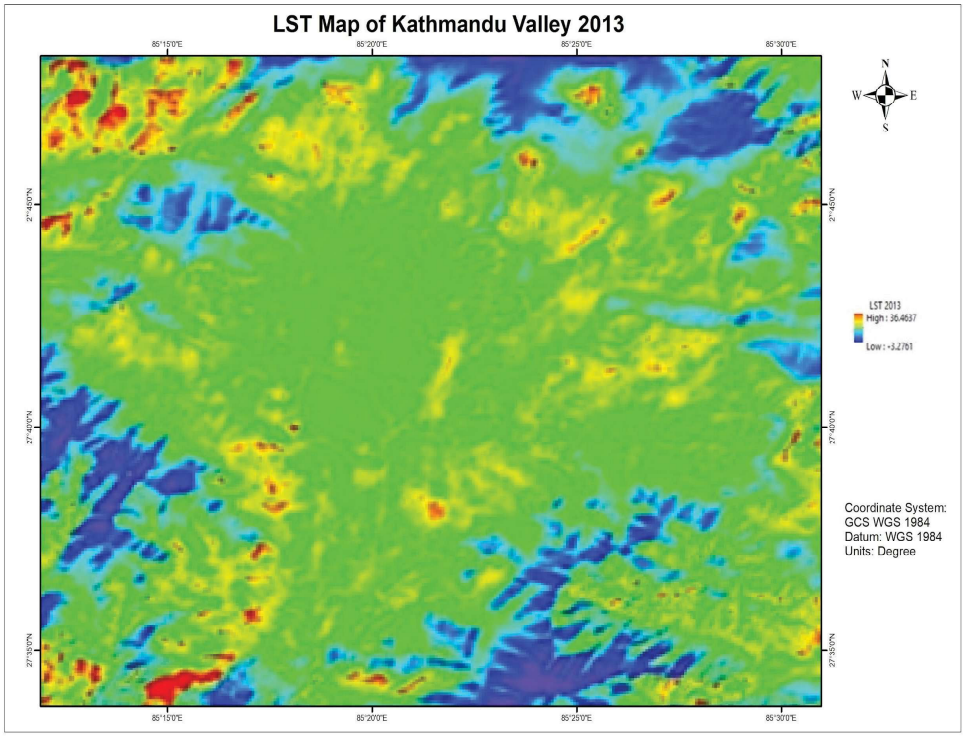

Figure 7. LST of Kathmandu of the years 2013.

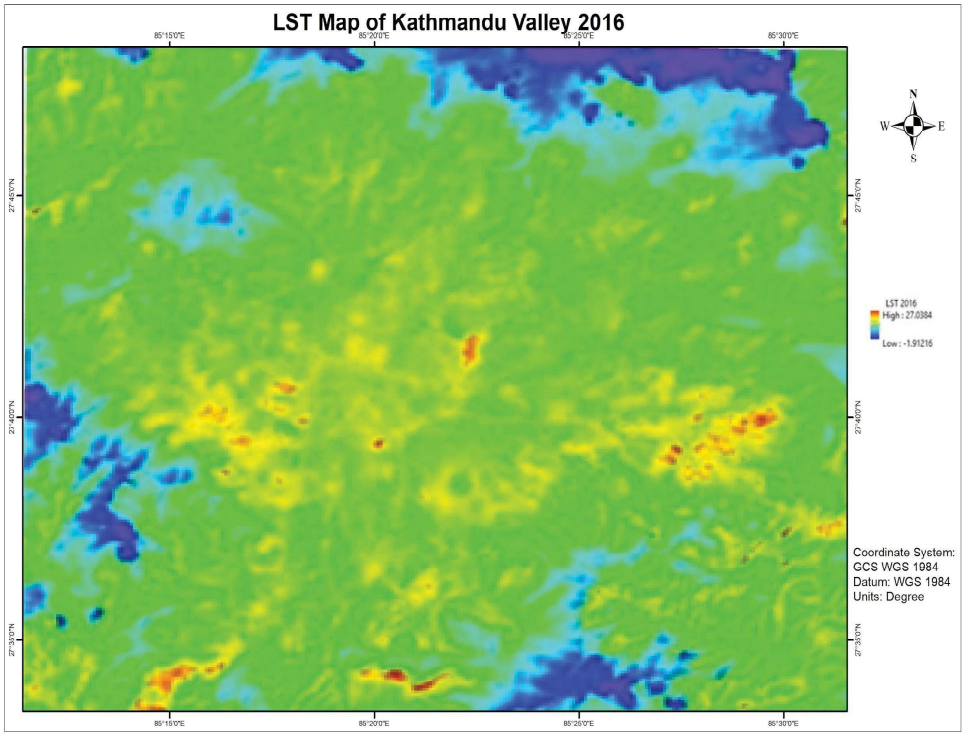

Figure 8. LST of Kathmandu of the years 2016.

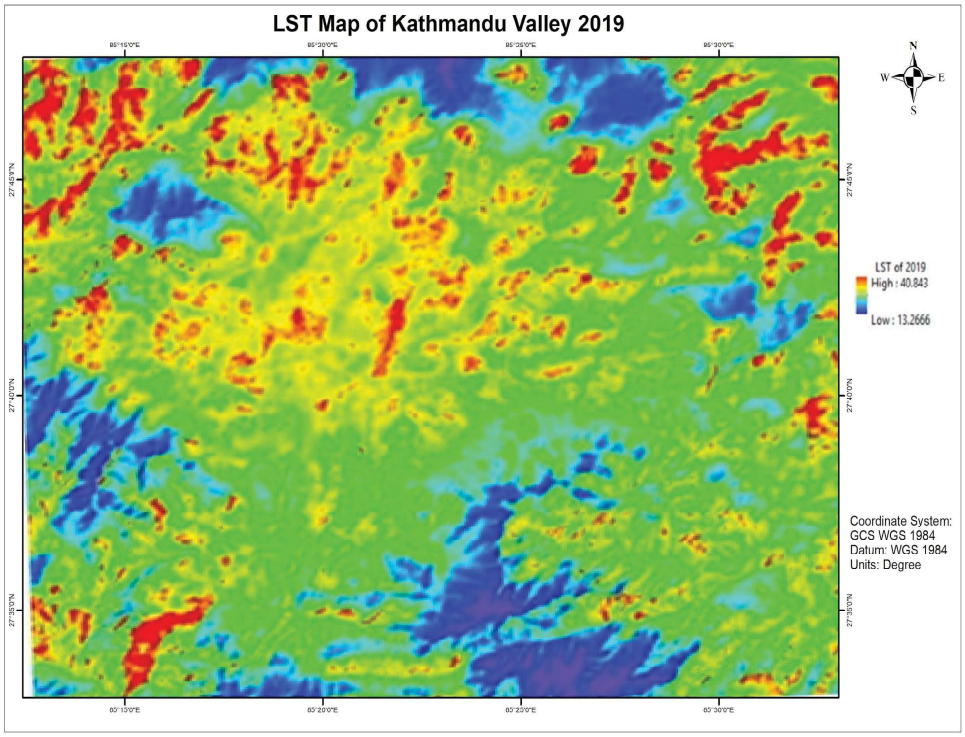

Figure 9. LST of Kathmandu of the years 2019.

Extreme fluctuations in temperature that were observed between 2013 and 2016 in this paper may have been driven by seasonal or meteorological conditions, a factor also noted by Rani et al. (2021) with respect to the temporal stability of Land Surface Temperature (LST). The observed spatial temperature distribution, which was cooler on the vegetated perimeter and hotter in the urban core, corresponds with recent research on the Urban Heat Island (UHI) effect in Kathmandu Valley. For example, Khatri et al. (2025) also documented an intense and intensifying UHI effect in the valley, linking land surface temperature increases directly with the expansion of built-up areas. Additionally, the distinct differences in LST that were observed based on land cover (i.e., built-up areas and bare soil having the highest) is consistent with the scientific literature on global land and the thermal properties of landscapes and other articles such as Guha et al. (2021). These comparisons reinforce that the dynamics of LST in the Kathmandu Valley configuration reflect localized urban expansion within the larger scope of globally observed climate patterns.

CONCLUSIONS

The study revealed a high rate of urban growth in the Kathmandu valley. The primary drivers of such growth are high population influx and inadequate land use planning. As a result, productive agricultural land and open areas are being replaced by concrete structures. This trend will become more severe unless proper land-use plans and policies are implemented. Based on our analysis of the thermal pattern of the study area over the given period, we found a gradual increase in temperature in the urban area. The study proved that the surface temperature is influenced by urban growth. However, the study had some limitations. The resolution of the images was just moderate for classification and change detection purposes. Despite a massive repository of Landsat imagery, it can sometimes be challenging to find suitable photos that meet our requirements.

Hence, we recommend that, as urban growth in the Kathmandu Valley is in a critical condition, it is high time that concerned authorities take necessary initiatives and that urban residents develop resilience to urban growth. We also recommend using high-resolution images and other classification methods to accurately classify land cover to detect urban development in the area.

REFERENCES

Akher, S. K., & Chattopadhyay, S. (2017). Impact of urbanization on land surface temperature-a case study of Kolkata New Town. Int J Eng Sci, 6(1), 71-81. https://doi.org/10.9790/1813-0601027181

Bhattarai, R., Alifu, H., Maitiniyazi, A., & Kondoh, A. (2017). Detection of land subsidence in Kathmandu Valley, Nepal, using DInSAR technique. Land, 6(2), 39. https://doi.org/10.3390/LAND6020039

Chander, G., Markham, B. L., & Helder, D. L. (2009). Summary of current radiometric calibration coefficients for Landsat MSS, TM, ETM+, and EO-1 ALI sensors. Remote sensing of environment, 113(5), 893-903. https://doi.org/10.1016/j.rse.2009.01.007

Guha, S., Govil, H., & Gill, N. (2021). A case study on the relationship between land surface temperature and land use/land cover over Bhubaneswar, India. Geology, Ecology, and Landscapes, 5(3), 218–228. https://doi.org/10.1080/24749508.2020.1757535

Hulley, G. C., Ghent, D., Göttsche, F. M., Guillevic, P. C., Mildrexler, D. J., & Coll, C. (2019). Land surface temperature. In Taking the Temperature of the Earth: Steps towards Integrated Understanding of Variability and Change (pp. 57–127). Elsevier. https://doi.org/10.1016/B978-0-12-814458-9.00003-4

Inu Pradhan Salike, L. F. (2015). Kathmandu Valley, Nepal: Climate Change Vulnerability Assessment.

Ishtiaque, A., Shrestha, M., & Chhetri, N. (2017). Rapid urban growth in the Kathmandu Valley, Nepal: Monitoring land use land cover dynamics of a himalayan city with landsat imageries. Environments, 4(4), 72. https://doi.org/10.3390/ENVIRONMENTS4040072

Joshi, D. R. (2023). Urbanization trend in Nepal. Contemporary Research: An Interdisciplinary Academic Journal, 6(1), 51-62. https://doi.org/10.3126/craiaj.v6i1.55367

K.C., B., & Shepherd, J. M. (2015). A study of urban heat island intensity in Kathmandu Valley, Nepal [Abstract]. AGU Fall Meeting Abstracts.

Khatri, B., & Khatri, R. (2024). Assessment on the relationship of spectral indices with land surface temperature using Google Earth Engine: A case study of Chitwan District, Nepal. Advances in Geomatics, 2(2), 74–87. https://doi.org/10.5281/zenodo.14555495

Khatri, B., Kharel, B., Dhakal, P., Acharya, S., & Thapa, U. (2025). Spatio-temporal dynamics of urban heat island using Google Earth Engine: Assessment and prediction—A case study of Kathmandu Valley, Nepal. Climate Services, 38, 100560. https://doi.org/10.1016/j.cliser.2025.100560

Liu, D., & Xia, F. (2010). Assessing object-based classification: advantages and limitations. Remote Sensing Letters, 1(4), 187–194. https://doi.org/10.1080/01431161003743173

Maxwell, A. E., Warner, T. A., & Fang, F. (2018). Implementation of machine-learning classification in remote sensing: An applied review. International Journal of Remote Sensing, 39(9), 2784–2817. https://doi.org/10.1080/01431161.2018.1433343

Rani, M., Kumar, P., Pandey, P. C., Srivastava, P. K., Chaudhary, B. S., Tomar, V., & Mandal, V. P. (2021). Multi-temporal NDVI and surface temperature analysis for Urban Heat Island impact assessment of Varanasi City, India. Quaternary International, 575-576, 249–259. https://doi.org/10.1016/j.quaint.2020.07.046

Rimal, B., Zhang, L., Keshtkar, H., Haack, B. N., Rijal, S., & Zhang, P. (2018). Land use/land cover dynamics and modeling of urban land expansion by the integration of cellular automata and markov chain. ISPRS International Journal of Geo-Information, 7(4), 154. https://doi.org/10.3390/ijgi7040154

Rumora, L., Miler, M., & Medak, D. (2020). Impact of various atmospheric corrections on sentinel-2 land cover classification accuracy using machine learning classifiers. ISPRS International Journal of Geo-Information, 9(4), 277. https://doi.org/10.3390/IJGI9040277

Talukdar, S., Singha, P., Mahato, S., Pal, S., Liou, Y. A., & Rahman, A. (2020). Land-use land-cover classification by machine learning classifiers for satellite observations—A review. Remote sensing, 12(7), 1135. https://doi.org/10.3390/rs12071135

Thapa, R. B., & Murayama, Y. (2012). Scenario based urban growth allocation in Kathmandu Valley, Nepal. Landscape and Urban Planning, 105(1-2), 140-148. https://doi.org/10.1016/j.landurbplan.2011.12.007

Timsina, N. P., Shrestha, A., Poudel, D. P. & Upadhyaya, R. (2020). Trend of urban growth in Nepal with a focus in Kathmandu Valley: A review of processes and drivers of change. https://doi.org/10.7488/ERA/722

Tran, D. X., Pla, F., Latorre-Carmona, P., Myint, S. W., Caetano, M., & Kieu, H. V. (2017). Characterizing the relationship between land use land cover change and land surface temperature. ISPRS Journal of Photogrammetry and Remote Sensing, 124, 119-132. https://doi.org/10.1016/J.ISPRSJPRS.2017.01.001

Wulder, M. A., Loveland, T. R., Roy, D. P., Crawford, C. J., Masek, J. G., Woodcock, C. E., Allen, R. G., Anderson, M. C., Belward, A. S., Cohen, W. B., Dwyer, J., Erb, A., Gao, F., Griffiths, P., Helder, D., Hermosilla, T., Hipple, J. D., Hostert, P., Hughes, M. J., … Zhu, Z. (2019). Current status of Landsat program, science, and applications. Remote Sensing of Environment, 225, 127–147. https://doi.org/10.1016/j.rse.2019.02.015

ADVANCES IN GEOMATICS

VOLUME 03 • ISSUE 01 • OCTOBER 2025
e-ISSN: 3023-4980

ORIGINAL ARTICLE

Submission: 08/09/2025
Accepted: 25/10/2025

ASSESSMENT OF TEMPORAL COASTLINE DYNAMICS AND LAND TRANSFORMATION USING CORINE, GIS AND REMOTE SENSING

Arzu ERENER[1]* Rabia HACIALİOĞLU[1]

[1] Department of Geomatics, Engineering Faculty, Kocaeli University, Türkiye.

* Corresponding Author: A. Erener, arzu.erener@kocaeli.edu.tr 0000-0002-9168-4254

ABSTRACT

Coastal areas where the majority of the society live are exposed to geographical changes. Observing the changing coastline and usage areas is important in terms of efficient use of the areas and directing the future. Remote Sensing (RS) is used effectively in change detection analyses and spatial studies in the recent years. This paper focuses mainly on the coastal line changes of Trabzon, Turkey by using Geographic Information Systems (GIS) and Remote Sensing (RS) by examining the Landsat and Google earth images. Landsat images were obtained for 2002, 2009, 2015, 2021 and Google earth data were provided for 2002, 2012, 2021 years. The land use type of the changing areas were examined using the 2000 and 2018 Corine data. According to the results of the study, it was observed that there was a remarkable growth in the coastal areas towards the sea. It has been concluded that this growth is mostly formed by the filling areas built into the sea. After the evaluation with Corine data, it has been determined that the areas that have changed have turned into sports, recreation, highway and port areas in 20 year period.

Keywords: Land Use, GIS, Corine, Change Analysis, Google Earth, Landsat, Remote Sensing.

Cited As:

Erener, A. & Hacıalioğlu, R. (2025). Assessment of temporal coastline dynamics and land transformation using Corine, GIS and remote sensing, Advances in Geomatics, 3(1), 55-71. https://doi.org/10.5281/zenodo.18087379

INTRODUCTION

For centuries, coastal areas have been one of the most preferred places for communities to settle. The fact that coastal areas are so important for communities has continued until today with factors such as trade, tourism, raw material source (sand, salt, mining areas), defence (sea bases, military areas), transportation, irrigation, energy, food and socio-cultural factors. Coastline is “the line formed by the junction of the points where water touches the land in seas, lakes and rivers, except in cases of flood”; The coastal edge line is defined as "the natural border of sandy, gravelly, rocky, stony, reedy, swamp and similar areas in seas, lakes and rivers where water movements occur in the land direction after the shore line" (Coastal Law No. 3621).

Changes in coastal areas include deterioration in the coastline that occur naturally or by human means. Coastal changes are called coastal advance or coastal regression. Coastal recession can occur due to factors such as melting of sand, coastal erosion, waves and sea currents. On the other hand, coastal progress can be formed by filling materials carried by water (Bird, 2008). The physical change of coastal areas affects many lives. In terms of ecological life, the routes of migrating birds are changing, and the habitats of many plants are affected. This situation disrupts the balance of nature and affects environmental pollution (Martínez et al., 2007). Turkey is surrounded by seas on three sides, has a total coastline of 8,333 km, and is a country where the concept of coast is of great importance. Coastal areas are globally recognized as focal points of human and economic activities, and this pattern is also observed in Türkiye (Akkaya, 2004; Kocadağlı, 2022).

Satellite remote sensing (RS) has revolutionized the observation of the Earth by enabling more accurate information to be obtained through the systematic evaluation of land surfaces (Yilmaz, 2004; Yongxue et al., 2019). There is an increase in the use of satellite images in the discipline of cartography due to the fact that satellite images provide continuous information, ease of updating, update speed, absence of legal obstacles in taking and evaluating images, and especially increasing geometric accuracy with high resolution satellite images (Mutluoğlu & Yakar, 2005; Müller et al., 2012; Mutluoglu et al., 2015; (Mutluoglu et al., 2016). Medium-resolution RS images have been widely used in various studies including, agriculture, landuse /cover mapping, change detection, object determination, urban expansion, deforestation, land degradation, shoreline change (Lu et al., 2007; Wu, 2007; Duveiller et al., 2008; Seto and Fragkias, 2005; Yu et al., 2011).

While Geographic Information System (GIS) is a system that performs location-based data acquisition, analysis, storage and presentation on the earth's surface for a specific purpose, RS technology is a technology for creating a data base. In recent years, RS and GIS technologies have been used effectively in coastline changes and spatial observations. Variation analysis provides a method for comparing images of an object taken at different times or under different conditions. There are many studies in this field in the national and international literature (Korkut et al., 2008; Doğan, 2008; Erener &

Düzgün, 2009; Kirui et al,. 2011; Chen et al., 2012; Olgun, 2012; Sekovski et al., 2012; Hussain et al., 2013; Kaya, & Toroğlu, 2015; Ma et al., 2016; Mishra et al., 2017; Nassar et al., 2018; Akdeniz, 2021; Erener & Yakar, 2012; Erener & Yakar, 2015; Uzan & Özcan, 2016; Sarı &Yüksel, 2020).

In the Akdeniz (2021) study, orthophoto maps of the years 1957, 1964, 1972, 1993, 2009, 2018, 2020 were used to examine the short- and long-term changes on the shores of the Küçük Menderes Delta. It was determined that there was an accumulation of up to 37.01 ha in the Küçük Menderes Delta between 1957 and 2020 and the length of the coastline decreased by 172.17 m. Nassar et al. (2018) examined the 27-year coastline change along the North Sinai coast of Egypt. Satellite data acquired at different times from the Landsat Thematic Mapper (TM), Enhanced Thematic Mapper Plus (ETM+), and Operational Land Imager/Thermal Infrared Sensor (OLI/TIRS) were processed in ArcGIS using scripts developed in the Python programming language. Kirui et al. (2011), the coastline change of Mangrove Forest land, which is very important to the people of Kenya, was analysed using red, near-infrared and middle-infrared bands of Landsat Thematic Mapper (TM) satellite images and aerial photographs and SRTM data for the years 1985, 1992, 2000 and 2010. In this study, it is aimed to monitor and analyse the change of the Trabzon coastline between 2002-2021. Google Earth and Landsat 5 and Landsat 8 satellite images with different resolutions were used for analysis. With the help of GIS-based analyses, areas of spatial change in the coastline have been determined over a 20-year period. The usage purposes of the landfills in coastal areas were examined with the help of Coordination of Information on the Environment (Corine) 2006 and 2018 data. With the help of the data obtained, the land use type of the areas that make up the change in the coastline has been revealed.

1. MATERIALS AND METHOD

1.1 Study area and data

The study area is the province of Trabzon, located in the northeast of Turkey. In the province, which has a coast to the Black Sea, they form small plains where the rivers reach the sea (Pural, 1995). These plains are places where crowded settlements are seen, although their lands are fertile (URL-1).

Due to the mountainous nature of the province, the settlements are scattered in the villages, on the other hand they are very close to each other at the coastal region. This both caused the formation of unplanned urbanization and led to studies to enlarge the city centre area by filling the sea. The study area is shown in Figure 1.

Figure 1. Study area.

In this study, 30 m resolution reflective bands Landsat 5 images of 2002 and 2009 and 30 m resolution reflective bands Landsat 8 images of 2015 and 2021 were used. Landsat images are downloaded free of charge from Earth explorer platform (https://earthexplorer.usgs.gov). Google Earth is a web-based computer program that displays photos of different resolutions obtained at different times from various satellites on Earth. Google Earth, which was initially released on June 11, 2001, has enabled detailed viewing of most cities worldwide since June 2006. In this study, using Landsat data as well as google earth data, analyses were applied from two different systems and compared. In this context, Google Earth images of the area for the years 2002, 2012, 2021 were downloaded and used. In addition, 100 m resolution Corine data for the years 2000 and 2018 were used to obtain land information. The Corine Project, which started in Portugal in 1985, is a system that includes the land cover and land use of all European countries (Tekin, 2019). The aim is to create a common database in the system where information is collected and shared over the cartographic map according to priority issues such as water, vegetation and land cover determined by the European Environment Agency (ACA). Turkey joined the project in 1998. Initial studies were completed in 2008 using 2000 Landsat satellite images.

A common classification language is used to express the areas that make up the land within the scope of the project. Classifications were made according to land use patterns. The classification, which consists of five basic classes, has 44 subclasses. Corine data was downloaded from the Corine Project website (https://land.copernicus.eu/). Also in the study, Turkey's Civil Boundaries Map was down-

loaded free of charge from the General Command of Mapping's website (https://www.hgk.msb.gov.tr/) and used as a base for the district borders map. The data used are shown in Table 1.

Table 1. Data Used.

Data Name	Year	Format	Resolution (m)
Landsat			
Landsat 5MS	2002 2009	Raster Raster	30(MS bands) 30(MS bands)
Landsat 8	2015 2021	Raster Raster	30(MS bands) 30(MS bands)
Google Earth			
Landsat/Copernicus Maxar Technologies	2002	Raster	30 0.3
Maxar Technologies	2012	Raster	0.3
Maxar Technologies CNES/Airbus	2021	Raster	0.3 0.5
Corine	2006 2018	Raster Raster	100 100
Türkiye administrative boundaries		Vector	

1.2 Method

The flow chart of the study is shown in Figure 2. In order to fit the images saved as images from the Google Earth Pro program to their real coordinates on the world, georeferencing has been included and the coordinate system has been defined. All satellite data, spatially overlapped with Landsat data, are masked for the Trabzon Değirmendere coastal region where the change occurred. Since the focus of the study is coastal change, two basic classes, sea and land, were created and samples were collected from the sea surface and the land surface. Supervised classification was applied with the samples. The classified raster data was converted into polygons and lines, and after editing, the changing areas of the coastline were determined using the polygon difference method. These processes were repeated for all satellite images. The obtained data and Corine data were masked with the district boundaries, then the Corine data were divided into categories and organized. Finally, the land use transformation was determined by overlapping the areas where the change occurred with the Corine data.

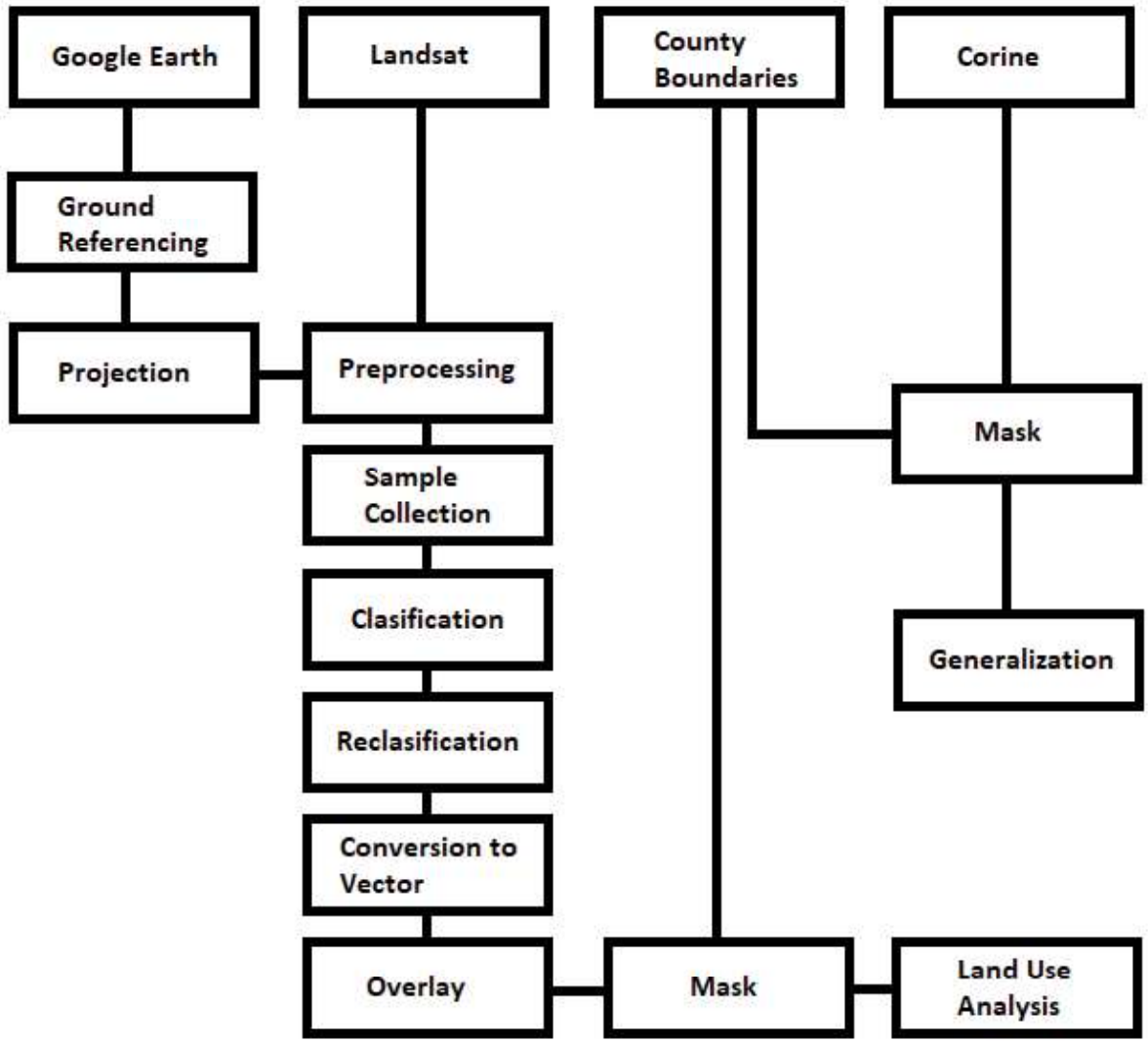

Figure 2. Process steps.

2. RESULTS

2.1 Landsat change analysis

The changing areas of the coastline were determined as a result of the supervised classification process by creating two basic classes, sea and land, with Landsat satellite images of 2002, 2009, 2015, 2021. Area calculations of images belonging to different years were obtained. It has been determined that the coastal area has grown by 142.18 hectares between 2002-2009, 61.34 hectares between 2009-2015, 56.76 hectares between 2015-2021. The area changes of the 260.30 ha growing area in total over the years are shown in Table 2.

Table 2. Landsat coastal change areas.

Year Range	Area Difference (ha)	Change Period (Annual)
2002 – 2009	142.18	7
2009 - 2015	61.34	6
2015 - 2021	56.76	6
2002 - 2021	260.30	19

By overlaying the images, the locations of the changed areas were determined. The changed areas are shown in Figure 3.

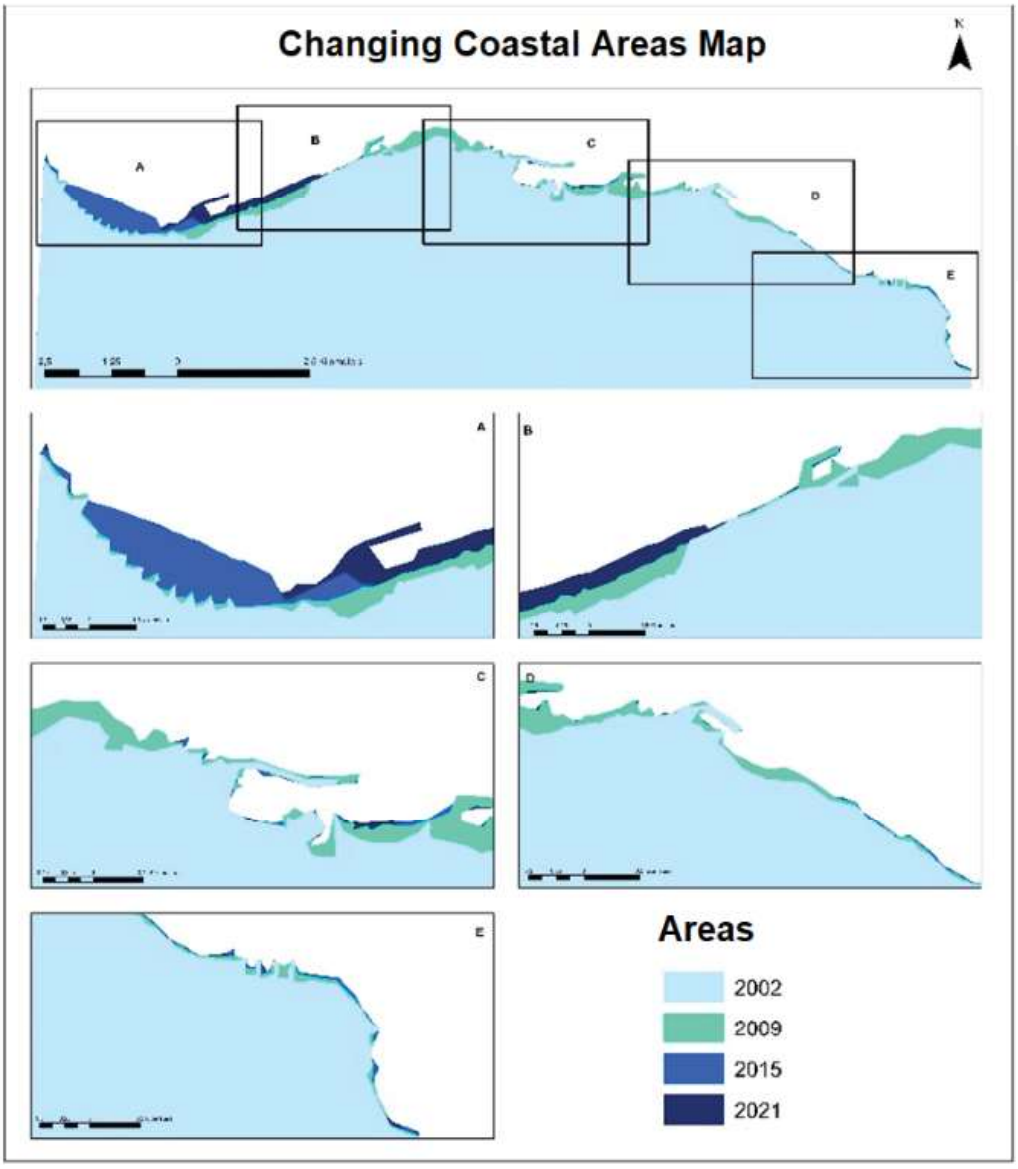

Figure 3. Coastline change map produced with Landsat images.

The change rates of Trabzon province, which underwent a coastal change of 260.30 hectares between 2002 and 2021, were converted into a pie chart and shown in Figure 4.

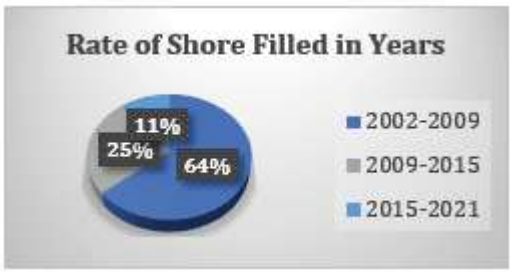

Figure 4. Ratio of fill areas of Trabzon coastline.

2.2 Google Earth change analysis

The changing areas of the coastline were determined as a result of the supervised classification process by creating two basic classes, sea and land, with Google Earth satellite images for the years 2002, 2012 and 2021. Area calculations of images belonging to different years were made. The area measurements derived from images acquired in different years were systematically evaluated. It has been determined that the coastal area has grown by 162.62 hectares between 2002-2021 and 72.44 hectares between 2012-2021. The area changes of the 235.06 hectares growing area in total over the years are shown in Table 3.

Table 3. Google Earth coastal change areas.

Year Period	Area Difference (ha)	Change Period (Annual)
2002 - 2012	162.62	10
2012 - 2021	72.44	9
2002 - 2021	235.06	19

By overlaying the images, the locations of the changed areas were determined. The changed areas are shown in Figure 5.

The change rates of Trabzon province, which underwent a coastal change of 235.06 hectares between 2002 and 2021, are shown in Figure 6, which has been converted into a pie chart. The percentage distribution indicates that 31% of the total coastline change occurred between 2002 and 2012, while the remaining 69% occurred between 2012 and 2021.

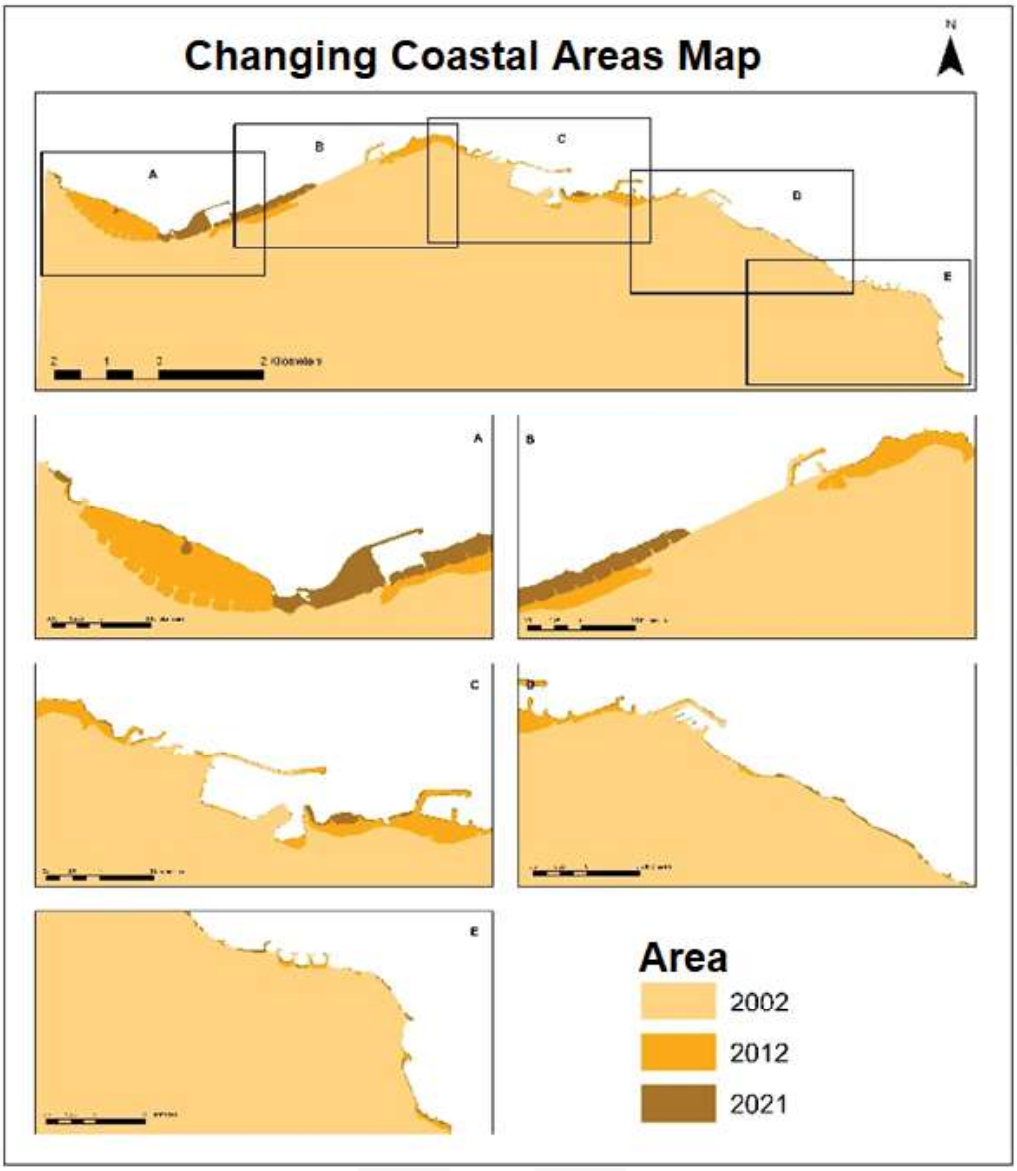

Figure 5. Coastline change map produced with Google Earth images.

Figure 6. Ratio of fill areas of Trabzon coastline.

2.3 Comparison of Landsat and Google Earth Studies

In the studies conducted for the same region between 2002-2021, the spatial change of the Trabzon coastline was 260.30 hectares with Landsat satellite images, while it was 235.06 hectares with Google Earth satellite images. The reason why the two spatial changes are different is the spatial resolution differences of the Google Earth satellite images. The change of the coastline is overlaid with Landsat and Google Earth satellite images and shown in Figure 7.

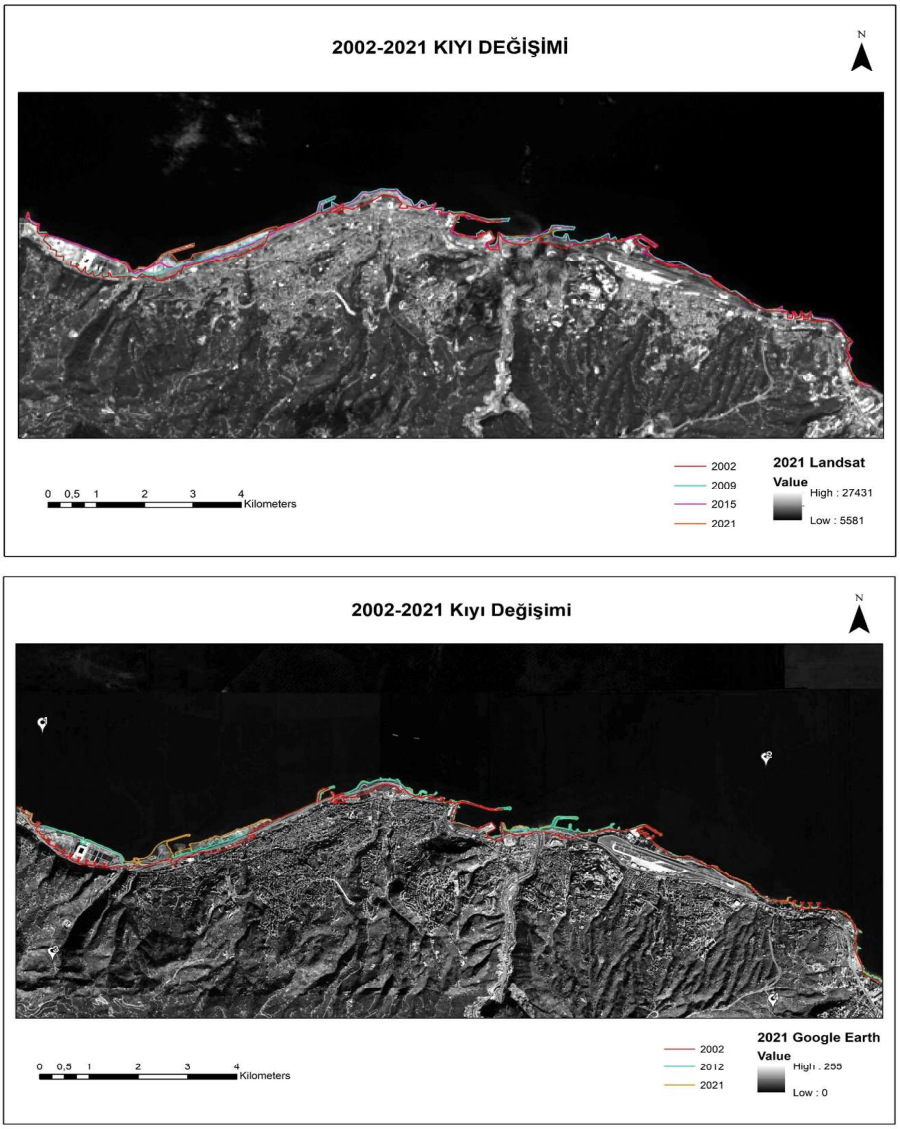

Figure 7. Demonstration of coastline change on Landsat satellite image and google earth images.

2.4 Corine land use maps

Once the coastline change analysis had been completed, the CORINE datasets were classified into their respective land cover categories and reorganized according to the official area codes. These categorized datasets were then spatially overlaid with the detected coastline change areas to identify the

corresponding land use types. The resulting land use maps for the years 2000 and 2018 are presented in Figure 8 and Figure 9.

The land use map of 2018 was overlaid with the coastal strip change data obtained with the Landsat images of 2002, and the land uses of the filled area were determined and shown in Figure 10.

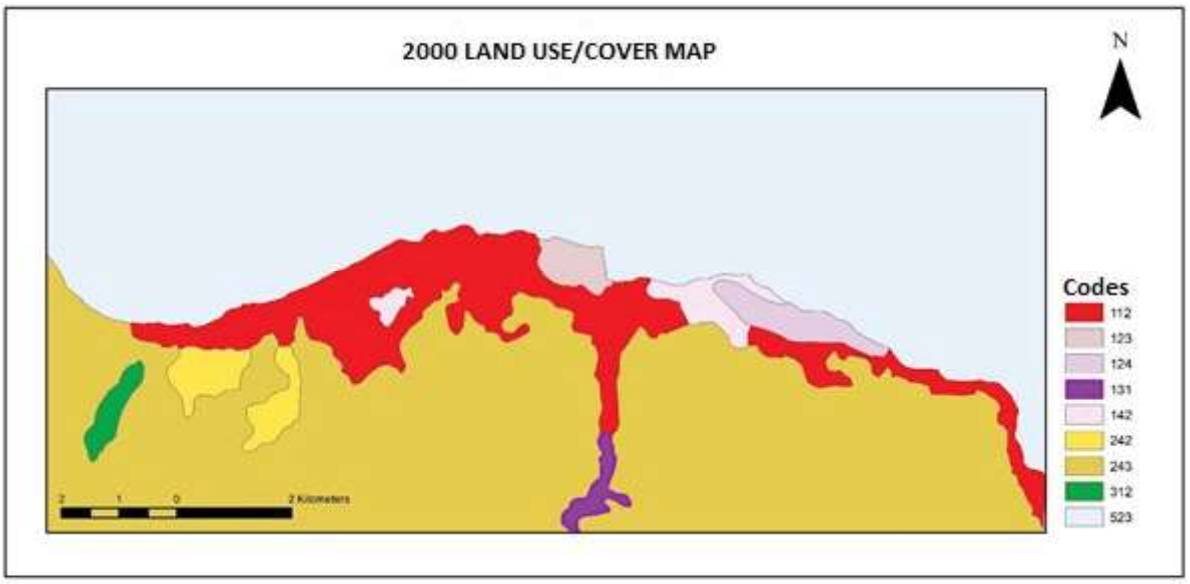

Figure 8. Trabzon coastline land use map in 2000.

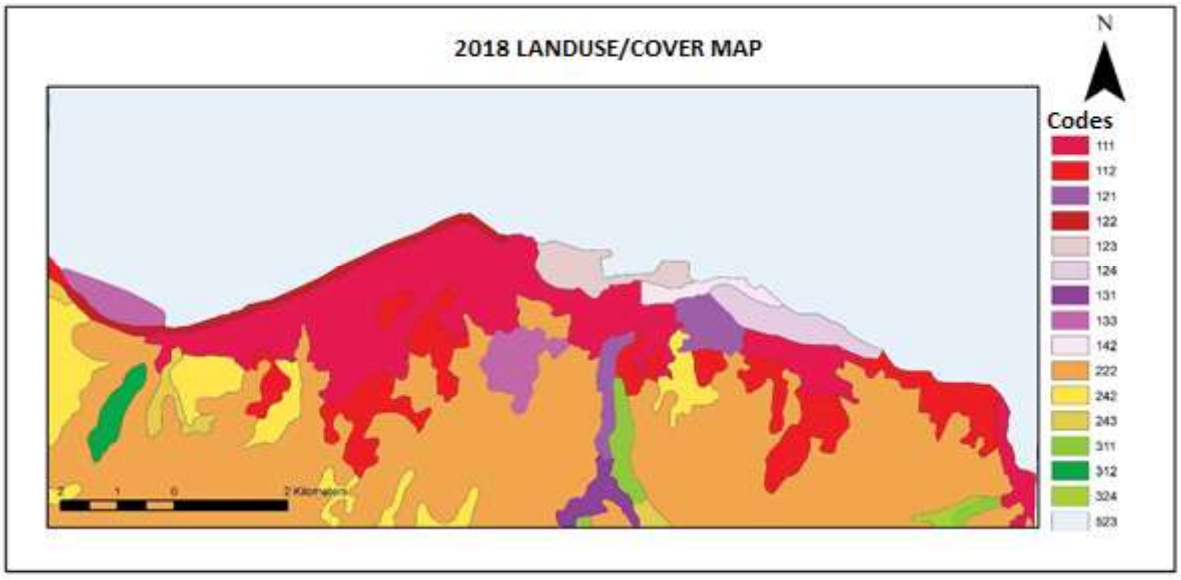

Figure 9. Trabzon coastline land use map for 2018.

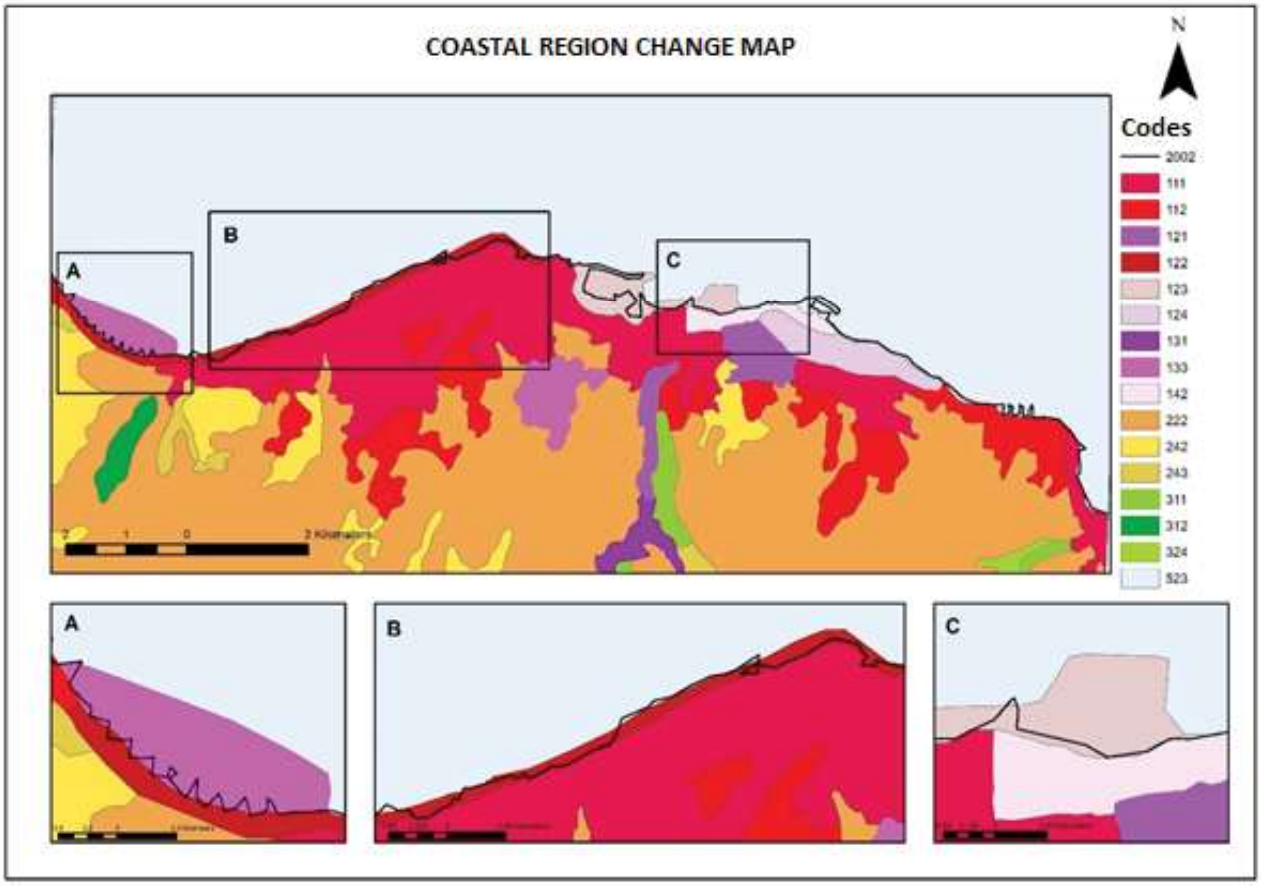

Figure 10. Demonstration of the change of coastal usage areas together with the coastline.

Area codes used in land use maps are explained in Table 4.

Table 4. Trabzon coastline land use Corine data.

Base Class	Codes	Sub-class
Structures	111	Continuous City Structure
	112	Discrete City Structure
	121	Industrial or Commercial Areas
	122	Road or Railroad Areas
	123	ports
	124	Airports
	131	Mining Fields
	133	Construction Sites
	142	Sports and Recreation Areas
	222	Orchards

Agricultural areas	242	Mixed Agricultural Fields
	243	Agricultural Areas With Natural Vegetation
Forest and	311	Broad Leaf Forests
Natural	312	Coniferous Forests
Areas	324	Plant Exchange Areas
Water Areas	523	Sea and Oceans

CONCLUSION

Change analyses are essential for monitoring spatial and temporal variations in land use, area size, and land characteristics. Understanding coastal change is particularly important, as it directly affects the physical and socio-economic conditions of communities residing along the shoreline. The results of this study indicate that coastline change has influenced urban development patterns, and that land reclamation activities extending toward the sea have created new areas of use within the coastal zone. In this context, RS techniques and GIS have been used effectively to detect temporal and spatial changes. Information about the land use of temporally changing areas was analysed with Corine data bases. Corine has been used as an efficient resource in change analysis, thanks to the spatial cartographic infrastructure of the Corine data and the effective classification of the attribute data.

In Trabzon, the mountains rise right after the sea, and the settlements originating from this mountainous area are scattered in the villages, while they are very close to the coastal coast. Settlements cause unplanned urbanization and the sea fill constructions done in order to gain space has provided a new place for the coastal area. The change of the coastal areas of Trabzon in the last 19 years has been obtained by determining the coastline of different years with different satellite images. Using Landsat satellite images, 142.18 hectares of land between 2002-2009, 61.34 hectares between 2009-2015, 56.76 hectares between 2015-2021, a total of 260.30 hectares of land between 2002-2021 detected. Using Google Earth satellite images, it has been determined that an area of 162.62 hectares between 2002-2012 and 72.44 hectares between 2012-2021 and a total area of 235.06 hectares between 2002-2021. It was concluded that the areal change caused land use change. Most of the areas changed are the filling areas made into the sea. It has been determined that the filled coastal areas have been transformed into sports and recreation areas, highway and port areas.

Consequently, coastlines can undergo rapid changes due to various human-driven alterations. Therefore, assessing these interventions is crucial for planning more orderly and sustainable coastal environments for the future.

REFERENCES

Akdeniz, H. B. (2021). Examination of shoreline temporal changes and development of coastal management system web (Publication No. 68221) [Master's Thesis, Konya Technical University]. YÖK National Thesis Center.

Akkaya, M. A. (2004). Coastal zone management in Turkey and legal regime, (Publication No. 150516) [Doctoral Thesis, İstanbul University]. YÖK National Thesis Center.

Bird, E. (2008). Coastal Geomorphology: An Introduction. Wiley-Blackwell.

Chen, G., Hay, G. J., Carvalho, L. M. T., & Wulder, M. A. (2012). Object-based change detection. International Journal of Remote Sensing, 33(14), 4434-4457. https://doi.org/10.1080/01431161.2011.648285

Doğan, İ. (2008). Coastline change detection using remote sensing data: Sample of Alaçatı, (Publication No. 237179) [Master's Thesis, Yıldız Technical University]. YÖK National Thesis Center.

Duveiller, G., Defourny, P., Desclée, B., & Mayaux, P. (2008). Deforestation in Central Africa: Estimates at regional, national and landscape levels by advanced processing of systematically-distributed Landsat extracts. Remote sensing of environment, 112(5), 1969-1981. https://doi.org/10.1016/j.rse.2007.07.026.

Erener, A., & Düzgün, H. S. B. (2009). Murgul bakır ocaklarındaki alansal değişimin uzaktan algılama yöntemi ile belirlenmesi (in Turkish). TMMOB Harita ve Kadastro Mühendisleri Odası 12. Türkiye Harita Bilimsel ve Teknik Kurultayı, 1-7.

Erener, A., & Yakar, M. (2012). Monitoring coastline change using remote sensing and GIS technologies. Lecture Notes in Information Technology, 30, 310-314.

Erener, A., & Yakar, M. (2015). Uzaktan Algılama Ve Cbs Teknolojileri İle Kıyı Sınır Değişim Analizi: Meke Gölü Örneği, TUFUAB VIII. Teknik Sempozyumu 21-23 Mayıs 2015 / Konya

Hussain, M., Chen, D., Cheng, A., Wei, H., & Stanley, D. (2013). Change detection from remotely sensed images: From pixel-based to object-based approaches. ISPRS Journal of photogrammetry and remote sensing, 80, 91-106. https://doi.org/10.1016/j.isprsjprs.2013.03.006

Kaya, Ö., & Toroğlu, E. (2015). Monitoring urban development of Kayseri and change detection analysis. Turkish Geographical Review, (65), 87-96. https://doi.org/10.17211/tcd.37722

Kirui, K. B., Kairo, J. G., Bosire, J., Viergever, K. M., Rudra, S., Huxham, M., & Briers, R. A. (2013). Mapping of mangrove forest land cover change along the Kenya coastline using Landsat imagery. Ocean & Coastal Management, 83, 19-24. https://doi.org/10.1016/j.ocecoaman.2011.12.004

Kocadağlı, A. Y. (2022). Türkiye'de Nüfusun Mekansal Dağılımında Kıyı Alanları. Eurasian Academy of Sciences Social Sciences Journal, 1-12.

Korkut, A., Şişman, E. E., Erdinç, Y. L., Özyavuz, M. (2008). Evaluation of land use of Tekirdağ coastal zone by GIS. Journal of Tekirdag Agricultural Faculty, 5(1), 13-25.

Lu, D., Batistella, M., Mausel, P., & Moran, E. (2007). Mapping and monitoring land degradation risks in the Western Brazilian Amazon using multitemporal Landsat TM/ETM+ images. Land Degradation & Development, 18(1), 41-54.

Ma, L., Li, M., Blaschke, T., Ma, X., Tiede, D., Cheng, L., Chen, Z., & Chen D. (2016). Object-based change detection in urban areas: The effects of segmentation strategy, scale, and feature space on unsupervised methods. Remote Sensing, 8(9), 761. https://doi.org/10.3390/rs8090761

Martínez, M. L., Intralawan, A., Vázquez, G., Pérez-Maqueo, O., Sutton, P., & Landgrave, R. (2007). "The coasts of our world: Ecological, economic and social importance." Ecological Economics, 63(2–3), 254-272.

Mishra, S., Shrivastava, P., & Dhurvey, P. (2017). Change detection techniques in remote sensing: A review. International Journal of Wireless and Mobile communication for Industrial systems, 4(1), 1-8. http://dx.doi.org/10.21742/ijwmcis.2017.4.1.01

Mutluoğlu, Ö., & Yakar, M. (2005). Accuracy and Cost Analysis in obtaining of spatial data from Mono Ikonos imagery. Selcuk University Journal of Engineering, Science and Technology, 20(1), 27-34.

Mutluoglu, O., Yakar, M., Yilmaz, H. M., & Yildiz, F. (2008). Comparisation of spatial accuracy of data acquired from mono and stereo images: a case study of campus area Konya Turkey. International Archive of Photogrammetry and Remote Sensing, 37(B4), 1045-1048.

Mutluoglu, O., Yakar, M., & Yilmaz, H. M. (2015). Investigation of effect of the number of ground control points and distribution on adjustment at WorldView-2 Stereo images. International Journal of Applied Mathematics, Electronics and Computers, 3(1), 37-41.

Mutluoğlu, Ö., Yakar, M., & Yılmaz, H. M. (2015). Worldview-2 Stereo uydu görüntüsünden üretilen sayısal ortofoto konum doğruluğunun araştırılması [Symposium presentation] (in Turkish). TUFUAB VIII. Teknik Sempozyumu, Konya, Turkey.

Mutluoğlu, Ö., Yakar, M., & Yılmaz, H. M. (2016). Investigation of spatial accuracy of high-resolution (50cm) Worldview-2 satellite images. Selcuk University Journal of Engineering, Science and Technology, 4(4), 321-329.

Müller, R., Krauß, T., Schneider, M., & Reinartz, P. (2012). Automated georeferencing of optical satellite data with integrated sensor model improvement. Photogrammetric Engineering & Remote Sensing, 78(1), 61-74. https://doi.org/10.14358/PERS.78.1.61

Nassar, K., Mahmod, W. E., Fath, H., Masria, A., Nadaoka, K., & Negm, A. (2019). Shoreline change detection using DSAS technique: Case of North Sinai coast, Egypt. Marine Georesources & Geotechnology, 37(1), 81-95. https://doi.org/10.1080/1064119X.2018.1448912

Olgun, A. (2012). Monitoring of coastline changes of the Goksu Delta by means of remote sensing and geographic information systems (Publication No. 315311) [Master's Thesis, İstanbul Technical University]. YÖK National Thesis Center.

Pural, A. (1995). Trabzon Tarihi Coğrafyası, İstanbul Üniversitesi, Yüksek Lisans Tezi, İstanbul

Sarı, Y. E. & Yüksel, H. (2020). Bilgi Teknolojileri İle Sezonsal Ve 20 Yıllık Periyotta Kentsel Isı Adası (KIA) Değişimi ve Etkileyen Faktör Analizi, Lisans Tezi, Kocaeli Üniversitesi, Kocaeli.

Sekovski, I., Newton, A., & Dennison, W. C. (2012). Megacities in the coastal zone: Using a driver-pressure-state-impact-response framework to address complex environmental problems. Estuarine, Coastal and Shelf Science, 96, 48-59.

Seto, K. C., & Fragkias, M. (2005). Quantifying spatiotemporal patterns of urban land-use change in four cities of China with time series landscape metrics. Landscape ecology, 20(7), 871-888.

Tekin, S. (2019). Corine Verileri İle Arazi Kullanım Değişimi: Türkiye Örneği, Lisans Tezi, Kocaeli Üniversitesi, Kocaeli

Uzan, M., & Özcan, S. (2016). Solaklıdere-İyidere Arasında(Trabzon/Of) Kıyı Kullanımının Zamansal Değişimi Ve Sürdürülebilirlik Yönetimi, Doğu Coğrafya Dergisi, Sayı 35

Wu, W. (2007). Coastline evolution monitoring and estimation—a case study in the region of Nouakchott, Mauritania. International Journal of Remote Sensing, 28(24), 5461-5484.

Yilmaz, H. M., Yakar, M., Mutluoglu, O., & Yildiz, F. (2004). Selection of the most suitable sizes of ground control points in the satellite images. ISPRS Congress Istanbul, Turkey.

Liu, Y., Hu, C., Dong, Y., Xu, B., Zhan, W., & Sun, C. (2019). Geometric accuracy of remote sensing images over oceans: The use of global offshore platforms. Remote Sensing of Environment, 222, 244-266.

Yu, K., Hu, C., Muller-Karger, F. E., Lu, D., & Soto, I. (2011). Shoreline changes in west-central Florida between 1987 and 2008 from Landsat observations. International Journal of Remote Sensing, 32(23), 8299-8313.

URL - 1 Geographical Structure of Trabzon. Retrieved May 10, 2023, from https://trabzon. net.tr/trabzon/trabzonun-cografi-yapisi.html?amp

ADVANCES IN GEOMATICS

VOLUME 03 • ISSUE 01 • OCTOBER 2025
e-ISSN: 3023-4980

ORIGINAL ARTICLE

Submission: 02/09/2025
Accepted: 27/10/2025

MULTI-CRITERIA GIS-BASED ASSESSMENT OF SOLAR POWER PLANT SITE SUITABILITY IN GÖNEN DISTRICT, ISPARTA, TÜRKİYE

Gülcan SARP[1]* Ceylin ZAMBAK[1]

[1] Faculty of Humanities and Social Sciences, Department of Geography, Süleyman Demirel University, Isparta, Türkiye.
* Corresponding Author: G. Sarp, gulcansarp@sdu.edu.tr 0000-0002-5021-4918

ABSTRACT

Solar energy has an important place among clean energy sources due to its environmental friendliness, energy supply security and sustainability features. In this research, the most suitable areas for Solar Power Plants (SPPs) in the Gönen district of Isparta were determined by applying a GIS-based Analytic Hierarchy Process (AHP) multi-criteria analysis. In the study, SPP site suitability factors such as elevation, slope, aspect, temperature, Global Horizontal Irradiance (GHI), annual precipitation, wind speed, Land Surface Temperature (LST), distance to roads and energy transmission lines, and land-use suitability were considered as the main criteria in SPP site selection. The top three criteria in SPP site selection were slope (18.8%), aspect (17.5%), and GHI (15.8%). Less influential factors are land use (3.9%), elevation (2.5%), and distance to roads (2.1%) and energy transmission lines (2.0%). According to the resulting SPP suitability map 16.55% of the district is in the "very high" suitability class, 27.55% in the "high" suitability class, and 27.21% in the "moderate" suitability class. Furthermore, more than 80% of the existing solar power plants lie in "high" and "very high" suitability classes. This emphasizes the appropriateness of the criteria used in this study and also the technique applied.

Keywords: Solar Power Plant (SPP), Analytic Hierarchy Process (AHP), Site Suitability, Gönen-Isparta.

Cited As:

Sarp, G., & Zambak, C. (2025). Multi-criteria GIS-based assessment of solar power plant site suitability in Gönen district, Isparta, Türkiye, Advances in Geomatics, 3(1), 72-86. https://doi.org/10.5281/zenodo.18087459

INTRODUCTION

Due to increasing consumption of fossil fuels, environmental issues such as climate change, global warming, and pollution have increased, thus accelerating the need for using sustainable and renewable energy sources. Among these energy alternatives, solar energy is considered a clean source, a reliable source, and an infinite source of energy in the future. To attain this objective, a radical shift towards the use of renewable energy sources such as solar, wind, and hydroelectric power, among others, after decreasing reliance on fossil fuels is mandatory. To facilitate this shift during the course of achieving this objective, a systematic and analytical methodology will be considered in selecting an investment location for clean and renewable energy sources. Furthermore, this is a mandatory requirement given the widespread emergence of SPP projects recently. Selecting a suitable location for a solar power plant not only considers high solar intensity but adopts a simultaneous assessment factor for other major parameters including slope, orientation, height, land use, wind speed, surface temperature, distance to roads, and distance to power lines. Integrating all these parameters will create a complicated situation in Multi-Criteria Decision Analysis (MCDA) / Multi-Criteria Decision Making (MCDM). Assessing inter-relationship among these parameters and their role in location selection is a complicated problem. To address these issues, studies conducted have effectively clarified that methods such as AHP analysis are very efficient in inter-linking these parameters with their relative weights successfully in AHP analysis (Aydin et al., 2013; Al Garni & Awasthi, 2017; Ozcelik & Sarp, 2018; Giamalaki et al., 2019; Gacu et al., 2023; Ahadi et al., 2023; Amiri et al., 2024). Past studies have clarified the significance of selecting a location for a solar power plant in literature (Bazmi & Zahedi, 2011; Mardani et al., 2015; Infield & Freris, 2020). Other studies undertaken clarify an integration strategy using GIS & MCDA/MCDM in order to reach an accuracy level in selecting a suitable location efficiently (Datta et al., 2011; Lund et al., 2024; Ukoba et al., 2024; Amiri et al., 2024). AHP analysis in these studies is used given its methodology, capacity to assess different parameters simultaneously based on priority parameters, and transparent analysis.

The Analytic Hierarchy Process (AHP) proposed by Saaty in 1972 is a technique used in MCDM. It is particularly useful in studies where decision makers must evaluate multi criteria to compare various options (Saaty, 1980). AHP has found many applications in renewable energy projects related to site selection (Al Garni&Awasthi, 2017; Yankiv-Vitkovska et al., 2020; Gacu et al., 2023; Amiri et al., 2024).

Despite the extensive literature on GIS–AHP-based solar site selection, region-specific studies that integrate long-term climatological variables with high-resolution spatial data at the district scale in Türkiye remain limited. Furthermore, the combined evaluation of static, quasi-static, and climatic parameters within a unified decision-support framework has not been sufficiently explored in local renewable energy planning contexts.

The present study proposes a GIS–AHP-based multi-criteria site suitability model to identify optimal solar power plant locations in the Gönen District (Isparta, Türkiye). The novelty of this study lies in the integration of a comprehensive set of carefully selected parameters representing topographic, climatic, environmental, and infrastructural conditions, the combined use of long-term climatological averages and high-resolution spatial datasets, and the production of a locally applicable suitability map to support regional renewable energy planning and decision-making. The selected parameters, such as elevation, slope, aspect, temperature, Global Horizontal Irradiance (GHI), annual precipitation, wind speed, Land Surface Temperature (LST), distance to roads, distance to energy transmission lines, and land-use suitability, which were selected based on their demonstrated relevance in previous GIS–MCDA/AHP studies and their direct influence on the technical feasibility, environmental compatibility, and economic viability of solar power plant installations.

Subsequently, the AHP method was performed in order to handle the complex decision-making processes among these parameters and to compute the importance, which continuously weighed the factors. Importance levels (weights) obtained from AHP were used to analyze and integrate the spatial data obtained through GIS, and the spatial distribution of suitable sites was determined. This integrated analysis is of immense value for identifying potential sites with high accuracy for the construction of a clean and sustainable solar power plant at Gönen.

1. STUDY AREA

The study area is the Gönen district of Isparta located in the Lakes Region of southwestern Türkiye (Fig.1a, b). The district has a high potential for solar power plant investments due to its location, and the widespread use of solar power plants in the district indicates this (Fig. 1c, d). According to Solar Energy Potential Atlas (GEPA) of Türkiye, the lowest radiation level observed in the district was 1.80 kWh/m²-day (December), and the highest radiation level was 6.73 kWh/m²-day (June). In May and August, radiation levels exceed 6 kWh/m²-day. On the other hand, while the sunshine duration in the district is around 3.85 hours in December and 4.33 hours in January during the winter months, these durations are around 11.06 hours and 11.64 hours in June and July during the summer months. This indicates a strong potential for SPP installation in the district (https://gepa.enerji.gov.tr/pages/32.aspx). These high radiation values support the economic viability of the project in the district. Therefore, Gönen is considered a suitable region for determining SPPs site suitability.

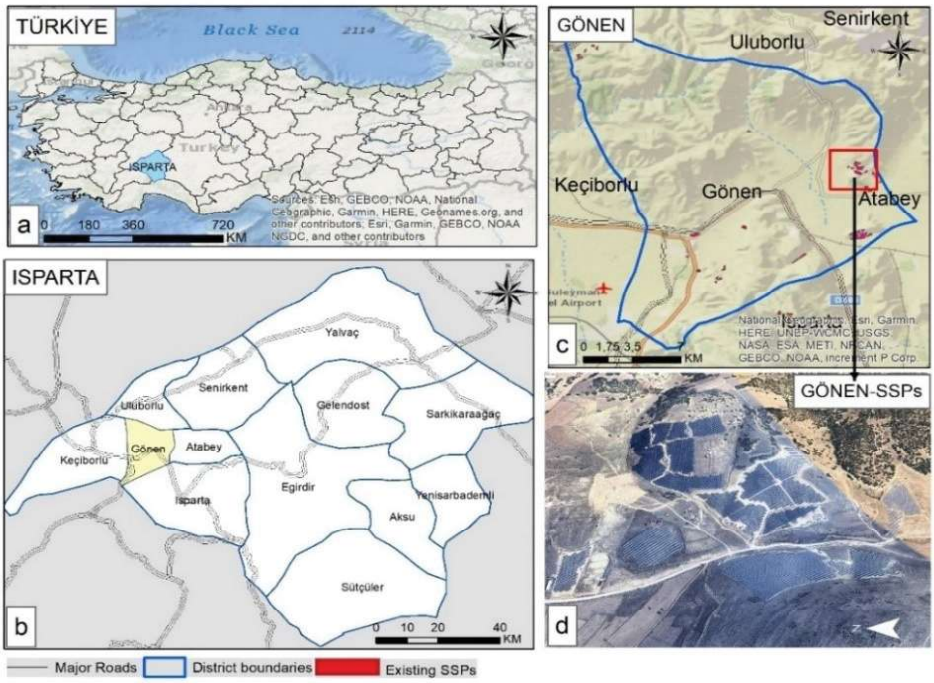

Figure 1. Study area maps: (a) Location of Isparta within Türkiye; (b) Location of Gönen within Isparta Province; (c) Detailed map of the Gönen district; (d) Example Google Earth imagery showing existing Solar Power Plants (SPPs) in Gönen.

2. MATERIALS AND METHODS

2.1 Data Sources and Preprocessing

Multiple datasets were used in this study to evaluate site suitability for SPPs. Topographic and morphometric parameters, including slope, aspect, and elevation, were derived from the SRTM 1 arc-second Digital Elevation Model (DEM) provided by NASA/USGS, which has a spatial resolution of 30 meters (https://www.earthdata.nasa.gov). Global Horizontal Irradiance (GHI) data were obtained from the Global Solar Atlas (World Bank Group), providing annual average values of GHI (https://globalsolaratlas.info/download/turkey), and wind speed data were retrieved from the Global Wind Atlas (https://globalwindatlas.info/en/). LST was calculated using Band 10 of the Thermal Infrared Sensor (TIRS) onboard Landsat 9 imagery acquired on 23 June 2025 from the USGS EarthExplorer (https://earthexplorer.usgs.gov/), with a spatial resolution of 100 meters. Precipitation and mean temperature data were obtained from the WorldClim v2.1 database at a spatial resolution of 30 arc-seconds (~1 km²), representing long-term climatic averages for the period 1970–2000 (Fick and Hijmans, 2017). Land cover and land use information were obtained from the CORINE Land Cover 2018 dataset (EEA) at 100-meter resolution, facilitating the identification of suitable and unsuitable terrain types (https://land.copernicus.eu/en/products/corine-land-cover). Road and power transmission line data were obtained from OpenStreetMap (OSM) using the Overpass Turbo query tool (https://over-

pass-turbo.eu/). Although the datasets originate from different temporal periods, long-term climatological averages were used to represent stable background conditions, while the most recent Landsat 9 imagery was selected to reflect the most recent surface thermal conditions important for evaluating solar power potential. This combination of multi-temporal datasets is commonly adopted in GIS-based spatial suitability analyses.

Preprocessing in a GIS environment was carried out before the analysis of all datasets. Preprocessing steps included geometric correction, coordinate transformation, and resampling to ensure consistency in spatial resolution across datasets. All layers were projected to a common coordinate system (UTM Zone 36N, WGS 84) and clipped to the district boundaries. To enable comparison across all datasets with the different units and scales, normalization to 0–1 range was performed.

2.2 Site Selection Criteria for Solar Power Plants

The performance and applicability of green energy systems depend on many factors, including the characteristics of energy sources, efficiency, physical and environmental characteristics of the technologies used, and potential installation sites. High-quality data is needed for economically viable and efficient location of solar power plants. The selection of criteria used in this study, including elevation, slope, aspect, temperature, GHI, annual precipitation, wind speed, LST, Euclidean distance to roads, Euclidean distance to power lines, and land use suitability (Fig.2), was based on an extensive literature review.

In the context of Gönen District, all these criteria have different spatial patterns that affect SPP suitability. According to the elevation data, the general altitude increases toward the northern and northwestern parts of the district, potentially limiting SPP installation in those areas due to cooler temperatures and stronger wind effects (Fig. 2a). Slope, on the other hand, was expressed as the steepness of the terrain. Steeper slope values were evident in northern and northwestern mountainous regions, which are considered as a limiting condition for SPP installation, while its gentler slopes in the southern and southeastern of the area seemed more favorable (Fig. 2b). Aspect maps showed slope orientation, which had an influence on the amount of exposure to solar radiation. South orientation offered favorable conditions (Fig. 2c). Temperature data were analyzed with respect to thermal conditions. Higher temperature values were evident in the centre and southeast part of the area, which would be favorable for energy generation (Fig. 2d). GHI was higher in the east and southeast, indicating greater solar potential in those areas (Fig. 2e). In some parts towards the north of the district, the annual precipitation is relatively higher than in other areas, which will affect the maintenance process of solar panels to be built in these parts (Fig. 2f). Wind speed shows higher values in the northern and northwestern parts of the district, where topographic exposure contributes to stronger air flow, potentially limiting the feasibility of SPP installations (Fig. 2g). LST results reveal lower temperatures in the northern and northwestern areas with higher elevation, while temperatures increase towards the cen-

tral and interior parts. Elevated temperatures in these central regions may enhance the performance and energy yield of solar power plants, making them more suitable for SPPs installation (Fig. 2h). Euclidean distances to roads and energy transmission lines were calculated to evaluate accessibility and connection efficiency. Proximity to a road offers convenience for construction and maintenance, while closeness to existing energy lines reduces connection costs. Accordingly, areas far from roads or transmission lines are considered less suitable (Fig. 2i–2j). Land use information from the CORINE Land Cover dataset has been reclassified into four suitability categories for SPPs installation: Highly Suitable (meadows, pastures, sparse vegetation, rocky areas, non-irrigated agricultural lands), Moderately Suitable (shrubland, mixed vegetation, orchards), Low Suitable (dense forests, built-up areas), and Not Suitable (wetlands, irrigated agricultural lands, water bodies), based on land-use compatibility, environmental protection constraints, and criteria widely adopted in GIS-based solar power plant site suitability studies (Carrión et al., 2008; Uyan, 2017; Khan et al., 2023). The spatial distribution of these land-use suitability classes is illustrated in Fig. 2k.

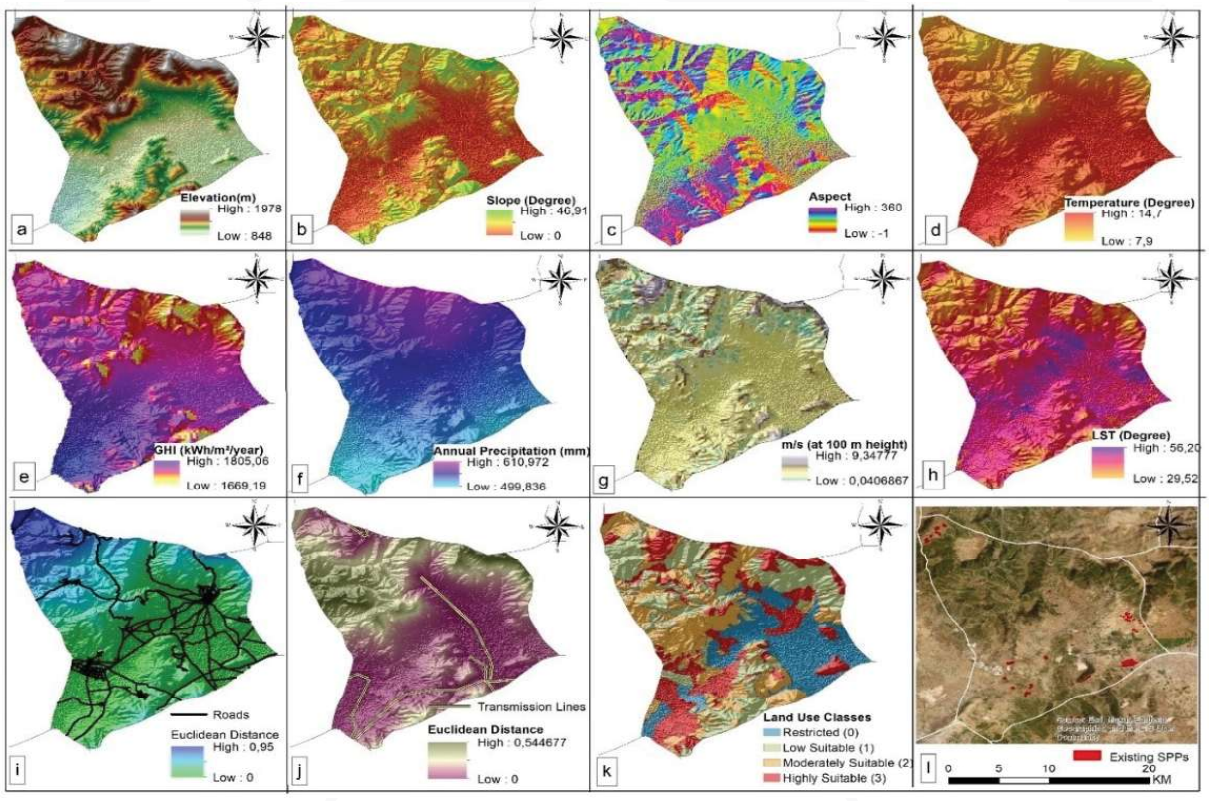

Figure 2. Thematic maps of the Gönen district illustrating topographic, climatic, and infrastructural factors influencing solar power plant (SPP) site suitability: (a) Elevation, (b) Slope, (c) Aspect, (d) Temperature, (e) Global Horizontal Irradiance (GHI), (f) Annual precipitation, (g) Wind speed, (h) Land Surface Temperature (LST), (i) Euclidean distance to roads, (j) Euclidean distance to energy transmission lines, (k) Land-Use suitability, and (l) Existing SPPs displayed over an ESRI basemap.

2.3 Criteria Normalization for Suitability Analysis

Datasets used in MCDA studies often have different units, scales, and value ranges. For this reason, data normalization is required to bring all criteria onto a comparable scale before applying weighting and overlay procedures. This step ensures that no single variable dominates the evaluation due to its numerical magnitude. In this study, all the continuous criteria were standardized to a 0–1 interval before the weighting and overlay stages. Slope, elevation, LST, wind speed, annual precipitation, and distances to roads and energy transmission lines were treated as cost criteria because they negatively affect site suitability with increasing values. These datasets were normalized using an inverse min–max transformation, based on the Linear Scale Transformation (Max–Min) technique given in Eq.1 (Çelen, 2014). This technique ensures that each attribute is rescaled within a strict interval of 0–1, within which its range is clear and comparable (Chakraborty & Yeh, 2007, 2009). GHI was considered a benefit criteria, since higher irradiation values indicate greater suitability for solar energy production. For this variable, standard min-max normalization was used (Eq.2):

$$Normalized\ Value = \frac{X_{\max} - X}{X_{\max} - X_{\min}} \tag{1}$$

where X is the raw value, and Xmin and Xmax are the minimum and maximum values of the dataset. This inversion ensures that larger values correspond to lower suitability.

$$Normalized\ Value = \frac{X - X_{\min}}{X_{\max} - X_{\min}} \tag{2}$$

where X is the value in the original cell, and Xmin and Xmax are the minimum and maximum values of the dataset. The result of this transformation rescales all values to a range between 0 and 1, which means higher normalized scores will result in a higher degree of suitability depending on the nature of the criterion.

The criteria pertaining to categories were considered individually. The aspect values were initially recoded into directional aspects, with all southern directions assigned a score of the highest suitability. Suitability scores were assigned to land cover classes based on their association with conducting a solar power plant setup. The categories were already in a standard scale and thus did not need any normalization.

By using this method, it can be ensured that both continuous and nominal variables possess a common scale of measurement so that they can be unified in AHP analysis.

2.4 Integration of Thematic Layers to Define Suitable Zones for SPPs

Suitable zones for SPPs in Isparta-Gönen were identified using the AHP, which was introduced by Saaty (1972). AHP is one of the MCDA techniques that allows both objective and subjective factors to be taken into consideration during decisions. As with other MCDA methods, it provides a structured approach for dealing with complex, unstructured decision-making problems. The process involves

establishing a hierarchy of decision criteria and allowing pairwise comparisons to be made between them in matrix form, assigning relative weights, and calculating a Consistency Ratio (CR). Comparisons are based on a numerical scale ranging from 1 to 9, indicating the relative importance of one criterion compared to another. All these values have to be determined with great care instead of arbitrary setting. The CR, proposed by Saaty (1977), should be checked for the consistency of the comparison matrix, and according to Saaty and Vargas (1991), the matrices having a CR value above 0.1 must be revised. CR is calculated as given in (Eq. 3):

$$CR = \frac{CI}{RI} \tag{3}$$

where CI is the consistency index and RI is the average consistency index for a randomly generated matrix. In this study, the CR was calculated based on the RI value that matched the size of the matrix in the AHP model. Given that there were 11 criteria involved in the pairwise comparison, the RI value was considered to be 1.51, according to Saaty and Vargas (1991). The CI is calculated from the pairwise comparison matrix through (Eq. 4):

$$CI = \frac{\lambda_{max} - n}{n - 1} \tag{4}$$

where λ_{max} is the largest eigenvalue of the comparison matrix, and n is the matrix order.

In the next step, the relative importance of the eleven thematic layers was assessed by a pairwise comparison method. In this respect, each pair of criteria was assigned a numerical value ranging between 1 and 9 to indicate the strength of preference among the concerned pairs. These values were determined by making comprehensive judgments with the aid of expertise in geoscience and remote sensing. The obtained pairwise comparison matrix is shown in Table 1.

Table 1. Pairwise comparison matrix of the eleven criteria.

Criteria	C1	C2	C3	C4	C5	C6	C7	C8	C9	C10	C11
C1	1	2	3	2	3	2	2	4	4	6	6
C2		1	3	4	3	1	1	6	6	7	7
C3			1	3	3	1	2	5	6	5	5
C4				1	2	1	1	3	8	6	4
C5					1	1	1	2	2	2	2
C6						1	7	5	6	6	6
C7							1	5	5	4	4
C8								1	4	3	3
C9									1	2	2
C10										1	1
C11											1

Criteria Exp: C1 – Slope; C2 – Aspect; C3 – Precipitation; C4 – Temperature; C5 – Wind speed; C6 – Solar radiation (GHI); C7 –Land surface temperature (LST); C8 – Land use; C9 – Elevation; C10 – Distance to roads; C11 – Distance to energy transmission lines.
Principal eigen value = 12.169
Eigen vector solutions: six iterations delta = 7.6E–8

Applying the principal eigenvector method, the final weights of the criteria were derived after pairwise comparison (Table 2). Among the thematic layers, slope received the highest weight (18.8%), followed by aspect (17.5%) and GHI (15.8%). Other important criteria included precipitation (13.1%), temperature (9.5%), LST (8.9%), and wind speed (6.0%). The criteria with the lowest influence were distance to energy transmission lines (2.0%) followed by distance to roads (2.1%), elevation (2.5%), and land use (3.9%), clearly reflecting the minor role of accessibility and land-use considerations in determining suitable sites for solar power plants. The CR of the pairwise comparison matrix was calculated as 0.077, which is below the threshold of 0.1 and indicates that the judgments are consistent enough for further analysis.

Table 2. Priority weights and rankings of criteria derived from AHP.

Criteria	Priority (%)	Rank	(+ %)	(- %)
Slope	18.8	1	9.0	9.0
Aspect	17.5	2	9.3	9.3
Precipitation	13.1	4	5.9	5.9
Temperature	9.5	5	4.1	4.1
Wind speed	6.0	7	3.1	3.1
Solar radiation (GHI)	15.8	3	13.8	13.8
Land surface temperature (LST)	8.9	6	4.5	4.5
Land use	3.9	8	2.1	2.1
Elevation	2.5	9	1.1	1.1
Euclidean distance to energy transmission lines	2.0	11	0.6	0.6
Euclidean distance to roads	2.1	10	0.6	0.6

2.5 GIS Integration and Weighted Overlay

The spatial suitability of potential solar power plant installation sites was assessed by integrating the AHP-derived weights of raster parameters used in the study within a GIS environment. The resulting weighting coefficients (Wi) were then applied to the raster layers using the Weighted Overlay

approach, one of the most common methods for MCDA, to obtain a suitability map of solar power plants in the study area. This process can be mathematically expressed as the Suitability Score (Eq.5):

$$Suitability\ Score = \sum_{i=1}^{n} w_i Xc_i \quad (5)$$

where wi is the AHP-derived weight of criterion i, n is the total number of criteria used in analysis and Xci is the normalized or classified raster value of criterion i.

3. RESULTS AND DISCUSSION

3.1 Effect of Criteria Weights and Spatial Distribution

The integration of the SPPs site selection parameters with the AHP methods reveals that slope was the most influential parameter, with a weight of 18.8%. On the other hand, the Euclidean distance to roads (2.1%) and energy transmission lines (2.0%), along with elevation (2.5%), were found to be less important criteria (Table 2). The prominence of slope factor in this analysis is in accordance with existing research work undertaken using GIS-MCDA for analysis of solar suitability, wherein slope factor has been proved to be a major factor in construction and installation cost favorability (Yankiv-Vitkovska et al., 2020). The lower priority weights given to accessibility factors such as Euclidean distance to roads and transmission lines have also been observed in existing research work based on GIS-AHP in solar site selection analysis (Al Garni & Awasthi, 2017).

Overall, the weighting results indicate a clear dominance of topographic and climatic factors over accessibility-related parameters, ensuring a consistent AHP-based foundation for the subsequent GIS weighted overlay analysis.

The AHP weighted overlay methodology has some intrinsic limitations. Some degree of “very high” suitability in moderately elevated or vegetated regions may reflect favorable solar radiation levels or localized topographic effects rather than actual site feasibility. Despite these limitations, the spatial distribution of suitability classes provides valuable insights into potential SPP locations.

The spatial distribution of suitability classes is illustrated in Fig. 3. “High” and “very high” suitability zones are mainly located in low slope areas and southern parts of this district, and regions of low suitability mainly exist in the northern and northeastern parts with high slopes.

The above results can be used for basic planning of SPP implementation, but verification and technical evaluation are very important in this case. Further research can improve model assessment using other validation methods, for instance, sensitivity analysis of AHP-weighting vector accuracy or comparisons based on other MCDA approaches.

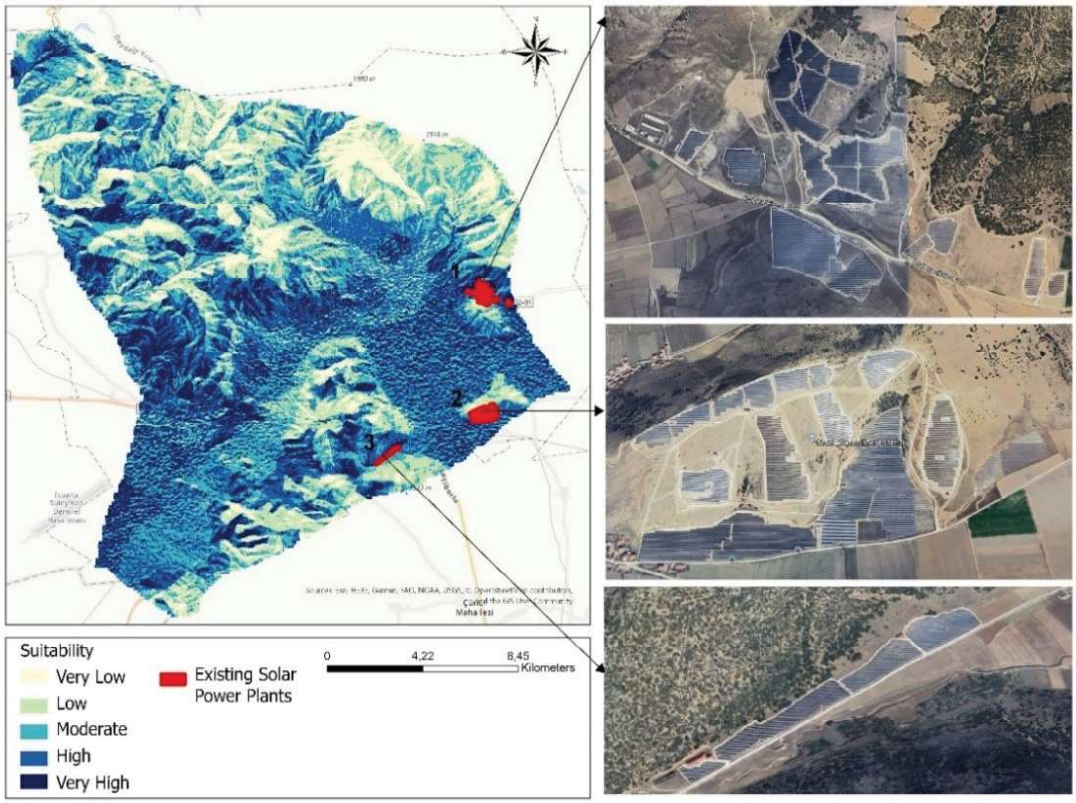

Figure 3. Final SPPs suitability map for Gönen District and detailed close-up Google Earth images of the three existing SPPs areas (on the right).

The numerical distribution of the suitability map is summarized in Table 3. The study region has been classified into five suitability classes. The results indicate that the "moderate suitability" and "high suitability" classes in Gönen occupy 27.21% and 27.55%, respectively, and "very high suitability" class occupies 16.55%. On the other hand, "very low" and "low" suitable regions occupy 9.32% and 19.36%, respectively, corresponding to a combined share of 28.68%, mainly covering the northern and northeastern part of this region with topography being less suitable in nature. Some apparent “very high” suitability in certain mountainous or vegetated areas may result from higher solar radiation values or local topographic variations, rather than reflecting true feasibility. These observations highlight the need for careful interpretation and on-site verification. The AHP-based weighted overlay results provide a relative suitability assessment rather than absolute feasibility; future studies may enhance realism by incorporating exclusionary constraint layers such as slope thresholds, forest masks, protected areas, or post-classification filtering procedures.

Table 3. Comparison of overall suitability classes with the spatial distribution of existing solar power plants (SPPs).

Suitability Class	Area Pixel Count	Total Area (%)	SPPs Pixel Count	SPPs(%)
Very Low	25306	9.32	0	0.00
Low	52532	19.36	59	5.67
Moderate	73818	27.21	119	11.44
High	74774	27.55	442	42.60
Very High	44925	16.55	419	40.29

3.2 Spatial Validation and Reliability Assessment of the Suitability Model

To determine the reliability of the proposed AHP-GIS based suitability model, the existing SPP sites have been traced using Google Earth images. The validation shows that 94.33% of the existing SPPs lie in moderate, high, and very high suitability classes, whereas only 5.67% lie in low and very low classes. Particularly, 82.89% of the existing SPPs lie in high and very high classes as shown in the proposed suitability model (Table 3). The presence of a high degree of similarity between the model output and existing SPPs indicates the reliability of the model output. Though discrepancies always exist in current studies due to certain economical, political, or infrastructural reasons, the present study indicates a preponderant influence of geographical factors for the selection of SPPs in the Gönen district.

Although the result of the accuracy assessment of this study relies exclusively on the comparison of the existing solar energy plants and the created suitability classes through spatial analysis, the fact that the concentration of existing solar energy plants lies in areas of moderate to high suitability suggests that there is a certain level of agreement between the two sets of model outputs and that of reality. Future studies should consider improving this aspect by using ROC/AUC analysis and presence/absence modeling among others.

CONCLUSIONS

This study demonstrates how the combined use of GIS and AHP methods can effectively select suitable sites for SPPs. Evaluation of the parameters used in site selection using the AHP method revealed that the top three factors in SPP site selection are slope (18.8%), aspect (17.5%), and solar radiation (15.8%), followed by precipitation (13.1%), temperature (9.5%), LST (8.9%) and wind speed (6.0%). Less influential factors in SPPs site selection are land use, elevation, and distance to power lines and roads.

According to the resulting map obtained from the analyses and weightings, 16.55% of the district is in the "very high" suitability class, 27.55% in the "high" suitability class, and 27.21% in the "moderate" suitability class. The concentration of more than 80% of existing solar power plants within the "high" and "very high" suitability classes highlights the relevance of the applied criteria and confirms the effectiveness of the proposed suitability assessment approach.

Beyond the identification of suitable sites, this study provides a district-scale GIS-AHP framework that combines long-term climatic variables with high-resolution spatial data and can be a useful decision-support tool for the preliminary solar power plant planning process. The results here express relative suitability, not absolute feasibility, and further studies can enhance the model by the inclusion of more constraint layers or by considering alternative MCDA methods.

REFERENCES

Ahadi, P., Fakhrabadi, F., Pourshaghaghy, A., & Kowsary, F. (2023). Optimal site selection for a solar power plant in Iran via the Analytic Hierarchy Process (AHP). Renewable Energy, 215, 118944. https://doi.org/10.1016/j.renene.2023.118944.

Al Garni, H. Z., & Awasthi, A. (2017). Solar PV power plant site selection using a GIS-AHP based approach with application in Saudi Arabia. Applied energy, 206, 1225-1240.

Amiri, A. A., Wahid, M. N., Al-Buraiki, A. S., & Al-Sharafi, A. (2024). A strategic multi-criteria decision-making framework for renewable energy source selection in Saudi Arabia using AHP-TOPSIS. Renewable Energy, 236, 121523.

Aydin, N. Y., Kentel, E., & Duzgun, H. S. (2013). GIS-based site selection methodology for hybrid renewable energy systems: A case study from western Turkey. Energy conversion and management, 70, 90-106.

Bazmi, A. A., & Zahedi, G. (2011). Sustainable energy systems: Role of optimization modeling techniques in power generation and supply—A review. Renewable and sustainable energy reviews, 15(8), 3480-3500.

Carrión, J. A., Estrella, A. E., Dols, F. A., Toro, M. Z., Rodríguez, M., & Ridao, A. R. (2008). Environmental decision-support systems for evaluating the carrying capacity of land areas: Optimal site selection for grid-connected photovoltaic power plants. Renewable and sustainable energy reviews, 12(9), 2358-2380.

Chakraborty, S., & Yeh, C. H. (2007). A simulation based comparative study of normalization procedures in multiattribute decision making. In Proceedings of the 6th Conference on 6th WSEAS Int. Conf. on Artificial Intelligence, Knowledge Engineering and Data Bases (Vol. 6, pp. 102-109).

Chakraborty, S., & Yeh, C. H. (2009). A simulation comparison of normalization procedures for TOPSIS. In 2009 International conference on computers & industrial engineering (pp. 1815-1820). IEEE.

Çelen, A. (2014). Comparative analysis of normalization procedures in TOPSIS method: with an application to Turkish deposit banking market. Informatica, 25(2), 185-208.

Datta, A., Ray, A., Bhattacharya, G., & Saha, H. (2011). Green energy sources (GES) selection based on multi-criteria decision analysis (MCDA). International Journal of Energy Sector Management, 5(2), 271-286.

Fick, S. E., & Hijmans, R. J. (2017). WorldClim 2: new 1-km spatial resolution climate surfaces for global land areas. International journal of climatology, 37(12), 4302-4315.

Gacu, J. G., Garcia, J. D., Fetalvero, E. G., Catajay-Mani, M. P., & Monjardin, C. E. F. (2023). Suitability analysis using GIS-based analytic hierarchy process (AHP) for solar power exploration. Energies, 16(18), 6724.

Giamalaki, M., & Tsoutsos, T. (2019). Sustainable siting of solar power installations in Mediterranean using a GIS/AHP approach. Renewable Energy, 141, 64-75.

Infield, D., & Freris, L. (2020). Renewable energy in power systems. John Wiley & Sons.

Khan, A., Ali, Y., & Pamucar, D. (2023). Solar PV power plant site selection using a GIS-based non-linear multi-criteria optimization technique. Environmental Science and Pollution Research, 30(20), 57378-57397.

Lund, H. (2024). Renewable energy systems: a smart energy systems approach to the choice and modeling of fully decarbonized societies. Elsevier.

Mardani, A., Jusoh, A., Zavadskas, E. K., Cavallaro, F., & Khalifah, Z. (2015). Sustainable and renewable energy: An overview of the application of multiple criteria decision making techniques and approaches. Sustainability, 7(10), 13947-13984.

Ozcelik, M., & Sarp, G. (2018). Evaluation of sustainable water supply alternatives in karstified rock masses using GIS and AHP methodology for Antalya (Turkey) urban area. Environmental Earth Sciences, 77(19), 696.

Saaty, T.L. (1972). An eigenvalue allocation model for prioritization and planning, Energy Manag. Policy Center, Univ. Pennsylvania, p.28–31.

Saaty, T. L. (1977). A scaling method for priorities in hierarchical structures. Journal of mathematical psychology, 15(3), 234-281.

Saaty, T. L., & Vargas, L. G. (1991). Prediction, projection, and forecasting: applications of the analytic hierarchy process in economics, finance, politics, games, and sports.

Saaty, T.L. (1980). The Analytic Hierarchy Process: Planning. Priority Setting. Resource Allocation, McGraw- Hill, New York International Book Company, New York.

Ukoba, K., Olatunji, K. O., Adeoye, E., Jen, T. C., & Madyira, D. M. (2024). Optimizing renewable energy systems through artificial intelligence: Review and future prospects. Energy & Environment, 35(7), 3833-3879.

Uyan, M. (2017). Optimal site selection for solar power plants using multi-criteria evaluation: a case study from the Ayranci region in Karaman, Turkey. Clean Technologies and Environmental Policy, 19(9), 2231-2244.

Yankiv-Vitkovska, L., Peresunko, B., Wyczalek, I., & Papis, J. (2020). Site selection for solar power plant in Zaporizhia city (Ukraine). Geodesy and Cartography, 69(1), 97-116.

ADVANCES IN GEOMATICS

https://aigjournal.com
advancesingeomatics@gmail.com
+90 262 303 32 46

e-ISSN: 3023-4980